POLITECNICO DI TORINO

MASTER COURSE IN ENERGY AND NUCLEAR ENGINEERING

Master Thesis

MODELLING, AUTHORIZATION AND RISK ANALYSIS OF AN INNOVATIVE RENEWABLE ENERGY STORAGE SYSTEM BASED ON REVERSIBLE SOLID OXIDE CELLS

Supervisors:

Prof. Massimo Santarelli

Ing. Domenico Ferrero

Candidate:

Paolo Elia Bortignon

December 2019

ABSTRACT

Current trends in energy sector are unsustainable and most studies agree in the necessity of an imminent and deep transformation of the sector. Hydrogen and fuel cells can play an important role in the framework of the future energy transition.

In the present thesis work a reversible solid oxide cells (rSOC) system working with hydrogen, natural gas or steam is studied as an innovative renewable energy storage system in a real environment microgrid. Relying on data available for an existing research project and from similar plants, the dynamic modelling of the rSOC stack and of most of the balance of plant components is carried out. 45 steady-state operating points are found and an annual simulation of the system behaviour in the integration with local renewables and office demand is performed. Four different cases are analysed to highlight the main features of the rSOC performance and hydrogen storage utilisation. The steady-state results are compared to them obtained by a single day simulation entirely carried out using the dynamic model. Remarkable similarities are obtained.

In the last chapters of the work authorization and risk analysis parts are presented. An overview on present regulations and standard for concerning hydrogen and fuel cells in both an Italian and European perspective is provided, highlighting the most impacting authorization barriers to the deployment of the technologies. A preliminary risk analysis based on literature review and semi-empirical methods evaluation of damage to people is carried out and no unacceptable deviations are found.

Keywords: Dynamic Modelling; Reversible Solid Oxide Cells; Hydrogen; Microgrid; Energy Storage; Risk Analysis; Authorization.

Table of Contents

ABSTRACT 2
LIST OF FIGURES 6
LIST OF TABLES 8
1. FOREWORD – Hydrogen and Fuel Cells 9
2. THEORETICAL ASPECTS OF FUEL CELLS AND ELECTROLYSERS 14
  2.1 FARADAY'S LAW 15
  2.2 CELL VOLTAGE 15
    2.2.1 OPEN CIRCUIT VOLTAGE 15
    2.2.2 EFFECTS OF TRANSPORT PROCESSES 16
  2.3 THERMAL BALANCE IN THE CELL 18
  2.4 FROM THE CELL TO THE STACK 19
3. SYSTEM DEFINITION 20
  3.1 REVERSIBLE SOLID OXIDE CELLS (rSOC) 20
  3.2 SYSTEM CONFIGURATION AND BALANCE OF PLANT 22
  3.3 CONCERNED PLANT 25
    3.3.1 NG-SOFC 26
    3.3.2 H2-SOFC 27
    3.3.3 SOEC 27
4. SYSTEM INTEGRATION 29
  4.1 SUPPLY SIDE 30
    4.1.1 PHOTOVOLTAIC PLANT 30
    4.1.2 HYDROELECTRIC POWER PLANT 37
  4.2 DEMAND SIDE 38
5. MODELLING 41
  5.1 MODELLING TECHNIQUE AND MAIN ASSUMPTIONS 41
  5.2 FEATURES OF THE STACK MODEL 43
    5.2.1 ELECTROCHEMICAL MODEL 43
    5.2.2 POLARIZATION MODEL 47
  5.3 DYNAMIC MODEL 50
    5.3.1 ELECTROCHEMICAL CALCULATOR 52
    5.3.2 OXIDANT LINE 53
    5.3.3 FUEL LINE 54

5.3.4 STACK MODULE 57
5.3.5 AFTERBURNER LINE 59
5.3.6 MIXER LINE 61
5.3.7 EXHAUST GAS LINE 62
5.3.8 EVAPORATOR LINE 63
5.4 MODIFICATIONS FOR LOW LOAD 63
5.4.1 SOFC MODES OF OPERATION 63
5.4.2 SOEC MODE OF OPERATION 65
6. MODELLING RESULTS – steady-state simulations 66
6.1 WORKSHEET 66
6.2 ANNUAL SIMULATION 73
6.2.1 DESCRIPTION OF THE MODEL 73
6.2.1 CASE 1 (10.9% supply – 10.9% demand) 78
6.2.2 CASE 2 (100% supply – 10.9% demand) 79
6.2.3 CASE 3 (30% supply – 10.9% demand) 79
6.2.4 CASE 4 (100% supply – 100% demand) 80
7. MODELLING RESULTS – dynamic simulations 82
7.1 RAMP UP SIMULATION 82
7.2 DAILY SIMULATION 85
8. REGULATIONS OVERVIEW 91
8.2 ITALIAN LEGISLATION 91
8.1.1 DECREE OF THE PRESIDENT OF THE REPUBLIC n. 151 - 1 August 2011 91
8.1.2 DECREE OF THE MINISTRY OF THE INTERIOR - 3 February 2016 93
8.1.3 MINISTERIAL DECREE - 13 July 2011 96
8.2 HYDROGEN REGULATION AND PROCEDURES IN AN EUROPEAN OVERVIEW 97
8.2.1 PRODUCTION OF HYDROGEN 98
8.2.2 STORAGE OF HYDROGEN 100
8.2.3 ELECTRICITY GRID ISSUES FOR ELECTROLYSERS 100
8.2.4 STATIONARY POWER FUEL CELLS 101
9. RISK ANALYSIS 103
9.1 RISK ANALYSIS WORKSHEET CREATION 103
9.2 SEMI-EMPIRICAL MODELS FOR EVALUATION OF DAMAGE 107
9.1.1 HYDROGEN 107
9.1.2 JET FIRE SCENARIO 109

9.1.3 EXPLOSION SCENARIO 112
9.1.4 INTERNAL RELEASE SCENARIO 114
9.3 RESULTS 115
10. CONCLUSIONS 116
11 APPENDIX 118
12 REFERENCES 127

LIST OF FIGURES

Figure 1 Schematic representation of today and hydrogen-based energy system [5] 12
Figure 2 Theoretical Aspects: Graphical representation of the bipolar plate 19
Figure 3 NG-SOFC configuration 26
Figure 4 H2-SOFC configuration 27
Figure 5 SOEC configuration 28
Figure 6 Schematic view of EnviPark 29
Figure 7 Supply side: View of PV power plant located in EnviPark 31
Figure 8 Map showing location of EnviPark, Totem Fotovoltaico and neighbouring buildings. Google Earth, earth.google.com/web/ 33
Figure 9 Supply side: schematic representation of the neighbouring buildings in EnviPark 33
Figure 10 Supply side: Example of calculation for PV obstacles 34
Figure 11 Supply side: Considered outline of horizon in PVGIS simulation 36
Figure 12 Supply Side: PV monthly production 36
Figure 13 Supply side: View of hydro power plant located in EnviPark, https://www.icanaliditorino.it/envronment-park 37
Figure 14 Supply side: Hydro power plant yearly profile 38
Figure 15 Demand side: View of building C in EnviPark 38
Figure 16 Demand side: Annual profile of electricity and heating 40
Figure 17 Modelling: Steam Methane Reforming dependence with temperature 45
Figure 18 Modelling: Water Gas Shift dependence with temperature 46
Figure 19 Modelling: Assumed ASR evolution with temperature 48
Figure 20 Modelling: Example of polarization curve for H2-SOFC 49
Figure 21 Modelling: SIMULINK© blocks worksheet 51
Figure 22 Modelling: Configuration of the considered blocks 51
Figure 23 Modelling: Electrochemical calculator 52
Figure 24 Modelling: Oxidant line 53
Figure 25 Modelling: Fuel line 55
Figure 26 Modelling: Stack module 57
Figure 27 Modelling: Afterburner line 59
Figure 28 Modelling: Mixer line 61
Figure 29 Modelling: Exhaust gas cooling line 62
Figure 30 Modelling: Fresh fuel flowrate depending on SOFC power 64
Figure 31 Modelling: SIMULINK© worksheet for low load in SOFCs 64
Figure 32 Results: SOFC electrical efficiency 69
Figure 33 Results: SOFC ancillary power consumption 70
Figure 34 Results: SOEC ancillary power consumption 71
Figure 35 Results: SOEC stack temperature 71
Figure 36 Results: Heat valorisation 72
Figure 37 Annual simulation: rSOC microgrid 73
Figure 38 Annual simulation: four cases 75
Figure 39 Annual simulation: net power for the four cases 76
Figure 40 Annual simulation: case 1 78

Figure 41 Annual simulation: case 2 79
Figure 42 Annual simulation: case 3 80
Figure 43 Annual simulation: case 4 81
Figure 44 Ramp up: NG-SOFC 83
Figure 45 Ramp up: H2-SOFC 83
Figure 46 Ramp up: SOEC 84
Figure 47 Daily Simulation: Modes of operation and Power values 86
Figure 48 Daily Simulation: Energy Storage Means Profile 86
Figure 49 Daily Simulation: Stack temperature, Ancillary power and Heat Valorisation 87
Figure 50 Daily Simulation: Time of hydrogen tank filling 88
Figure 51 Daily Simulation: Hydrogen tank filling at the end of the day 89
Figure 52 Daily Simulation: Daily Ancillary Energy Consumption 90
Figure 53 Daily Simulation: Daily Heat Recovery 90
Figure 54 Risk analysis: system configuration 103
Figure 55 Risk analysis: Risk matrices 106
Figure 56 Risk Analysis: Schematic representation of outer and inner zone 108

LIST OF TABLES

Table 1 Theoretical aspects: Fuel cells reactions 14
Table 2 System definition: Main parameters of the rSOC system 28
Table 3 Supply side: PVGIS simulation input data 31
Table 4 Supply side: Example of calculation for PV obstacles 34
Table 5 Supply side: Angle results for PV obstacles 35
Table 6 Demand side: considered yearly energy density and energy 39
Table 7 Modelling: Bossel coefficients for SMR and WGS equilibrium constants 45
Table 8 NG-SOFC steady-state worksheet 67
Table 9 H2-SOFC steady-state worksheet 68
Table 10 SOEC steady-state worksheet 68
Table 11 Annual simulation: results for the four cases 76
Table 12 Categorization of storage vessels for fire prevention procedures 91
Table 13 Safety distances depending on storage vessel category 95
Table 14 Risk Analysis: Frequency levels 104
Table 15 Risk Analysis: Damage levels 105
Table 17 Risk Analysis: Enclosure characteristics 108
Table 18 Risk Analysis: Storage vessel characteristics 108
Table 19 Jet Fire Scenario: Released hydrogen quantities 109
Table 20 Jet Fire Scenario: Consequence levels 111
Table 21 Jet Fire Scenario: Results 1 111
Table 22 Jet Fire Scenario: Results 2 111
Table 23 Explosion Scenario: Consequence levels 113
Table 24 Explosion Scenario: Results 113
Table 25 Internal Release Scenario: Released hydrogen quantities 114
Table 26 Appendix: Supply side: Considered angular views 118

1. FOREWORD – Hydrogen and Fuel Cells

The world is experiencing a series of clear and alarming issues regard to which we are called to promptly and effectively act. Current trends in fields on which our society has laid the basis for many years are alarming and are leading us to a socially, economically and environmentally unsustainable world to which upcoming changes are needed.

In 2015 the Paris Agreement has brought virtually all the countries into a common response to strengthen the efforts for facing climate change, in terms of mitigation, adaptation and support to developing countries. The Agreement set the target of limiting the rise in global average temperature to well below 2°C above pre-industrial levels and pursuing efforts to reach the target of 1.5°C level, "recognizing that this would significantly reduce the risks and impacts of climate change" [1].

According to IPCC (Intergovernmental Panel on Climate Change) 2018 report, to fulfil the 2°C target a reduction of 25% of carbon dioxide emissions with respect to 2010 levels must be obtained by 2030 and the "net zero" by around 2070. For limiting the average temperature increase below 1.5 °C, the reduction should be at least of 45% in 2030, reaching the net zero emissions level in 2050 [2]. Energy-related carbon dioxide emissions are responsible for around two-thirds of global greenhouse gas emissions and in 2017 they grew by 1.4% after three years of flat behavior, reaching a historic peak of 32.5 Gt.

In the same year, the global total primary energy supply was covered by 81% by fossil fuels (oil, coal and natural gas), while the rest includes among others hydro, wind, solar, biofuels, waste and nuclear. Renewables, without considering biofuels, contributed to around 4% [3]. Some changes in the actual global energy system are emerging, in terms of renewable power supply, electrification and energy efficiency measures, but they are not enough. Moreover, in the following years growth in population and GDP will cause an additional stress in the energy sector, increasing the global demand. A deep change of the energy sector is needed and the pathway by which the transformation would be obtained is referred to *energy transition*.

Hydrogen has the potential to play an important role in the future energy transition. It can significantly contribute to tackle several actual energy issues as decarbonization, air pollution and energy security; it can produce a relevant increase in the renewable energy penetration; it has the capability to connect different energy sectors and energy networks improving the flexibility of the energy system. For these reasons, even if relevant barriers and challenges are present, the interest around hydrogen is increasing more and more.

Hydrogen is an energy carrier, as electricity. It means that, differently from the energy sources, it has to be produced, from energy sources (such as natural gas, coal, biomass) or from other energy carriers (as electricity in electrolysers). The analogy with electricity can be continued. As electricity, hydrogen is a clean energy carrier: containing not carbon, from its use only a product of water or steam is generated. Though, it can be associated to a large carbon footprint, depending on the energy source and process employed for its production. As electricity, it is a versatile commodity, which can be used in various applications. However, differently from electricity, it is a chemical species, which can be treated basically as other fuels: it can be transported at long distances, it can be stored, it can be mixed with other chemicals, it can be burnt.

Today, hydrogen is massively produced. Around 120 million tonnes of hydrogen are used every year, almost totally employed as a feedstock in some specific industrial sectors, especially in refining – where it is added to heavy oil for transport fuel production – and in chemical industry – where it is employed to produce ammonia, mainly used as a fertilizer [2]. The use as an energy carrier is up to now negligible. This quantity corresponds to 14.4 exajoules, about 4% of global final energy and non-energy use [2]. The vast majority of the produced hydrogen today comes from fossil fuels, via natural gas steam reforming and coal gasification, and it is responsible for the emission of 830 million tonnes of carbon dioxide per year, equivalent to the ones released by Indonesia and the United Kingdom combined [4].

The energy source from which hydrogen is produced is usually referred to color names: it is 'black hydrogen' if it comes from coal, 'grey hydrogen' from natural gas, 'brown hydrogen' from lignite, 'blue hydrogen' if it is produced from a fossil energy source but in a plant equipped with carbon capture and sequestration (CCS) system, then it is 'green hydrogen' if it is produced via electrolysis from power coming from renewable energy sources. It is clear that in the framework of energy transition, only 'green hydrogen' represents a sustainable approach, while 'blue hydrogen' could be an interesting but challenging bridging solution.

Today, natural gas steam reforming is the less expensive way to produce hydrogen and constitutes its benchmark: depending on the regions, it is around USD 0.9 per kg in the United States, USD 2.2 in Europe and USD 3.2 in Japan [5]. Up to now, converting electricity from the grid to hydrogen via electrolysis costs around three times more than via steam reforming [6]. To reduce it, three main parameters are considered as critical: electrolyser capital investment, cost of the renewable electricity and number of operating hours of electrolyser [2].

Hydrogen and fuel cells technology are directly linked, even if for both different integrations are possible. As electrochemical devices, fuel cells have the possibility to directly convert chemical energy into electrical energy without passing through combustion, thermal cycle and electric motor as in traditional power cycles. Thus, the same reaction is obtained with less entropy generation and with higher efficiency. Fuel cells can be fed with other fuels than hydrogen, such as natural gas and liquid hydrocarbons, thus possibly helping their early adoption [5].

The electricity grid is always characterized by the instantaneously balance between power supply and power demand. The increasing penetration of variable renewable energy sources as solar photovoltaics and wind rises the issue of grid management, since their patterns of power generation cannot be exactly a priori evaluated and they are not necessarily aligned with the patterns of power demand, basically alternating surplus and deficit conditions. In this framework, energy storage technologies represent the key element.

Hydrogen is one of the most promising options for storing energy from renewables. Indeed it can be massively stored in various forms – such as a compressed gas in a pressurized vessel, as a cryogenic liquid, or in a mixture with other species – over days, weeks or even months, as well as theoretically transported at long distances via truck, ship or pipeline, allowing in such a way the shifting both in space and time of power supply and demand. Electrolysers can convert surplus electricity into hydrogen, while fuel cells can cover electricity deficit generating power if fed with hydrogen, and modern electrochemical devices are characterized by a sufficiently fast production ramp up and down to follow the grid requirements. However, electrolysers cannot work only with “otherwise curtailed” electricity because the load factor would be to low and the operative cost of the device would be not competitive. Thus, a tradeoff between using electricity in low-price periods and having an adequate utilization rate is necessary [2].

Renewables power can be stored in hydrogen and converted in different forms. The use of electrolysers and fuel cells expressed above is referred to *power-to-power* and it is subjected to a power loss of around 70% in the overall transformation. But other possibilities are present, too. The produced hydrogen can be injected in gas grid in a mixture with natural gas or it can be treated in a chemical plant and converted to synthetic methane (*power-to-gas*); moreover, hydrogen can be sold as a transport fuel in FCEVs (*power-to-fuel*). Therefore, an energy system in which hydrogen have a central place could in turn drag an even higher share of renewables.

Beyond the grid energy storage, hydrogen could be theoretically used in all the three main energy end uses – transport, building and industry – with the potential to contribute to deeply decarbonize the sectors as well as tackling air pollution, substituting fossil fuels responsible for the release of greenhouse gases and particulates.

Transport sector still much relies on fossil fuels and in particular road transport is responsible for 75% of all transport carbon emissions [5]. Electric vehicles (EVs) market is growing very fast, but they suit especially for passenger cars, urban and short-range applications. Moreover, still issues concerning their low energy density and slow recharging time are present. Hydrogen fuel cell electric vehicles (FCEVs) can represent a parallel solution: they can drive long distances without need of refuel (already more than 500 km), the refueling time is close to the oil-based fuel in the order of 3-5 minutes, the ratio between weight and stored energy is better than batteries [7]. For these reasons, FCEVs by now represents the most promising technology for long distance and heavy-duty transport. Moreover, hydrogen infrastructure can build on existing gasoline pipeline distribution and retail system. In the last years, first mass-produced hydrogen passenger cars have been sold and several examples of bus fleets and trucks can be found. According to [5], achieving a 25% share of FCEVs in road transport by 2050 would contribute up to 10% emissions reduction of the total ones related to transport sector. In aviation, ships and trains too, hydrogen can play an important role in the future.

For concerning buildings, hydrogen can be used in stationary power fuel cell systems. They generate electricity to cover partly or entirely the users’ demands, as well as a by-product of heat which can be used in the absence of a district heating network connection. They represent a high-efficiency cogeneration unit, which constitutes a promising alternative to conventional internal combustion engines. One of the most relevant experience of fuel cell systems is the Japanese *Ene-Farm* program, which was born in 2009 from a consortium of major Japanese energy suppliers and fuel cells manufacturers. Devices are fed with LPG, from which hydrogen is extracted, producing up to 1 kW of power output and the heat necessary to entirely cover the domestic hot water demand. Since it started, around 220 000 units of micro CHP stationary fuel cells have been installed by 2018 and the unit price for PEM devices has been cut to around two-thirds [8], allowing the reduction over time of the incentives guaranteed by the Japanese government. Future goals are to reach 2.5 million units by 2030.

Industrial sector is today called for a significant decarbonization. The change will be complex and slow to obtain, since the processes have taken decades to maximize efficiency and reduce losses. Some industrial sectors are very difficult to be electrified with grid or batteries and hydrogen can potentially be a promising solution in long term, especially in compartments where it is already largely used. Hydrogen could be employed to generate high temperature heat for industrial processes using fuel cells or hydrogen burners; moreover, hydrogen produced via electrolysis could exploit waste heat provided from industrial processes to improve overall efficiency [7].

In the future energy systems, the need of emissions reduction could probably be complemented by the necessity of treatment of the carbon dioxide sequestered by CCS systems. In the framework of circular economy, green hydrogen will be required for converting carbon dioxide in usable chemicals, such as methanol, methane, formic acid or urea [7]. In Iceland, the George Olah Renewable Methanol Plant converts carbon dioxide captured from a geothermal power plant nearby into methanol using hydrogen produced via electrolysis. Started in 2012, it is the first industrial scale production of fuel from carbon dioxide[1] and similar concept plants are planned to be installed also in Sweden and Germany.

Since the wide possibilities potentially provided by the hydrogen, it could occupy a pivotal role in the energy transition by connecting different energy sectors and transmission and distribution networks in a low-carbon energy system [5]. A graphical representation of the present and of the hydrogen-based potential future energy system is given in *Figure1*, taken from [5].

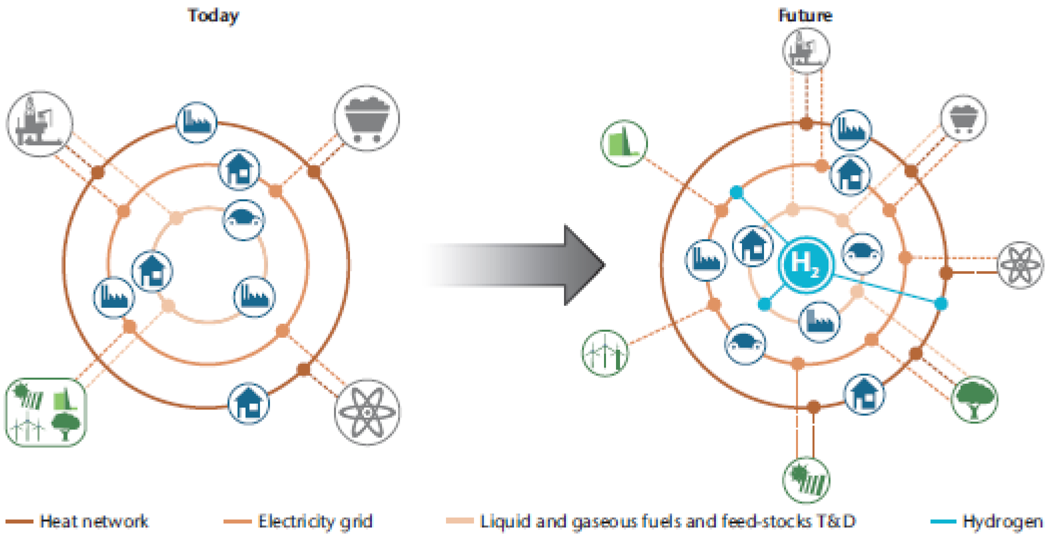

Figure 1 Schematic representation of today and hydrogen-based energy system [5]

---

[1] https://static1.squarespace.com/static/56926c502399a318016c5ed8/t/5daefd1f358b762b8348189d/1571749152527/GO+Plant-+Profile.pdf

The actual energy system is characterized by a large use of fossil fuels for all the end use sectors and by a lack of connections among the different commodity grids and networks of electricity, heat and fuels. Hydrogen could provide the missing linking element among them and at the same time an energy carrier usable for transport, buildings and industry.

Besides its great potential, hydrogen has to face some important obstacles before effectively enter the energy system.

As it has been said, up to now green hydrogen represents a costly commodity with respect to fossil fuel-based alternatives. Costs of fuel cells and electrolysers are high and the technology is still in the early stages of commercialization. Governments can help accelerate the deployment of hydrogen and fuel cells by ensuring research, development and demonstrations (RD&D) funding to make the technology competitive with alternatives [5].

Even if pipelines carrying pure hydrogen are technically feasible and have been operated for years, their extent is limited [2]. The existing broad natural gas infrastructure cannot be used for transporting pure hydrogen, and it could be theoretically possible only with a huge money investment for the conversion of the infrastructure, that is unfeasible. At present, hydrogen can be injected at low shares (around 10-20%) with natural gas in the grid without significant technical challenges, or it can be converted in SNG, which is fully compatible with the existing network, but with high expenditure. In the future, the co-injection of natural gas and hydrogen at higher shares could help both the widespread of hydrogen and the use of natural gas as low-carbon transitional fuel [2]. However, this remains an important challenge.

The major driver of the deployment of green hydrogen as energy carrier is the climate change. Thus, in the absence of binding requirements and restrictions for fossil fuels and carbon emissions, the widespread of hydrogen remains unimaginable. Policy and incentives measures must be created by Governments to support in near-term the energy transition, helping the deployment of clean technologies. Since hydrogen can be generated from sources with very different carbon emissions, standards for measuring lifecycle environmental impacts must be agreed; moreover, regulations have to be updated and geographically homogenized to include hydrogen technologies. The lack of a clear legislation is now a unnecessary barrier for the development of a clean hydrogen industry [2].

A further aspect to be considered is the people acceptance towards hydrogen, recognized to be an extremely flammable gas with potential safety concerns, and the balance between these issues and the promising environmental benefits related to its use.

“Clean hydrogen is enjoying unprecedented political and business momentum, with the number of policies and projects around the world expanding rapidly” [2][4]. Previous waves of interest towards hydrogen has been already experienced in the past and still substantial barriers are present. However, the urgency of climate change mitigation, the high and high penetration of variable renewable energy sources, the reduction of the costs of hydrogen technologies suggest that this time could be different.

2. THEORETICAL ASPECTS OF FUEL CELLS AND ELECTROLYSERS

Fuel cells and electrolysers are electrochemical devices which directly converts chemical energy of a fuel into electricity and vice versa. The conversion is direct in the sense that, differently from classical thermal machines, nor thermal nor mechanical energy take part in the transformation, thus giving less entropy generation and higher efficiency.

The core of the electrochemical cell is constituted by the so-called membrane electrodes assembly (MEA), which consists of three packed layers: two electrodes at the sides and the interposed electrolyte between them. The occurring chemical reaction is constituted by a couple of redox reactions: the oxidation takes place in the anodic electrode, where the electrons are delivered, while the reduction takes place in the cathodic electrode, where electrons are recombined. The electrons are exchanged by the two sides through an external electronic conductor; the produced ions at one electrode, instead, pass through the electrolyte to reach the other electrode. In fuel cells spontaneous reactions are carried on ($\Delta g < 0$) and the moving of the electrons is due to the presence of a voltage gradient between the electrodes, which is created in the charge separation and which guarantees the possibility to obtain power; in electrolysers power is supplied to the device creating the voltage gradient to force the occurring of non-spontaneous chemical reactions ($\Delta g > 0$).

The first demonstration of a fuel cell was realized by Sir William Grove in 1839 using hydrogen as the fuel reacting with oxygen of the air to form water and producing power (the reverse is valid for an electrolyser). This is the simplest overall chemical reaction that can occur in an electrochemical device:

$$H_2 + \frac{1}{2}O_2 \leftrightarrow H_2O$$

In different types of fuel cells, the previous overall reaction is obtained with different configurations. The main difference is in the ion species which is transferred through the electrolyte, which causes the choice of the inlet molecular species to be delivered to the electrodes. In a solid oxide fuel cell, oxygen ions O^{2-} are exchanged; thus, the following semi-reactions occur in the two electrodes:

	Anode	Electrolyte	Cathode
Fuel cell	$H_2 + O^{2-} \rightarrow H_2O + 2e^-$	$\leftarrow O^{2-}$	$\frac{1}{2}O_2 + 2e^- \rightarrow O^{2-}$
Electrolyser	$O^{2-} \rightarrow \frac{1}{2}O_2 + 2e^-$	$\leftarrow O^{2-}$	$H_2O + 2e^- \rightarrow H_2 + O^{2-}$

Table 1 Theoretical aspects: Fuel cells reactions

Since in a reversible cell, i.e. a single device in which both fuel cell mode and electrolyser mode of operation are possible, typically in the same electrode the same chemical species are used, the anode in fuel cell mode is physically the same electrode of the cathode in the electrolyser mode and it is referred as fuel electrode, while the other is referred as oxidant electrode.

2.1 FARADAY'S LAW

The equation which links the electric and the chemical aspects of the phenomenon is the Faraday's law. It states the relation between the electric current I released in a fuel cell (or to be provided to an electrolyser) and the molar flowrate $\dot{n}_i$ of the chemical species to be provided (or produced):

$$\dot{n}_i = \frac{I}{z_i \cdot F} \quad \left[\frac{mol}{s}\right]$$

Where:

z_i represents the charge number of the chemical species i, defined as the number of electrons associated to the electrochemical reaction of one molecule of the species (for hydrogen and water is 2, for oxygen is 4, for methane is 8);

F is the Faraday constant, obtained by the product of the Avogadro's number N_A and the electric charge of the electron q: $F = N_A \cdot q = 6.022\ x\ 10^{23} \cdot 1.602\ x\ 10^{-19} \approx 96485\ [C/mol]$.

2.2 CELL VOLTAGE

2.2.1 OPEN CIRCUIT VOLTAGE

When the external circuit is open, the electrons cannot flow. However, the charge separation in the electrodes occurs anyway: in this case the rates of production and recombination of the reactions are in equilibrium. For this reason, a cell voltage can be measured in this condition, and it is named in various ways: Nernst voltage, reversible voltage, equilibrium voltage or open circuit voltage (OCV).

From an energy point of view and applying the first and second principle of thermodynamics, the available work per unit of mole in a fuel cell (or electrolyser) is equal to the molar Gibbs free energy variation of the reaction, neglecting the sign. Since the available work corresponds to the electrical work, i.e. the product of charge and voltage, the following expressions are obtained for fuel cells:

$$\Delta\bar{g}_{reaction}(T, p_i) = -z_{fuel} \cdot F \cdot OCV \quad \left[\frac{J}{mol}\right]$$

And for electrolysers:

$$\Delta\bar{g}_{reaction}(T, p_i) = +z_{fuel} \cdot F \cdot OCV \quad \left[\frac{J}{mol}\right]$$

Where $\Delta\bar{g}_{reaction}$ is the molar Gibbs free energy change expressed in terms of partial pressure p_i of the species. Evaluating the relation at the reference pressure p_0 and reversing the relation, another expression for the Nernst voltage is obtained for fuel cells:

$$OCV = -\frac{\Delta \bar{g}_{reaction}(T, p_0)}{z_{fuel} \cdot F} + \frac{\bar{R}T}{z_{fuel}F} \cdot \log\left(\frac{\prod_R \left(\frac{p_i}{p_0}\right)^{\nu_R}}{\prod_P \left(\frac{p_i}{p_0}\right)^{\nu_P}}\right) \; [V]$$

And for electrolysers:

$$OCV = \frac{\Delta \bar{g}_{reaction}(T, p_0)}{z_{fuel} \cdot F} - \frac{\bar{R}T}{z_{fuel}F} \cdot \log\left(\frac{\prod_R \left(\frac{p_i}{p_0}\right)^{\nu_R}}{\prod_P \left(\frac{p_i}{p_0}\right)^{\nu_P}}\right) \; [V]$$

Where ν_R and ν_P are the stoichiometric coefficient in the electrochemical reaction for each reactant and each product respectively. Recalling that the Gibbs free energy change of the reaction $\Delta \bar{g}_{reaction}(T, p_0)$ is negative for a fuel cell system and is positive for an electrolyser unit, the Nernst voltage is of course a positive quantity. Other formulations of the Nernst voltage are also considered, evaluating it in terms of activity or concentrations instead of pressure ratio.

The Nernst voltage depends only on the electrochemical reaction and on the temperature and pressure conditions, because, since its formulation is based only on thermodynamics, transport effects or geometry considerations are not present. From the last formulation, some important considerations about pressure can be done, taking into consideration that for concerning fuel cells, higher the Nernst voltage higher the produced power at the same current, while for concerning electrolysers, lower the Nernst voltage lower the power to be provided at the same current:

- for reactants, it is better to send them at high pressure and pure (higher partial pressure);
- for products, it is better to released them at low pressure and dilute (lower partial pressure).

For concerning the temperature, an increase has the consequence of reducing the Nernst voltage.

2.2.2 EFFECTS OF TRANSPORT PROCESSES

When the external circuit is closed and electrons can flow, transport phenomena introduce irreversibility in the process and the measured cell voltage is different from OCV:

$$V_{cell} = OCV \mp \sum \eta_j(i)$$

Where $i \; [A/cm^2]$ is the electric current density, calculated as the ratio between the absolute electric current I and the surface area of the cell S.

Three main phenomena are considered and their modifications of OCV, decreasing it in fuel cell mode and increasing it in electrolyser mode, are named overvoltage $\eta \; [V]$:

- ACTIVATION OVERVOLTAGE

The first overvoltage is related to kinetics in the activation of the electrochemical reactions. The molecular species entering the cell must be ionized and recombined in the active parts of the two electrodes, where the so-called three phase boundary (TPB) is present: it means a zone where a catalyst species is surrounded by three phases – a porous, an electronic and an ionic one – which allow an adequate flow of molecular species, electrons and ions respectively. The Butler-Volmer equation is typically used to describe this overvoltage; one of the possible relations is the following:

$$\eta_{ACT}(i) = \frac{\bar{R} \cdot T}{\beta \cdot n_{RDS} \cdot z_{fuel} \cdot F} \cdot \sinh^{-1}\left(\frac{i}{2 \cdot i_0}\right) \qquad [V]$$

Where $\beta \approx 0.5$ is the so-called symmetry factor, n_{RDS} is the number of charges transferred in the rate determining step of the considered electrochemical reaction, while i_0 $[A/cm^2]$ is the exchange current density, which represents a parameter of quality of the electrode evaluating its capability of transferring charges. The activation overvoltage is relevant at low current, while it has a quite negligible effects at higher values. Since it refers to the single electrode, the activation overvoltage must be considered twice, one for anode and one for cathode.

- OHMIC OVERVOLTAGE

It is related to the resistance to the flow of electrons and ions. The contribution of electrons, that is due to the flow in the external circuit and partly in the electrodes, is in general small and may be neglected, while the very main part is due to ionic contribution, which refers to ion flow in the electrolyte and partly in the electrodes. The Ohm law is applied to account for this term:

$$\eta_{OHM}(i) = R \cdot I = \rho_{el} \cdot \frac{L}{S} \cdot i \cdot S = (\rho_{el} \cdot L) \cdot i = ASR \cdot i \qquad [V]$$

Where ASR $[\Omega \cdot m^2]$ is named area specific resistance and constitutes a main parameter for evaluating the cell performance. This overvoltage introduces a contribution that is almost linear with respect to electric current.

- DIFFUSION OVERVOLTAGE

Diffusion overvoltage does not represent a real physical overvoltage, but it is introduced to account for the mass transport effects, which could be expressed in principle inside the Nernst equation of OCV but in a more complex way. More precisely, at very high current density the cell voltage shows a sudden variation (decrease in fuel cell mode and increase in electrolyser mode), because the provision of molecules is not as fast as the requirements of the catalyst in those conditions. This effect is considered by the diffusion overvoltage by the following relation:

$$\eta_{DIFF}(i) = \left| \frac{\bar{R} \cdot T}{z_{fuel} \cdot F} \cdot \ln\left(1 - \frac{i}{i_L}\right) \right| \qquad [V]$$

Where i_L is the so-called limiting current density, which represents a parameter of quality of the electrode evaluating the capability of diffusing molecular species. As for the activation overvoltage, also the diffusion overvoltage must be considered for both the electrodes.

2.3 THERMAL BALANCE IN THE CELL

From an energy viewpoint, the electrochemical cell exchanges mass flows, power and heat with the environment. For concerning heat, two contributions can be highlighted:

- Reversible heat. It is related to the thermodynamics of the reaction and more precisely to the entropy variation:

  $$\dot{Q}_{rev} = T \cdot \Delta\bar{s} \cdot \dot{n}_{fuel} = T \cdot \Delta\bar{s} \cdot \frac{I}{z_{fuel} \cdot F} \qquad [W]$$

  The sign of the term depends on the entropy variation term, so it is a consequence of the mode of operation: it is positive (exothermic) in fuel cells and it is negative (endothermic) in electrolysers.

- Irreversible heat. It is related to the transport phenomena which cause the overvoltage terms; it is negative, i.e. exothermic, both for fuel cell and electrolyser mode.

  $$\dot{Q}_{irr} = -I \cdot \sum_{j=1}^{3} \eta_j(i) \qquad [W]$$

Therefore, the thermal management of the solid oxide cell system can be very different depending if it operates in fuel cell or in electrolyser mode:

- FUEL CELL mode of operation. Both terms are positive, thus it always works in exothermic conditions and the released heat from the cell is equal to:

  $$\dot{Q}_{cell} = |\dot{Q}_{rev}| + |\dot{Q}_{irr}| = I \cdot \left(-\frac{\Delta\bar{h}}{z_{fuel} \cdot F} + \frac{\Delta\bar{g}}{z_{fuel} \cdot F} + \sum_{j=1}^{3} \eta_j(i) \right)$$
  $$= I \cdot \left(-\frac{\Delta\bar{h}}{z_{fuel} \cdot F} - V_{cell} \right) \qquad [W]$$

- ELECTOLYSER mode of operation. The two terms have opposite sign; thus, the cell may work both in endothermic or exothermic conditions and the exchanged heat is:

  $$\dot{Q}_{cell} = \dot{Q}_{rev} - |\dot{Q}_{irr}| = I \cdot \left(\frac{\Delta\bar{h}}{z_{fuel} \cdot F} - \frac{\Delta\bar{g}}{z_{fuel} \cdot F} - \sum_{j=1}^{3} \eta_j(i) \right)$$
  $$= I \cdot \left(\frac{\Delta\bar{h}}{z_{fuel} \cdot F} - V_{cell} \right) \qquad [W]$$

Three situations can occur in electrolyser mode:

1. $\frac{\Delta\bar{h}}{z_{fuel} \cdot F} < V_{cell}$: endothermic condition (heat must be provided to the cell), at low current densities;
2. $\frac{\Delta\bar{h}}{z_{fuel} \cdot F} > V_{cell}$: exothermic condition (as for fuel cells, heat must be taken off the cell), at high current densities;

3. $\frac{\Delta\bar{h}}{z_{fuel} \cdot F} = V_{cell}$: thermoneutral condition, which occurs when the heat released by the irreversibilities is balanced by the heat required for the reaction; it means that no thermal management is needed at this condition and the thermal balance is already satisfied. The potential at which this situation occurs is named thermoneutral point:

$$TNV = \frac{\Delta\bar{h}}{z_{fuel} \cdot F} \qquad [V]$$

2.4 FROM THE CELL TO THE STACK

The voltage of a single cell is quite small, typically less than 1 V. Therefore, in order to produce a useful voltage, many cells must be connected in series, forming the so-called “stack”. The series connection is obtained by connecting the fuel electrode of a cell to the oxidant electrode of the next inserting another layer, named interconnector, between them. In planar configuration this structure is referred as “bipolar plate”. The interconnector material allows the passage of electrons between the electrodes of neighboring cells inside the stack. At the same time, in the interconnector ducts for feeding the electrodes with molecular species are placed. A graphical representation of the structure is given in *Figure2* [9].

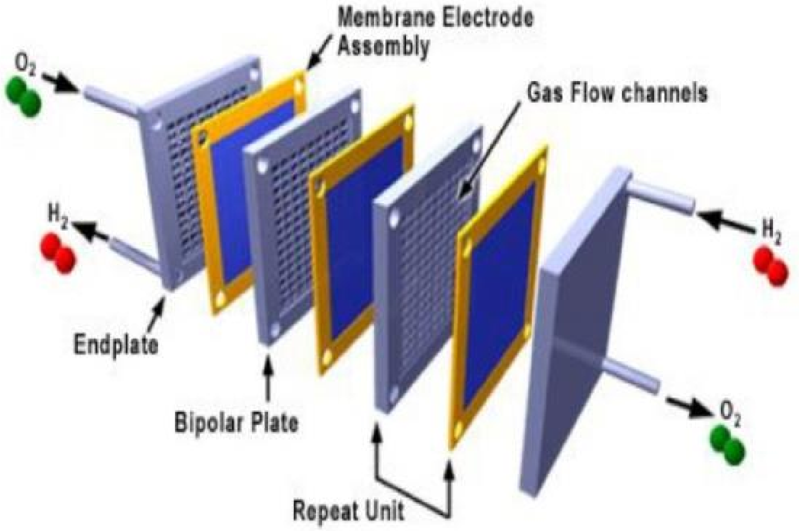

Figure 2 Theoretical Aspects: Graphical representation of the bipolar plate

Several bipolar plates constitute the stack and guarantee an adequate value of voltage and power. The approximated stack voltage may be simply calculated as the product of the single cell voltage and the number of cells in series:

$$V_{stack} = n_{cell} \cdot V_{cell} \qquad [V]$$

Thus, the produced DC power in a fuel cell (or provided in an electrolyser) is:

$$W_{stack} = V_{stack} \cdot I = n_{cell} \cdot V_{cell} \cdot i \cdot S \qquad [W]$$

3. SYSTEM DEFINITION

In the present chapter, the general description of the concerned plant system is provided. In the first part, the concept of reversible solid oxide cell is given, with particular reference to the stack module, referring to most used materials and shapes. In the second part, a general overview of the entire system configuration is provided, with the explanation of the main functions and design parameters of the balance of plant components. Then, the representation of the plant concerned in this work is given.

3.1 REVERSIBLE SOLID OXIDE CELLS (rSOC)

Electrochemical devices can play a key role in the framework of the energy storage. The main idea is combining a fuel cell and an electrolyser in the same system, in order to store electricity surplus in chemicals using the latter device and to restitute electricity from the stored chemicals through the chemical reactions occurring in the fuel cell (Power-to-Power paradigm). However, a more interesting and challenging option is to couple the two devices in the same unit, which can operate reversibly. It basically consists in a redox battery, whose capacity is determined by the size of the fuel gas (and in some cases also in the oxidant gas) reservoirs. These single-unit devices are generally referred as Unitized Regenerative Fuel Cells (URFC) [10].

URFC can operate at different temperature conditions, as for the fuel cells and electrolysers; at high or intermediate-high temperatures (650-900 °C), the solid oxide technology is mainly adopted and the regenerative electrochemical system is typically named reversible solid oxide cell, which is abbreviated as rSOC or ReSOC. The rSOC technology theoretically shows significant advantages with respect to the low-temperature one. Due to higher temperature levels, the transport processes are enhanced so giving higher efficiencies both in fuel cell and electrolyser modes of operation. Moreover, typically lower quality catalysts are required (such as Nickel with respect to Platinum) and several chemical species may be used. On the other hand, the higher temperatures cause higher degradation and thermal stresses, with more stringent requests for the materials. Moreover, the high temperature electrolysis technology is up-to-now less mature than the low-temperature one. However, the high kinetic performances due to high temperature make possible the construction of SOEC as SOFC, only with the reverse reactions. For this reason, the considered configuration for r-SOC are basically the one of the more popular SOFC.

Several geometric cell configurations are present in the high-temperature solid oxide technology. The earlier developments were using tubular shape, which can simplify issues concerned with sealing; however, in the last decades mainly the planar configuration have been developed, which benefit from improved power density [10][11]. A general description of the planar cell configuration is given in the present chapter.

The membrane electrode assembly (MEA) is a laminated ceramic and metal structure composed by three main layers: two porous electrodes separated by a dense electrolyte. Other important elements of the structure are the interconnects and the sealing.

- ELECTROLYTE

Currently, the most used material for the electrolyte of a solid oxide cell is zirconia (zirconium oxide, ZrO_2) stabilized by a small amount of yttria (yttrium oxide, Y_2O_3), typically between 3 and 10% [12]. It is named Yttria-Stabilized-Zirconia (YSZ) and is a solid, dense and ceramic material. The addition of some Y^{3+} ions in the fluorite crystal structure of zirconia instead of some Zr^{4+} ions causes the presence of a number of vacancies in the oxide-ions O^{2-} sites which are responsible for the excellent ability to conduct oxide-ions. The ionic conductivity of YSZ is $0.02\ S \cdot cm^{-1}$ at 800 °C and very thin layers of about 25-50 µm can be made, ensuring that the ohmic losses are comparable with other cell types [13].

Most recently, other materials have been produced with high oxide-ion conductivity at lower temperatures with respect to the required ones by zirconia-based electrolytes. The most interesting one is Lanthanum Strontium Gallium Manganite (LSGM).

- FUEL ELECTRODE

The state-of-the-art material used for the fuel electrode (anode in SOFC and cathode in SOEC mode of operation) is a composite ceramic and metallic (cermet) made of metallic nickel (Ni) dispersed in the ceramic YSZ matrix. The ceramic material is responsible for the high ionic conductivity, while nickel both behaves as the electrocatalyst and provides high electronic conductivity. Moreover, the high porosity in the structure allows mass transport of reactant and product gases. Zirconia is adopted both to inhibit the sintering of the metal particles and to provide a thermal expansion ratio close to that of the electrolyte [12].

Most recently, the attention has been directed to completely ceramic fuel electrodes. In this way, problems such as carbon deposition due to nickel catalyst can be reduced. The most relevant examples of these materials are Gadolinia-Doped-Ceria (GDP) mixed with Zr and Y, and various TiO_2-based systems [13].

- OXYGEN ELECTRODE

The same requirements are for the oxygen electrode. The porous layer is in general constituted by the ceramic YSZ – which ensure enough ionic conductivity – and a material belonging to the perovskite family, such as Strontium-doped Lanthanum Manganite (LSM, $La_{1-x}Sr_xMnO_{3-\delta}$) – which is a very good electronic conductor. This material is particularly suitable to operations above 800 °C [10]. For cells operating at lower temperatures, mixed ionic and electronic conductors are typically preferred as oxygen electrode materials and another perovskite material is used, such as lanthanum strontium cobalt ferrite (LSCF, $La_{1-x}Sr_xCo_{1-y}Fe_yO_{3-\delta}$).

- INTERCONNECT

The interconnect material serves to create the connection among the cells to increase the voltage level associated to the stack unit. In that component, the electric current is carried along by transferring the electrons from the adjacent electrodes: for this reason, the interconnect material must have very good electrical conductivity. Especially for high temperature electrochemical devices, it must show a similar expansion coefficient with the electrodes to reduce the mechanical stresses, and it must avoid the possibility of poisoning the oxidant electrode with chromium evaporation and successive deposition, which can cause a rapid deactivation of the electrode. Moreover, in the interconnects the fuel and oxidant channels for feeding the cells take place.

Various materials have been employed for the interconnect. Metallic interconnects, as ferritic stainless steels, are used for their low cost, suitability for shaping and welding, adequate expansion behavior and resistance to high temperature. The composition of the alloys is studied for reducing also the risk of chromium emission and the *Crofer 22* (an iron-chromium alloy containing 22% chromium in weight) has been typically employed. An alternative, which is favoured especially for the tubular configuration, is the use of a ceramic material, such as lanthanum chromite.

- SEALING

One of the main issues related to solid oxide cells, especially for planar configuration, is the possibility of leakages among the different layers, due to the very high temperatures that are reached. For this reason, the choice of the sealing material has an important role to guarantee an adequate gas tightness. Moreover, it must show good adhesion from one side to ceramic and from the other side to metallic materials, it must be able to sustain thermal cycles and it should not be conductive for electrons.

The most used materials are glasses with transition temperature close to the operating temperature of the cells. Thus, they soften as the cells are heated up forming a seal all around the cell [13]. Glass-ceramics are used too, for which a better control of their crystallization can be done [10]. A possible issue is the migration of silica from the glasses to the electrodes, causing degradation of the performances.

3.2 SYSTEM CONFIGURATION AND BALANCE OF PLANT

Medium- and high-temperature fuel cells systems “can never be considered simply as fuel cells, but they must always be thought of as an integral part of a complete fuel processing and heat generating system” [13]. In fact, several balance of plant components are necessary for driving these plants and many different system configurations are possible [11].

- FUEL PROCESSING

In fuel cell mode of operation, the used fuel is usually constituted by a mixture of hydrogen, carbon oxides, hydrocarbons and other gases for which a pre-treatment before entering the stack can be necessary for kinetic reasons and durability issues. Two main aspects can constitute a problem for the stack: degradation by contaminants and carbon deposition.

The risk of degradation of the cell performance is a specific problem of electrochemical devices with respect to conventional thermal machines, that is due to the presence of catalyst, which may be dramatically degraded if it interacts with some contaminants. The most dangerous poisons are probably siloxanes and sulphur compounds and a maximum value of respectively 30 and 100 ppb are typically considered in the fuel inlet mixture. For concerning natural gas, only the sulphur compounds added as odorants by the utility company for safety reasons are present and a clean-up section is needed. To this end, different desulphurization systems are considered in the practice, such as hydrodesulphurization reactors or, especially for solid oxide cells, activated carbon absorbent system [13].

The second issue is the risk of carbon formation in different areas of the system if a fuel containing carbon is used. At temperature above 650 °C, methane may decompose with the following pyrolysis reaction: $CH_4 \rightarrow C + 2\ H_2$. Another source of carbon formation is the carbon monoxide produced in the electrochemical reactions, via the so-called Boudouard reaction, $2\ CO \rightarrow C + CO_2$, which is catalyzed by the nickel catalyst present in the anode of the solid oxide cells. If the carbon deposition phenomenon occurs, the pores of the cell may be blocked by the carbon and no fuel stream is fed to the stack, with the consequence of the deactivation of the catalyst. The risk of carbon deposition is prevented by adding an oxygen carrier into the fuel mixture, in order to shift the equilibrium of the reactions towards a desired one. The oxygen carrier is in general water (steam reforming), but also oxygen (partial oxidation) or both (autothermal oxidation).

In order to have higher overall efficiency, a precise choice in the thermal integration between the stack and the fuel reforming section is needed. Different implementations have been considered and the main three are:

- **External reforming**. The reformer unit and the stack unit are physically separated and between them heat transfer occurs. An external pre-reforming section is generally used also for internal reforming configurations, in order to avoid overcooling [14].
- **Indirect internal reforming**. The reformer section is placed in close thermal contact with the stack: reforming plates may be coupled with small cell packages and the reformate exiting the plates is fed to the adjacent cells [13].
- **Direct internal reforming**. The fuel conversion directly occurs within the anode compartment of the fuel cell stack, taking advantage of its catalytic properties in the solid oxide configuration. This implementation allows good heat transfer and chemical integration [13].

➢ FUEL UTILIZATION AND RECIRCULATION

When hydrogen is supplied to a fuel cell as part of a mixture with other species, its concentration decreases along the length of the stack due to the electrochemical reaction which utilizes it, while the quantity of other species, as carbon dioxide, remains constant. Therefore, the stack voltage shows a relevant decrease due to the dropping down of the Nernst potential. Consequently, in the case of a reformed fuel containing carbon dioxide or when internal reforming is present, hydrogen cannot be entirely used in the fuel cell and a redundant flowrate must be provided, so that a part of it passes unreacted through the stack. The fuel utilization factor FU is defined as the ratio between the consumed hydrogen in the stack and the inlet hydrogen in it:

$$FU = \frac{moles\ H_2^{react}}{moles\ H_2^{inlet}}$$

The unreacted hydrogen is then anyway used when a recirculation loop is present. Thus, the fuel electrode outlet stream is partly recirculated back mixing with a fresh fuel flowrate passing again through the stack. Consequently, two values of fuel utilization factor are present: one for the single loop ("per pass" fuel utilization [11]) and one comprising the recirculated flowrate (system fuel utilization).

Recirculation has several effects. As it has been seen, it can raise system efficiency by converting a higher quantity of hydrogen (SOFC mode) and steam (SOEC). Moreover, for internal reforming devices, it is usually needed for providing the steam content required for methane and carbon monoxide conversion into hydrogen, thus reducing the risk of carbon deposition. For SOEC mode of operation, the recirculation line provides a small amount of hydrogen to the stack inlet in order to create a reducing atmosphere fostering a longer lifetime.

Recirculation is typically achieved by splitting the outlet stream from the stack and using a high temperature ejector or a mechanical pump to mix the recycled stream to the fresh fuel stream. Mechanical pumps consume electrical energy and can be subjected to corrosion and degradation but allow more flexible operation and are in general less expensive [15].

- AIR UTILIZATION AND THERMAL MANAGEMENT

As for the anode side, also in the cathode line of a fuel cell air is provided in excess with respect to the strictly required for chemical reasons. Thus, an air utilization factor is defined as:

$$AU = \frac{moles\ stoichiometric\ air}{moles\ inlet\ air}$$

Moreover, air flowrate can also be used as thermal control medium of the stack. In this case, the air utilization factor decreases more. In natural gas fed fuel cell systems with internal reforming, the amount of air necessary for thermal management is less than in hydrogen fed ones, due to the highly endothermic reaction of steam reforming.

Other possibilities for thermal management of the fuel cell stack are systems with a cooling fluid passing through the stack [16] as for low-temperature devices or by heat pipes located in the interconnector [17]. However, for simplicity reasons, the widely used system is by air excess.

In electrolysers, oxygen is not required as a reactant, but it is created in the cell as a product. As it has been seen (2.3) thermal management in SOEC is more complex, because depending on the operating voltage the electrochemical reaction can be endo- or exothermic; thus, both conditions where heat must be provided and conditions where heat must be removed are present. In exothermic conditions the general approach is to cool down the stack as in fuel cells, by injecting a quantity of air, while in endothermic conditions various configurations are possible, but typically the circulation of a hot fluid in the stack is performed. Heat pipes with a heat transfer fluids or additional channels created in the stack where the inlet gases are injected are examples of proposed solutions; a simpler possibility is to send air at high temperature to heat up the stack [18]. Moreover, the sweep air flowrate has the positive effect of reducing the oxygen concentration in the oxidant electrode side, so reducing the operating voltage due to Nernst equation and to avoid possible delamination at the interface between oxidant electrode and electrolyte caused by oxygen anions movement [16].

- DOWNSTREAM OF THE STACK

One of the advantages of high temperature electrochemical devices is the presence of hot gases downstream of the stack, whose chemical and thermal content may be exploited for increasing the overall efficiency of the system. Various configurations for this purpose are possible.

Hot streams exiting the stack are typically used for preheating the inlet streams in fuel and oxidant lines by using recuperators. This aspect is referred as "process integration" and it is necessary for increasing electrical and thermal system efficiencies [13]. Thus, procedures as minimization of exergy losses and pinch analysis are carried out at design stage.

Moreover, in the exhaust gas stream exiting the stack a quantity of unreacted fuel is present, as expressed by the fuel utilization factor. A part of that is recirculated to be then converted into electrical energy into the device, but the remaining part downstream the splitter can be exploited in other ways. An interesting possibility is to create a bottoming cycle with the use of a gas turbine with an additional generation of electrical energy to increase the overall efficiency. Another possibility is to simply burn the remaining fuel species in an afterburner with an additional increase in hot gas temperature, that can be exploited in other parts of the system or to provide heat to users.

3.3 CONCERNED PLANT

The rSOC system that has been studied in this work relies on an existing research project. The available data have been integrated with other values obtained from similar concept real plants. The concerned system can operate in three modes of operation. In fuel cell conditions, hydrogen or natural gas can be supplied to the stack, while in electrolyser mode only steam is supplied and hydrogen is generated. The plant will be installed in 2020 in Environment Park (EnviPark), a technological park located in Turin, Italy. EnviPark is seat of offices and laboratories and of a small photovoltaic plant (16.3 kW_p) and a hydro power plant (380 kWe). The concerned r-SOC plant aims to demonstrate the storage of local renewable energy sources (RES) and its auto consumption for the delivery of electricity and heat to commercial buildings. The storage means is hydrogen, which is produced in SOEC mode in periods when surplus of electrical energy is present and then compressed towards a pressurized vessel when it is stored. On the other hand, when a need of power to the users is present, electricity can be provided by the SOFC through the conversion of the stored hydrogen. Another possibility is to generate power feeding the fuel cell system with natural gas coming from the gas grid. The system is then completed by a set of battery of 50 kWh.

The three r-SOC modes of operation have been tagged as NG-SOFC, H2-SOFC and SOEC in the following part. The base system configurations that have been studied in the following part are represented and briefly described for their three modes of operation. Then, after the modelling part (5), some changes in the configurations will have been performed for low-load conditions and will have discussed later.

3.3.1 NG-SOFC

In this configuration the rSOC devices works as fuel cell fed by a natural gas stream coming from the gas grid. As expressed previously, before entering the reforming catalysts natural gas must be cleaned up from the sulphur added for safety reason in the grid. Thus, a desulphurization section is needed. The fresh natural gas stream is mixed with recycled fuel coming from the recirculation loop and the mixture passes through the fuel line. The temperature of the stream is increased by a recovery heat exchanger and by an electric pre-heater before entering the pre-reformer unit, where the conversion of methane into hydrogen partly occurs. Then, the fuel is heated up by an electric heater to reach at least 890 K for avoiding thermal stresses in the stack module.

The required oxidant for the electrochemical reaction is constituted by the oxygen contained into outer air. Air stream pressure is compressed in a blower and passes through the oxidant line where only a temperature rising occurs, thanks to a recovery heat exchanger and an electric heater. At the stack inlet section, a minimum temperature of 830 K is set.

In the anode side of the stack unit an internal reforming section is present where the remaining methane and carbon monoxide are converted into hydrogen, which reacts with oxygen of the cathode side to form water and generating electrical energy, which is delivered to the users. The stack operating temperature is 1003 K (730 °C).

At the anode outlet section, a stream rich in water and carbon dioxide and with unreacted fuel species is recirculated back to preheat the fuel line and then is split into two streams: 65% of the flowrate is mixed with the fresh fuel by using an ejector, while the remaining 35% is delivered to the combustion chamber of an afterburner, where oxygen and nitrogen coming from cathode exit section are also provided. There the fuel is burnt, and the hot exhaust gases are used for preheating the oxidant line and the residual heat is recovered by a water stream to be delivered to the users for heating demand. Then, the exhaust gases are released into atmosphere.

In *Figure3* the schematic representation of NG-SOFC mode of operation is given.

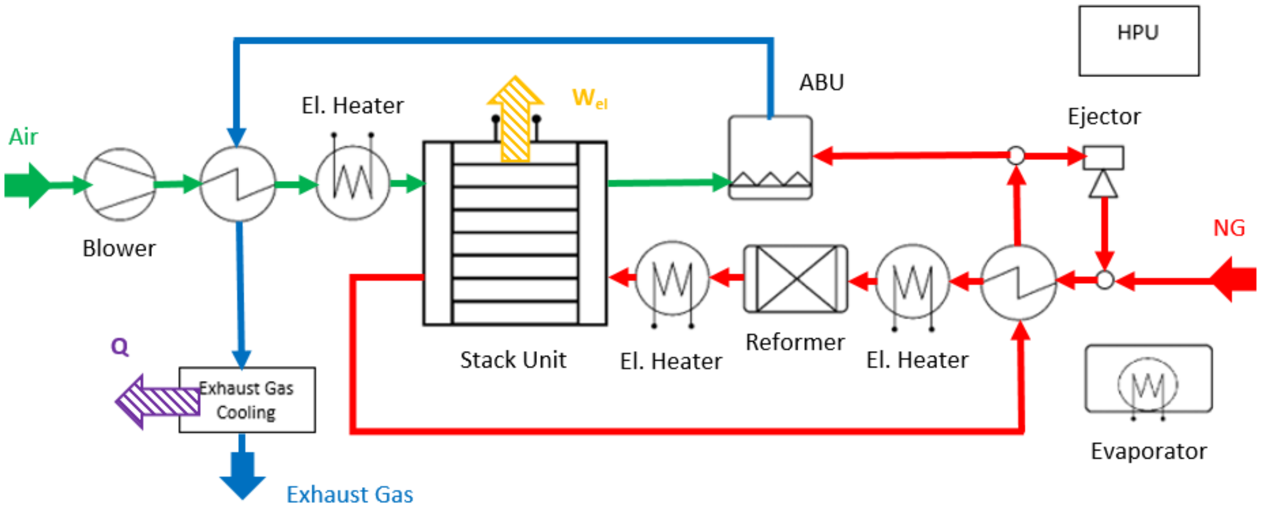

Figure 3 NG-SOFC configuration

3.3.2 H2-SOFC

In this mode of operation, hydrogen replaces natural gas as the fuel. Hydrogen comes from the hydrogen processing unit (HPU), where it is expanded from the high pressure of the storage vessel to the operating pressure of the system and it is delivered to the mixer component, where it is mixed with the recycled stream from the anode of the stack and the resulting stream is constituted by a mixture of steam and hydrogen. That mixture passes through the fuel line as in NG-SOFC, with the difference that no reforming reactions occur and in the pre-reformer the composition and the temperature of the stream remain unchanged. In this case too, the minimum inlet anode temperature is set to 890 K.

For the cathode side, the situation is identical to the previous case. In the stack unit only the exothermic electrochemical reaction of formation of water from hydrogen and oxygen occurs, which provides electrical power. As in NG-SOFC, the produced electrical power in the stack is partly used for the auxiliaries, i.e. blower and electric heater, which needs power to work. The net power is then the effective power delivered to the users.

The rest of the system performs the same functions as in NG-SOFC, as it can be seen from *Figure4*, where this configuration is represented.

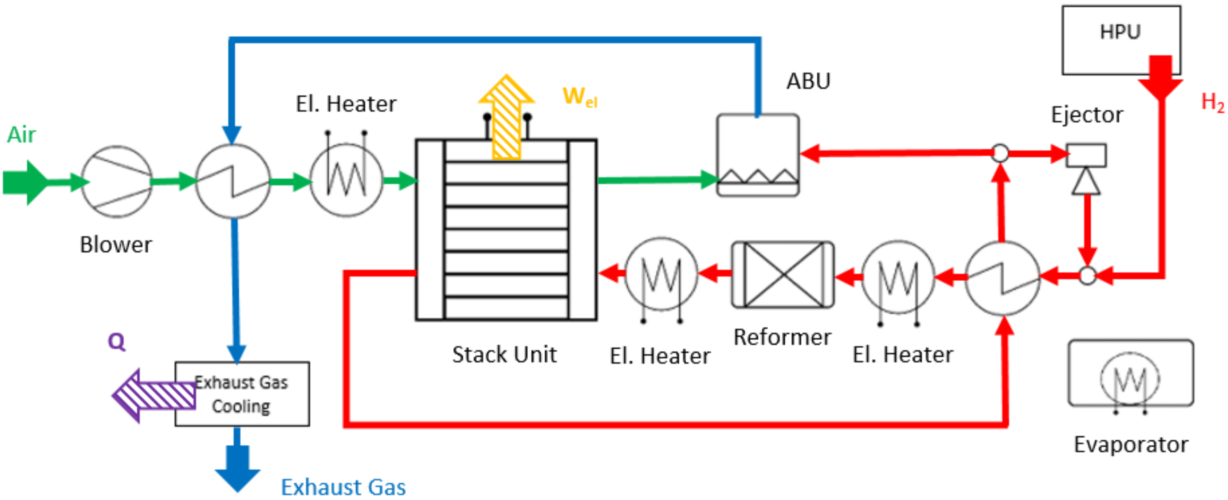

Figure 4 H2-SOFC configuration

3.3.3 SOEC

In this configuration (*Figure5*), power is provided to stack to perform electrolysis of water. Water is supplied at ambient temperature and is then converted into steam in the evaporator, where heat is provided by an electric heater. Fresh steam is mixed with a recycled stream constituted by unreacted steam and produced hydrogen. The mixture passes through the fuel line increasing its temperature before entering the stack module. In this configuration too, the stream passes through pre-reformer without reacting. Temperature in the inlet stream can have very different values, depending on the exo- or endothermic conditions inside the stack. In exothermic conditions the stream must be supplied at lower temperature, while in endothermic conditions it must be at higher temperature to sustain the reactions.

In the oxidant line, air is provided for thermal management of the stack and its stack inlet temperature depends at the same way on voltage values of the stack.

In the stack unit the steam electrolysis occurs, forming oxygen in the anode and hydrogen in the cathode. The produced oxygen mixes with inlet air and it is not recovered; the stream is exploited for its high temperature to preheat the oxidant line and, if possible, for heating demand of the users. The fuel electrode outlet stream is constituted by produced hydrogen and unreacted steam and it is recirculated back to heat up the fuel line. In the splitter the stream is divided: a part is recycled, while the other is delivered to HPU. In HPU hydrogen is pressurized to 200 bar by a set of compressors and it is stored as compressed gas into a vessel.

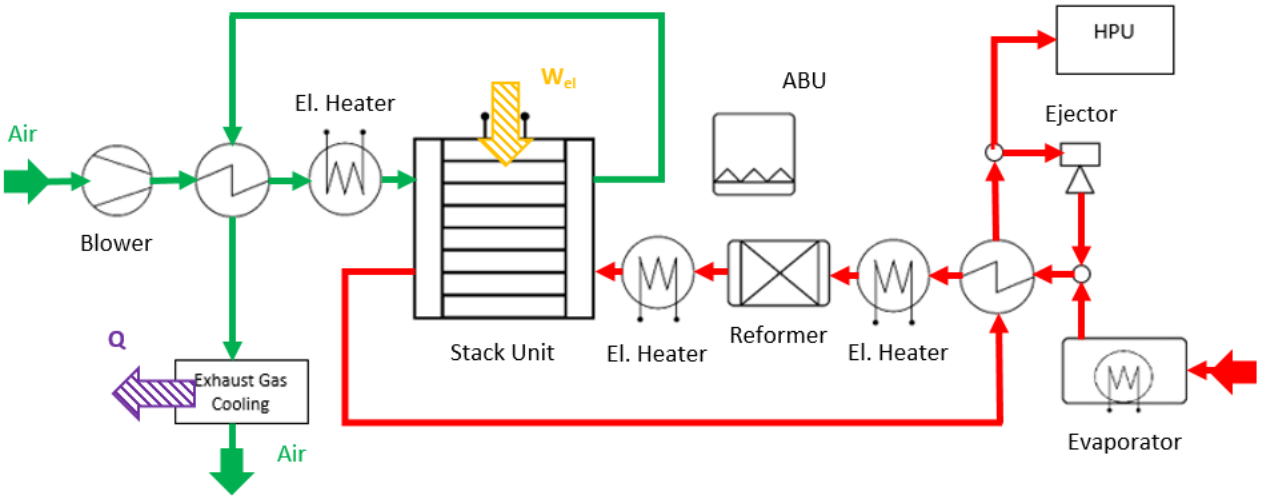

Figure 5 SOEC configuration

The main quantities and parameters characterizing the concerned system or assumed for the modelling have been resumed in *Table2*.

Maximum Produced Power in NG-SOFC mode	P_{NG}^{MAX}	13.5 kW
Maximum Produced Power in H2-SOFC mode	$P_{H_2}^{MAX}$	11.5 kW
Maximum Consumed Power in SOEC mode	P_{SOEC}^{MAX}	75 kW
Inverter Efficiency	η_{INV}	0.9
Blower and H2-compressor isentropic efficiency	η_c	0.8
Air Recovery Heat Exchanger Effectiveness	ϵ_{ARHX}	0.65
Air Electric Heater Rated Power	W_{AEHX}^{NOM}	5.5 kW
Evaporator Electric Heater Rated Power	W_{EVA}^{NOM}	3 kW
Fuel Recovery Heat Exchanger Effectiveness	ϵ_{FRHX}	0.8
Reformer Electric Heater Rated Power	W_{REHX}^{NOM}	3 kW
Fuel Electric Heater Rated Power	W_{FEHX}^{NOM}	1.5 kW
“Per Pass” Fuel Utilization in SOFC modes	FU	0.665
“Per Pass” Steam Conversion in SOEC	SC	0.7
Recirculation Ratio (Ejector)	RR	0.65
Surface area of cells in the stack	A_{cell}	200 cm^2
Number of cells in the stack	n_{cell}	300
Hydrogen Storage Maximum Pressure	$p_{storage}$	200 bar

Table 2 System definition: Main parameters of the rSOC system

4. SYSTEM INTEGRATION

The concerned r-SOC system will be installed as a pilot plant in a real environment in order to validate the technology. The chosen site is Environment Park, located in Turin, Italy.

Environment Park (EnviPark) is a Technology Park created in 1996 and extending over around 30 000 m^2. It is constituted by a set of 10 building units surrounded by greenery, which hosts offices and laboratories which are operated by the various companies located in the Park. More than 500 people daily work in the overall site, and besides offices and laboratories a restaurant and cafeteria area and a directional building with a conference centre are present.

The Park management company (Environment Park S.p.A.) manages the site and provides the tenants with several services, including energy both in terms of heat and electricity. It operates as an innovation agency with great attention on clean technologies, following the mission of the Park. The energy demand of the Park is covered for around 65% by renewable energies generated on its site, and more precisely by:

- A district and cooling network fed by two biomass boilers (1.8 MW power);
- A mini hydroelectric power plant installed inside the park (Kaplan 380 kW$_e$ power, 1300 MWh per year);
- A photovoltaic (PV) plant of 16.3 kW of peak power (15 MWh per year), integrated into the energy grid of the park;
- Solar thermal energy solutions integrated into heating and Domestic Hot Water systems.

The r-SOC system interacts with the electrical renewable energy sources, i.e. the PV and hydro power plant. In *Figure6*, a schematic representation of EnviPark is provided, in which the location of the renewables has been highlighted. The r-SOC system will be installed in a dedicated enclosure located underground, next to a parking area, beneath the so-called building C, which is marked in a similar way in the figure. The hydrogen processing unit, instead, will be installed outside, in an open area located in front of building C.

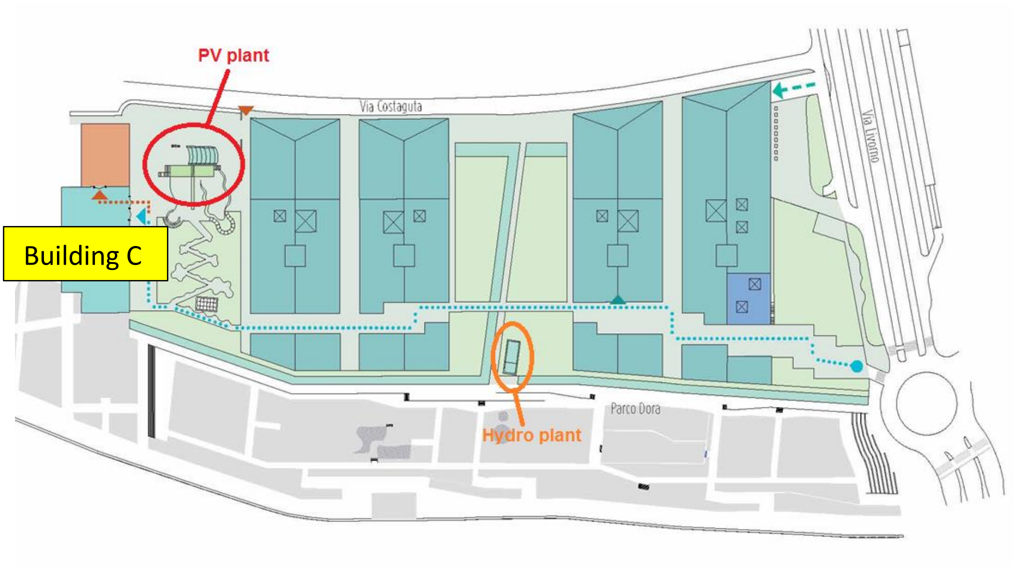

Figure 6 Schematic view of EnviPark

The r-SOC system will interface with the Renewable Energy Sources power generation and the Park energy requests. In SOFC mode of operation, the system will produce power and heat that will be delivered to the commercial buildings of the Park by using hydrogen stored in the tank (H2-SOFC) or natural gas caught directly from the grid (NG-SOFC). In electrolyser mode of operation (SOEC), the electricity provided from PV and Hydro will be used to produce hydrogen that will be stored in the tank. A battery unit of 50 kWh provides short term electrical storage and the electricity grid connection to deliver surplus power and require deficit power completes the overall system. An extensive testing period on-site is planned, with 8000 hours of test and more than 200 full cycles between SOFC and SOEC and back.

For studying the r-SOC system behaviour, an evaluation of the energy profiles for renewables at supply side and for users at demand side to which it interacts is necessary. For this reason, in the following part the methods whereby they have been obtained and the main assumptions that have been used are presented. An hourly-resolution annual energy profile has been obtained for each system.

4.1 SUPPLY SIDE

4.1.1 PHOTOVOLTAIC PLANT

Totem Fotovoltaico (*Figure7*) is the PV plant installed in Environment Park. It consists of 8 rows of PV polycrystalline silicon panels with different slope, arranged in a support frame constituted by six big arches made of treated larch wood and six columns and six hinges. On top of the frame, a superstructure formed by uprights and traverses in extruded aluminum ensures the stand for the PV panels. Each row is made by 20 panels, so giving a total number of PV modules equal to 160 and the total intercepting surface of the plant is about 200 m^2. The peak power is 16.32 kW_p [19]. The PV plant was constructed in 2002 and its architecture was designed as a light sail and permeable to light, which provides a shaded area and at the same time represents a peculiar attraction of EnviPark[1].

Monthly-resolution power production data for four past years (2010-2014) are the only available data for the plant, since no specific research studies were recently made on it. Thus, in order to create an hourly-resolution profile of power production of a typical year, the software PVGIS [20] is used. PVGIS stands for PhotoVoltaic Geographical Information System and is an online free solar photovoltaic energy calculator for stand-alone or connected to the grid PV systems located in Europe, Africa, America and Asia which provides results on solar radiation and annual output power of the PV panels, with defined modules tilt, orientation and main features [21]. From the software results, values of yearly energy production and in-plane irradiation are obtained, as well as a .csv file with hourly values of energy production, in-plane irradiation, sun elevation, ambient temperature and wind speed along the year. In the following part the description of the procedure adopted with the software is described.

[1] http://www.comune.torino.it/comitatoparcodora/servizi/attivita/visiteguidate/envipark.pdf

Figure 7 Supply side: View of PV power plant located in EnviPark

For calculating the desired results, some input data are needed by the PVGIS software. They are summed up in *Table3* and for some of them an explanatory description is provided, based on the PVGIS user manual [22] and on the specific documentation of the plant at the time of installation.

Latitude [°]	45.087
Longitude [°]	7.674
Solar radiation database	PVGIS-COSMO
PV technology	Crystalline silicon
Installed peak PV power [kWp]	16.3
System loss [%]	25
Mounting position	Free-standing
Slope [°]	30
Azimuth [°]	20

Table 3 Supply side: PVGIS simulation input data

Four solar radiation databases are available for choice. Two of them, PVGIS-CMSAF and PVGIS-SARAH are calculated from satellite data using methods developed by the CM SAF consortium; the others are based on Climate Reanalysis data sets and they are PVGIS-ERA5 – which uses data provided from the European Centre for Medium-Range Weather Forecast (ECMWF) – and PVGIS-COSMO – which covers the European region. The latter one is chosen because the provided results are closer to the empirical measurements.

The system loss parameter represents all the losses in the system which decrease the power actually delivered to the electricity grid with respect to the produced power by the PV panels. They include, among others, losses in cables, power inverters, dirt and snow on the modules and degradation in time. A default value of 14% for standard systems is recommended by the software; however, in the plant documentation the considered ratio between the power provided downstream the inverter and the produced power is around 20% and it includes average losses due to temperature, mismatch and ohmic effects and the conversion efficiency in the inverter. Considering also the old age of the concerned plant, a value of 25% has been chosen.

For concerning the slope, the eight rows of panels are mounted in the arch support frame and are characterized by very different slopes. An average value of 30 degrees has been considered, following the plant documentation.

Azimuth of the PV system has been calculated using the software *Google Earth*: the plant is oriented towards South-West with an angle of around 20 degrees from the South.

The calculation of solar radiation and PV performance requires information about the local horizon to estimate the effects of the presence of local hills, mountains, trees or buildings that block the light of the sun during some periods of the day. The software provides a calculated horizon for the specific location of the plant, which uses data about ground elevation with a resolution of around 90 meters; however, this is not enough to evaluate the shadows created by the very nearby things such as houses and trees. Since the plant is located at around 3 meters above the ground and is inserted in an urban environment, with particularly tall and near buildings in the south-west direction, a more precise calculation on the horizon height has been carried out. It is possible to upload in the software a simple text file, with one number per line and each number representing the horizon height expressed in degrees in a certain direction. The values account for equal angular distances around the horizon, given in a clockwise direction starting from the North (i.e. North – East – South – West): in the present work an angular distribution of 5 degrees has been considered, so with a total number of 72 values.

In *Figure8* the satellite view of the site from *Google Earth* is given. The PV plant is marked with a big filled red circle and the most view-impacting buildings for the system are identified with letters from A to G (the building F is a group of three skyscrapers outside the map); moreover, north of the plant, some trees are present. In *Figure9* the schematic approximated map that has been used for the shadow calculation is provided, where only the relevant buildings and trees are represented. The buildings have been considered as oriented with the azimuth-direction of the PV system for the sake of simplicity, since the actual orientation is not far from that. To compute angles and distances, a Cartesian coordinate system x-y-z is considered: the x-axis follows the azimuth-direction of the plant (i.e. creating an angle of 20 degrees with the South direction), the y-axis is orthogonal to it in the surface plane and the z-axis represents the elevation from the ground level. The origin of the coordinate system is located approximately at the center of the PV plant.

Figure 8 Map showing location of EnviPark, Totem Fotovoltaico and neighbouring buildings. Google Earth, earth.google.com/web/

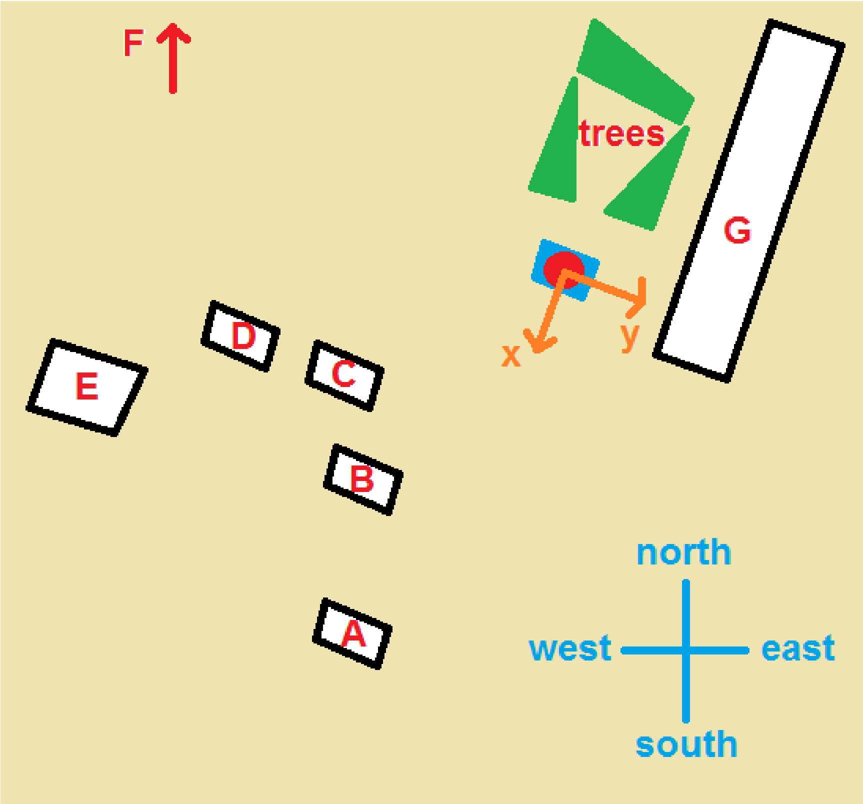

Figure 9 Supply side: schematic representation of the neighbouring buildings in EnviPark

An example of the calculation procedure is provided for concerning the building C, the closest one to the plant. For concerning buildings, because of the choice of the coordinate system and of the approximated orientation of the buildings, three points for each building are considered to completely evaluate the shadow profile.

For the distances along the x-axis and y-axis, the three points are the two vertexes of the buildings that constitute the borders of the shadow (1 and 2 *Figure10*) and the closest one to the PV system (3). For concerning the elevation, a single value for the entire building is chosen. The distances are measured by using the software *Google Earth* and *Google Earth Pro*.

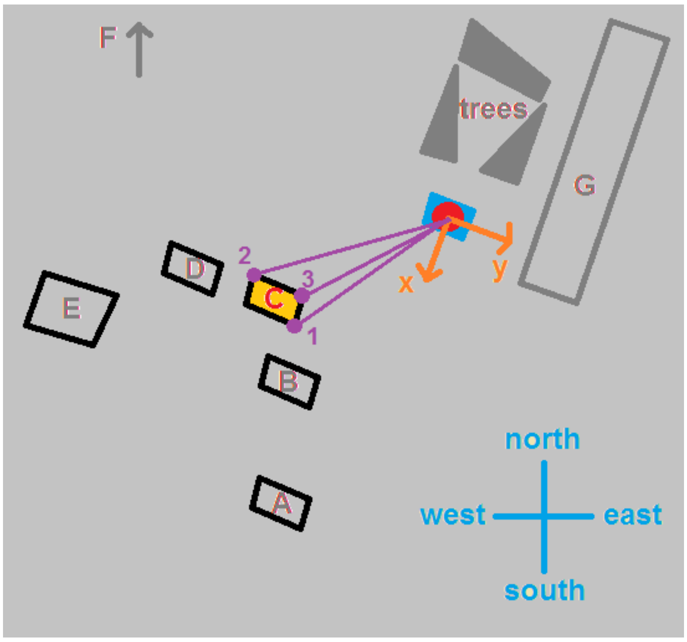

Figure 10 Supply side: Example of calculation for PV obstacles

For the building C, the values are collected in *Table4*.

x_1 $[m]$	y_1 $[m]$	x_2 $[m]$	y_2 $[m]$	x_3 $[m]$	y_3 $[m]$	z $[m]$
47	-45	34	-65	34	-45	39

Table 4 Supply side: Example of calculation for PV obstacles

From these values, the clockwise azimuth angle (with respect to the x-y coordinate system, ϕ, and with respect to the South, θ) and the distance L of the three points are calculated. For point 1 of building C is:

$$\phi_1 = \arctan\left(\frac{|y_1|}{|x_1|}\right) = \arctan\left(\frac{45}{47}\right) = 43.8\ [°]$$

$$\theta_1 = \phi_1 + 20° = 63.8\ [°]$$

$$L_1 = \sqrt{x_1^2 + y_1^2} = \sqrt{47^2 + 45^2} = 65.1\ [m]$$

Then, the horizon height angle α is computed:

$$\alpha_1 = \arctan\left(\frac{z}{L_1}\right) = \arctan\left(\frac{39}{65.1}\right) = 30.9\ [°]$$

The same procedure has been carried out for all the buildings and the trees (divided in three parts as in *Figure10*), and the obtained results are given in *Table5*. Distances are expressed in meters while angles in degrees.

	A	B	C	D	E	F	G	TreesNW	TreesN	TreesNE
x_1	140	84	47	47	103	-385	15	-30	-71	-30
y_1	-10	-20	-45	-78	-130	-240	35	-21	21	9
x_2	126	72	34	34	80	-350	-63	-30	-80	-30
y_2	-34	-66	-65	-146	-155	-368	35	-10	-20	20
x_3	126	72	34	34	80	-350	0	-	-75	-
y_3	-10	-20	-45	-78	-130	-240	35	-	0	-
z	39	36	39	34	67	73	6	6	6	6
ϕ_1	4.1	13.4	43.8	58.9	51.6	148.1	293.2	145.0	163.5	196.7
θ_1	24.1	33.4	63.8	78.9	71.6	168.1	313.2	165.0	183.5	216.7
L_1	140.4	86.3	65.1	91.1	165.9	453.7	38.1	36.6	74.0	31.3
α_1	15.5	22.6	30.9	20.5	22.0	9.1	9.0	9.3	4.6	10.8
ϕ_2	15.1	42.5	62.4	76.9	62.7	133.6	209.1	161.6	195.7	213.7
θ_2	35.1	62.5	82.4	96.9	82.7	153.6	229.1	181.6	215.7	233.7
L_2	130.5	97.7	73.4	149.9	174.4	507.9	72.1	31.6	82.5	36.1
α_2	16.6	20.2	28.0	12.8	21.0	8.2	4.8	10.7	4.2	9.4
ϕ_3	4.5	15.5	52.9	66.4	58.4	145.6	270	-	180	-
θ_3	24.5	35.5	72.9	86.4	78.4	165.6	290	-	200	-
L_3	126.4	74.7	56.4	85.1	152.6	424.4	35.0	-	75	-
α_3	17.1	25.7	34.7	21.8	23.7	9.8	9.7	-	4.6	-

Table 5 Supply side: Angle results for PV obstacles

The horizon height angle distribution follows a linear profile for each building, with two minima in the extremes and the maximum in Point 3. Given these profiles, the angular distribution with a step of 5 degrees in the azimuth angle θ is computed, by evaluating the maximum of the horizon height angle α if a superposition among different building shadows occurs. For the angles in which no obstacles have been considered, a constant value of 2 degrees has been set, which in any case is not relevant for the results. It is important to notice the difference in the azimuth angle system between the previous study and the software PVGIS: the uploaded file shall start from North (which corresponds to $\theta = 180\ [°]$) proceeding in a clockwise direction. The resulting angular distribution of the horizon height is provided in a tabular form in (11) and in the graphical representation by the software PVGIS in *Figure11* below.

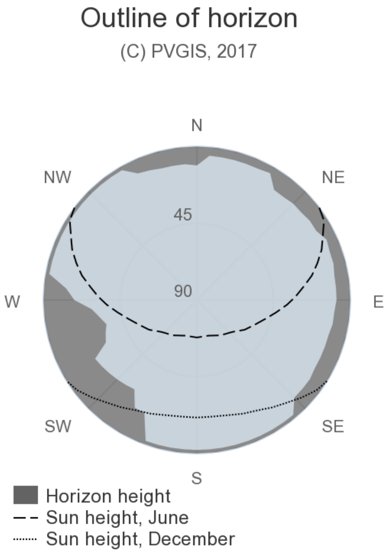

Figure 11 Supply side: Considered outline of horizon in PVGIS simulation

In *Figure12* the calculated PV energy production along the year (marked as ‘reference year’) is represented besides the measured values in the period 2011-2014. For some months (namely July, October and November) the results are bigger than the measured ones, but in a yearly perspective there is a quite good agreement between the values.

As expected, the highest values are present in summer months and the lowest ones in winter season. Of course, the main variation is in the daily profile, because power production is obtained only during days.

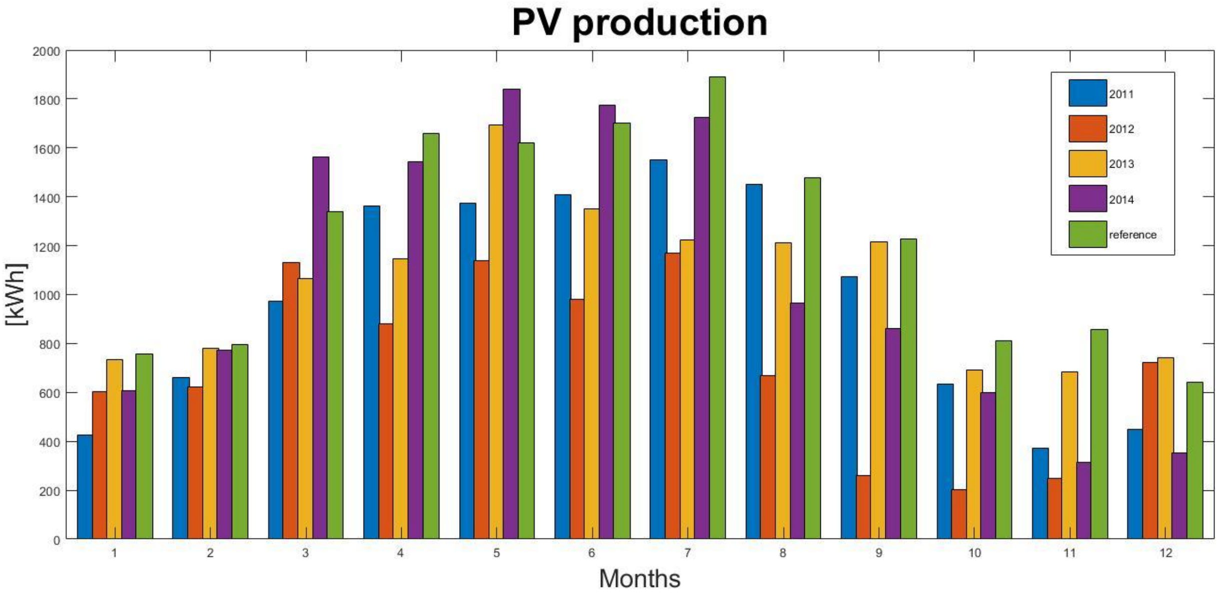

Figure 12 Supply Side: PV monthly production

4.1.2 HYDROELECTRIC POWER PLANT

The mini hydroelectric power station *Franco Mana*, located inside Environment Park, is constituted by a 380 kWe Kaplan hydro turbine. The plant was installed in 2008 and it was the first hydro power plant located in an urban context in Italy [23]. The water is taken from the Dora Riparia river, using an existing derivation located in the river bend to create the Meana channel, which passes through the park. The channel, which was constructed in mid-18th century, represents the earliest evidence of the connection between the river and the area, which played an important role in the urban activity and industrialization [24]. The local total head of water is about 5 meters.

Figure 13 Supply side: View of hydro power plant located in EnviPark, https://www.icanaliditorino.it/envronment-park

In this case, the power output values are available with hourly resolution for the entire year (*Figure14*) and no further calculations are needed. The distribution of the values shows a seasonal oscillation, with the highest results in late spring, when almost 400 kW are reached, and the lowest between September and October, when the mean value is slightly above 100 kW. A smaller daily variation can be observed, but without a precise pattern and mainly due to changes in the river water conditions. Finally, some plant stops are present during the year. Typically, they are constituted by few hours or single day blocks, but a significantly longer stop can be observed between 12 and 30 Mars.

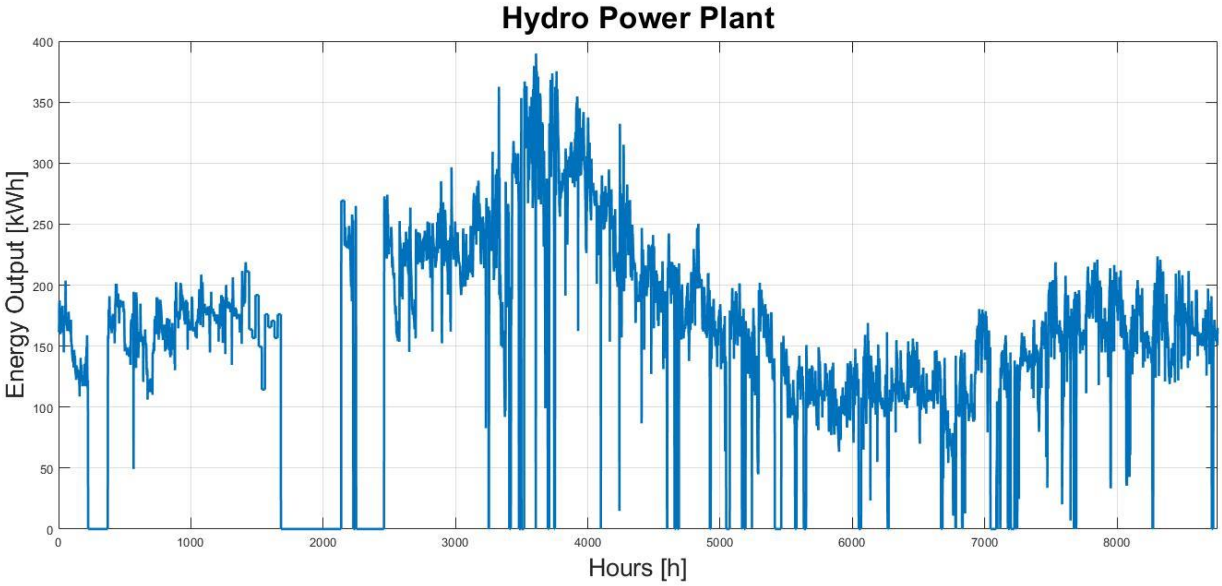

Figure 14 Supply side: Hydro power plant yearly profile

4.2 DEMAND SIDE

The r-SOC system will be installed in a basement located in building C of EnviPark (represented in *Figure15*) and will be connected to the hydrogen processing unit that will be placed in an open area near the same building.

Figure 15 Demand side: View of building C in EnviPark

From a recent study on the installation of the Air Treatment Units serving the offices and the laboratories of the Park, accurate values on monthly energy needs for space heating and cooling purposes have been obtained, as well as precise measurements for surfaces and volumes of the different zones of building C. The annual energy requirements for space heating and cooling has been considered for the whole building and the yearly energy density expressed in $[kWh/m^3_{gross}y]$ has been evaluated.

The two values have been compared with reference values from [25], in order to class the office type by the demand requirements and to assess a suitable value for electricity needs, for which a precise measurement is not available. More precisely, the calculated values for heating and cooling are close to the referenced ones tagged as "Office 60s-80s Sandwich Largely Glazed" for top floor and intermediate thermal zones (20.16 $[kWh/m^3_{gross}y]$ for space heating and 10.22 $[kWh/m^3_{gross}y]$ for space cooling). Thus, the referenced value of 14.15 $[kWh/m^3_{gross}y]$ expressed for electricity needs has been chosen for evaluating building C demand. The considered yearly energy density and the overall yearly energy demand values are collected in *Table6*.

	Energy density $[kWh/m^3_{gross}y]$	Overall Energy $[MWh/y]$
Space Heating	20.44	313.5
Space Cooling	11.44	175.4
Electricity	14.15	217.0

Table 6 Demand side: considered yearly energy density and energy

For evaluating the hourly distribution of the demands over the year the following approach has been used. As expressed in [26] and [27], such detailed data are present in literature only for USA. In particular, the U.S. Department of Energy's Office of Energy Efficiency and Renewable Energy (EERE) developed commercial building benchmark models which covers 16 building types across 16 locations representing the US climate zones [28]. For this reason, it has been chosen to consider the hourly load profile provided for a US office rescaled with the yearly values calculated above.

For the concerned work, the "Medium Office" building type and the "4A" climate zone (representative city is Baltimore, Maryland) have been considered as the closest to the actual conditions. The downloadable database [29] contains hourly load profile of 365 days in a normal year for electricity and gas demand, differentiated for more precise purpose (electricity and gas for space heating, electricity for space cooling, for fans, for interior lights and for interior equipment, gas for domestic hot water).

Space heating demand profile has been obtained by summing up the electricity and natural gas contribution of the US reference model; electricity demand profile has been gained by summing the electricity load for fans, equipment and lights; space cooling demand profile has been obtained by evaluating only the space cooling contribution of the US reference model. The three profiles are then rescaled to the calculated yearly overall values present in *Table6*.

The demand side of the fuel cell system is characterized by two contributions: power and heat. Thus, the hourly power demand profile is obtained by summing up each value of the electricity and space cooling load profiles calculated before hour by hour, while heat demand covers both space heating and domestic hot water (DHW). For this reason, an assessment of the DHW requirements for the Park is necessary.

That has been done following the technical standards for the determination of energy needs at design stage, according to the UNI/TS 11300-2:2019. The energy requirements for DHW have been calculated following [30] with the next formula:

$$Q_{DHW} = \sum \rho_{water} \cdot c_{water} \cdot (T_{supply} - T_0) \cdot V_{water} \cdot G$$

Where

$\rho_{water} = 1000\ [kg/m^3]$ is the water density.

$c_{water} = 1.162\ x\ 10^{-3}\ [kWh/(kg \cdot K)]$ is the specific heat capacity for liquid water.

T_{supply} is the supply water temperature, which is conventionally evaluated equal to 40 °C.

T_0 is the water inlet temperature to the DHW system, which depends on the outlet air temperature, but may be considered constant for the whole year and equal to 15 °C: with that choice, the temperature drop contribution is $\left(T_{supply} - T_0\right) = 25\ [°C]$ for every months.

$V_{water}\ [m^3/G]$ represents the heated volume of water per unit of time and it is evaluated according to the technical standard with different formulas depending on the characteristics of the demand; for offices the value depends on the surface area in the following way: $V_{water} = 0.2\ [l/(m^2 \cdot G)]$; the surface area of the building C in EnviPark is 3070 m^2.

$G\ [G]$ is the number of days in the time period for which the domestic hot water demand is calculated.

The evaluation of the DHW energy demand has been done for each month, by considering the days of full and partial load from the US profile. The 12 values have been then summed up to obtain the annual energy demand, which is used to rescale the DHW energy profile given from [29].

In *Figure16* the annual representation of the electricity and heat demand are given. The heating profile is standard, with almost null needs in summer months, where only domestic hot water demand is present, while having very high values in winter periods, with maximum hourly peak of 850 kWh. For concerning electricity, the assumed energy profile is characterized by a non-stop occupation during summer, when the highest demand is required, mainly due to cooling needs. Over the entire year, a minimum electricity demand due to interior equipment is found to be equal around to 15 kWh in weekdays and nearly half in weekends during night hours

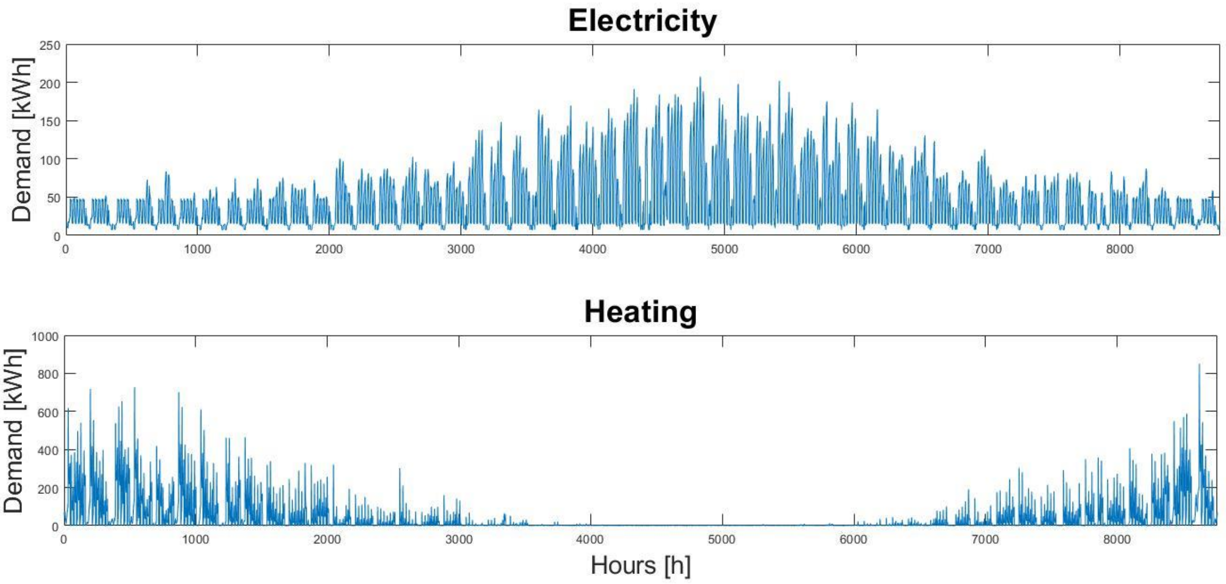

Figure 16 Demand side: Annual profile of electricity and heating

5. MODELLING

5.1 MODELLING TECHNIQUE AND MAIN ASSUMPTIONS

The objective of modelling is to represent the real physical system by a model, that is used to simulate its behavior [31]. It consists in creating a mathematical formulation describing the system, which elaborates the input signals in order to get a sufficiently accurate representation of the output signal and of the state of the process. Models are typically used to understand and predict the behavior of a system, to optimize control strategies and thermal balancing, to obtain information on the optimal parameters, to perform a predictive evaluation of the system [14]. It offers a fundamental complement to experimental works, which allows to reduce time necessary for the analysis and to highlight mathematical relations otherwise difficult to be obtained.

Several types of modelling approach for fuel cells and electrolysers are present in literature. One of the most important characterization is given by the dimensionality of the model [32], which clearly depends on the level of detail of requested results or available data that are the specific needs of the model.

Zero-dimensional modelling allows examining system without considering spatial configuration and geometry. It is typically used for system-level studies and with the introduction of heat capacity of components, it can be able to represent the dynamic response of the system. The main advantages are low computational cost and simple formulation of the model, but it cannot be used for furtherly studying spatial distribution and effects due to geometry and size [14]. In one-, two- and three-dimensional models, space-dependent equations are solved, and further information can be obtained. Investigations on property variation in space, dangerous operational modes and heat transfer are typically performed using these models. Computational fluid dynamics codes can be employed, but significantly increasing computational power. They are mainly used for analysis only related to the cell.

In this work a zero-dimensional dynamic model of the entire r-SOC system has been constructed using SIMULINK©. The system is constituted by the stack module and most of the balance of plant (BoP) components. Time-dependent differential equations have been solved for each subsystem in a lumped parameter approach and the evolution of component temperature in different conditions has been studied. All the three modes of operation have been analyzed. In the following part, the main assumptions and some features of the model are resumed.

Seven chemical species have been considered in the model. Inlet air has been assumed to be constituted only by the main two species, oxygen 21% and nitrogen 79% in molar basis. For concerning fuel, only one species has been assumed to be delivered in each mode of operation: methane in NG-SOFC, hydrogen in H2-SOFC and steam in SOEC. Due to the presence of recirculation loop and pre-reforming unit, the composition in the fuel line is however always constituted by a mixture of species: only hydrogen and water in H2-SOFC and SOEC, while also methane, carbon monoxide and carbon dioxide in NG-SOFC. The considered assumptions for chemical reactions in reformer, stack and afterburner will be more precisely discussed below in the description of the modelling technique for each subsystem.

Molar properties of the above species, such as heat capacity, enthalpy and entropy, have been obtained by the NIST chemistry web book [33]. The standard gas phase thermochemistry data of the species are provided through fixed expressions and specific coefficients from A to H for each species, depending on the temperature T [K]:

$$\overline{c_p^0} = A + B \cdot t + C \cdot t^2 + D \cdot t^3 + \frac{E}{t^2} \qquad \left[\frac{J}{mol \cdot K}\right]$$

$$\overline{h^0} = \overline{h_{298.15}^0} + A \cdot t + \frac{B}{2} \cdot t^2 + \frac{C}{3} \cdot t^3 + \frac{D}{4} \cdot t^4 + \frac{E}{t} + F - H \qquad \left[\frac{kJ}{mol}\right]$$

$$\overline{s^0} = A \cdot \ln t + B \cdot t + C \cdot \frac{t^2}{2} + D \cdot \frac{t^3}{3} - \frac{E}{2 \cdot t^2} + G \qquad \left[\frac{J}{mol \cdot K}\right]$$

Where $t = T/1000$ and $\overline{h_{298.15}^0}$ represents the standard enthalpy of formation of the species, which is tabulated.

The Gibbs free energy of the species has been calculated at different temperature T as in [34] with the following expression:

$$\Delta\bar{g} = \Delta\bar{g}_{298.15}^0 + \left[\left(\overline{h^0} - \overline{h_{298.15}^0}\right) - \left(T \cdot \overline{s^0} - T_0 \cdot \overline{s_{298.15}^0}\right)\right] \qquad \left[\frac{kJ}{mol}\right]$$

Where $\Delta\bar{g}_{298.15}^0$ is the standard Gibbs free energy and values have been obtained by [35], $T_0 = 298.15\ [K]$ represents the reference temperature and $\overline{s_{298.15}^0}$ is the enthalpy of formation of the species in standard conditions, provided by NIST.

All the occurring reactions have been considered in equilibrium conditions. Thus, for steam methane reforming and water gas shift reactions, the equilibrium constants have been used to evaluate the conversion of reactants. As in other works [36], only hydrogen ion transportation have been assumed to be responsible for electrical flow. While the methane contribution is wherever considered null, due to its relative slow kinetics [37], this is not typically the case of carbon monoxide. However, when an internal reforming section is present inside the stack module, the conversion of carbon monoxide into hydrogen is already evaluated and only the hydrogen contribution to power generation can be assumed [38]. Moreover, direct oxidation of carbon monoxide has not been considered, as well as methane has been converted to hydrogen only [34]. The conversion of hydrogen into steam in SOFCs and vice versa in SOEC have been assumed by considering fixed constant fuel utilization and steam conversion factors for most of the operating points as input values, available by project studies and found in literature.

Pressure drops along the system have been neglected. The air blower has been assumed to increase the stream pressure to 0.05 barg.

Both anode and cathode side outlet streams have been considered exiting the stack at the same temperature, equal to the lumped parameter one of the stack.

Other assumptions and parameter choices will be in any case discussed in the following part.

The core of the model is the stack module. Since some relevant features of the modelling technique are present and deserve a precise explanation, the electrochemical and the polarization model for the stack subsystem are widely presented in the next part, leaving a faster systematic description of the dynamic models for each considered subsystem in the subsequent part.

5.2 FEATURES OF THE STACK MODEL

5.2.1 ELECTROCHEMICAL MODEL

Inside the solid oxide cell several electrochemical reactions occur. In the more general and complex case, i.e. NG-SOFC mode of operation, three main reactions have been considered in the present model:

- steam methane reforming (SMR) $CH_4 + H_2O \rightarrow CO + 3H_2$
- water gas shift (WGS) $CO + H_2O \rightarrow CO_2 + H_2$
- hydrogen oxidation (HOX) $H_2 + \frac{1}{2}O_2 \rightarrow H_2O$

SMR is highly endothermic at standard condition ($\overline{\Delta H^0_{SMR}} = +206\ kJ/mol$) and is responsible for the conversion of methane into hydrogen and carbon monoxide. Carbon monoxide is converted too into hydrogen and carbon dioxide in WGS, which is exothermic at standard condition ($\overline{\Delta H^0_{WGS}} = -41.1\ kJ/mol$). Both reactions need the presence of steam water as a reactant. They represent the reactions occurring in the internal reforming section of the stack. The real electrochemical reaction is the third one, which is exothermic ($\overline{\Delta H^0_{HOX}} = -241.8\ kJ/mol$ for water in steam phase) and is responsible for the output power as expressed in the polarization model part.

For evaluating the molar flowrate exiting the stack, the moles of methane, carbon monoxide and hydrogen that react in a certain time in the three above reactions have been indicated with three variables – a, b and c respectively – in order to simplify the notation:

$$a = \dot{n}_{CH_4,SMR} \quad [mol/s]$$

$$b = \dot{n}_{CO,WGS} \quad [mol/s]$$

$$c = \dot{n}_{H_2,HOX} \quad [mol/s]$$

For the five chemical species considered reacting in the fuel electrode of the model, the equilibrium molar flows have been evaluated. Considering the assumption of equilibrium conditions for the reactions, they correspond to the molar flows in the outlet section of the unit. Applying a simple material balance, they depend both from the inlet molar flow in the stack and from molar flows of other species that are transformed by the three above reactions. The molar flowrates of the species at equilibrium conditions are expressed below:

$$\dot{n}_{CH_4(o)} = \dot{n}_{CH_4(i)} - a$$

$$\dot{n}_{H_2(o)} = \dot{n}_{H_2(i)} + 3a + b - c$$

$$\dot{n}_{CO(o)} = \dot{n}_{CO(i)} + a - b$$

$$\dot{n}_{H_2O(o)} = \dot{n}_{H_2O(i)} - a - b + c$$

$$\dot{n}_{CO_2(o)} = \dot{n}_{CO_2(i)} + b$$

As an example, the hydrogen molar flow at equilibrium ($\dot{n}_{H_2(o)}$) is obtained by the sum of the inlet hydrogen molar flowrate in the stack unit ($\dot{n}_{H_2(i)}$), three times the methane molar flow reacting in SMR ($3a$), the carbon monoxide molar flow reacting in WGS (b) and minus the hydrogen molar flow reacting with oxygen in HOX (c). The other expressions are obtained using the same approach.

The total molar flowrate in the outlet section of the stack module at equilibrium conditions is given by the sum of the molar flowrates of each species in the previous equations, obtaining:

$$\dot{n}_{TOT(o)} = \dot{n}_{TOT(i)} + 2a$$

Thus, in order to evaluate the composition of the outlet flow exiting the stack unit, the reacting molar flowrates a, b and c must be calculated.

For the considered assumptions, the unknown c can be directly calculated by evaluating the fuel utilization factor FU as:

$$c = FU \cdot (\dot{n}_{H_2(i)} + 4 \cdot \dot{n}_{CH_4(i)} + \dot{n}_{CO(i)})$$

In order to evaluate the other two unknowns, for both reforming and shifting reactions the constants of equilibrium of the reaction $K_p(T)$ have been used. Considering a reaction occurring at a pressure p and constituted by N reactants and M products, each one with a stoichiometric coefficient v_i (positive for the products and negative for the reactants), it is defined as:

$$K_p(T) = \left(\frac{p}{p_0}\right)^{\sum_{i=1}^{N+M} v_i} \cdot \prod_{i=1}^{N+M} y_i^{v_i}$$

Where p_0 is a reference pressure, conventionally assumed equal to 1 bar, and y_i are the molar fractions of the species, defined as the ratio between the molar flowrates of the species i-th in a stream and the total molar flowrate of the stream:

$$y_i = \frac{\dot{n}_i}{\dot{n}_{TOT}}$$

Applied to SMR and WGS, the following expressions are generated:

- $K_{p,SMR}(T) = p_{cell}^2 \cdot \frac{y_{CO} \cdot y_{H_2}^3}{y_{CH_4} \cdot y_{H_2O}}$
- $K_{p,WGS}(T) = \frac{y_{CO_2} \cdot y_{H_2}}{y_{CO} \cdot y_{H_2O}}$

The constant of equilibrium highlights if the reaction is spontaneously directed towards the products ($K_p(T) > 1$), towards the reactants ($K_p(T) < 1$) or in equilibrium ($K_p(T) = 1$). The value of the constant is dependent only by the temperature at which the reaction occurs and different correlations are available in literature. Following the approach chosen by [36][34], the polynomial expression proposed by Bossel is used:

$$\log K_p(T) = A \cdot T^4 + B \cdot T^3 + C \cdot T^2 + D \cdot T + E$$

Where the constant values are:

	SMR	WGS
A	-2.6312$\cdot 10^{-11}$	5.47$\cdot 10^{-12}$
B	1.2406$\cdot 10^{-7}$	-2.574$\cdot 10^{-8}$
C	-2.2523$\cdot 10^{-4}$	4.6374$\cdot 10^{-5}$
D	1.95027$\cdot 10^{-1}$	-3.9150$\cdot 10^{-2}$
E	-66.139488	13.209723

Table 7 Modelling: Bossel coefficients for SMR and WGS equilibrium constants

The graphical representation of the considered constants of equilibrium in dependence of temperature are plotted in *Figures17-18*. It is possible to see how SMR reaction is favored at higher temperatures, while WGS reaction shows the opposite trend.

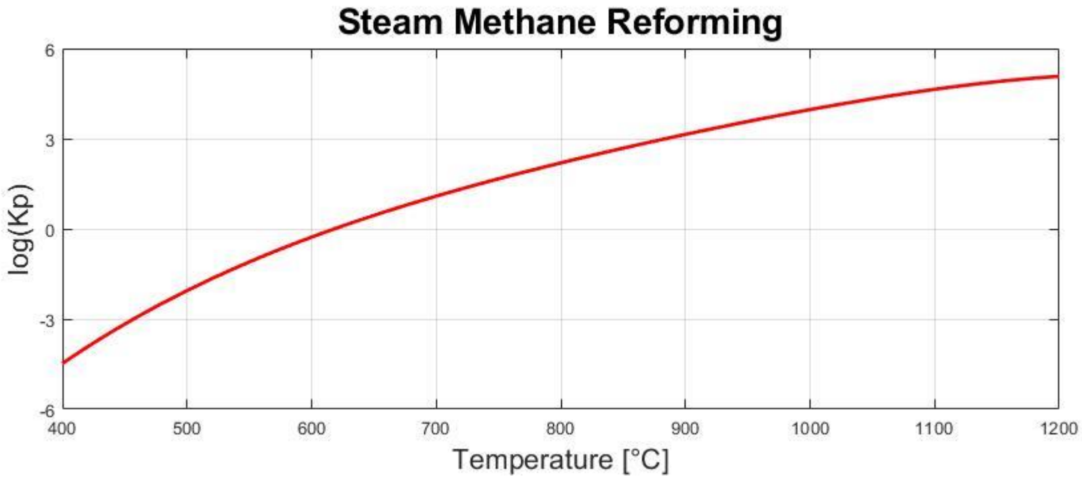

Figure 17 Modelling: Steam Methane Reforming dependence with temperature

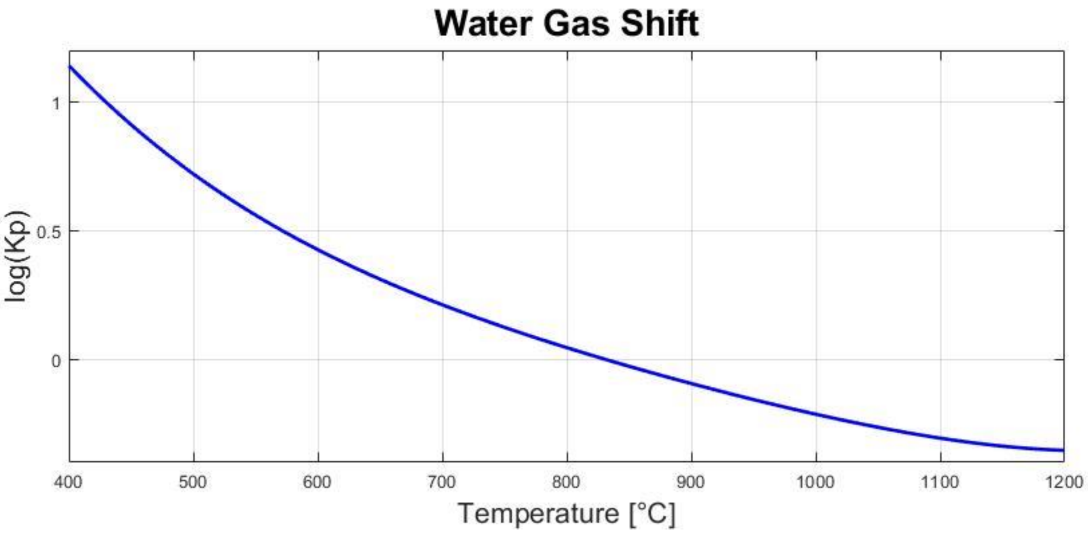

Figure 18 Modelling: Water Gas Shift dependence with temperature

Thus, knowing the temperature inside the stack unit, the constants of equilibrium of the reactions are obtained and the following system of three non-linear equations results:

$$\left\{\begin{array}{c} K_{p,SMR}(T) = p_{cell}^2 \cdot \dfrac{\left(\dfrac{\dot{n}_{CO(i)} + a - b}{\dot{n}_{TOT(i)} + 2a}\right) \cdot \left(\dfrac{\dot{n}_{H_2(i)} + 3a + b - c}{\dot{n}_{TOT(i)} + 2a}\right)^3}{\left(\dfrac{\dot{n}_{CH_4(i)} - a}{\dot{n}_{TOT(i)} + 2a}\right) \cdot \left(\dfrac{\dot{n}_{H_2O(i)} - a - b + c}{\dot{n}_{TOT(i)} + 2a}\right)} \\ K_{p,WGS}(T) = \dfrac{\left(\dfrac{\dot{n}_{CO_2(i)} + b}{\dot{n}_{TOT(i)} + 2a}\right) \cdot \left(\dfrac{\dot{n}_{H_2(i)} + 3a + b - c}{\dot{n}_{TOT(i)} + 2a}\right)}{\left(\dfrac{\dot{n}_{CO(i)} + a - b}{\dot{n}_{TOT(i)} + 2a}\right) \cdot \left(\dfrac{\dot{n}_{H_2O(i)} - a - b + c}{\dot{n}_{TOT(i)} + 2a}\right)} \\ c = FU \cdot \left(\dot{n}_{H_2(i)} + 4 \cdot \dot{n}_{CH_4(i)} + \dot{n}_{CO(i)}\right) \end{array}\right\}$$

It is a system made of 3 equations and 3 unknowns (a, b and c) and it can be solved using different methods. In this work, the Newton-Raphson method has been applied in MATLAB© [39].

For concerning H2-SOFC mode of operation, the previous approach is not really required, since no internal reforming reactions occur. Only the last equation remains and the reacting hydrogen molar flowrate inside the stack can be directly evaluated from the assumed value of fuel utilization:

$$a = 0$$

$$b = 0$$

$$c = FU \cdot \dot{n}_{H_2(in)}$$

For concerning SOEC mode of operation, the approach is similar to H2-SOFC. Instead of fuel utilization, steam conversion factor has been used to determine the reacting steam molar flowrate from the inlet one in the stack:

$$\dot{n}_{H_2O}^{reacting} = SC \cdot \dot{n}_{H_2O(in)}$$

5.2.2 POLARIZATION MODEL

For high temperature electrochemical devices activation overvoltage (2.2.2) can be typically neglected. Moreover, it may be assumed that normal operations do not occur at very high current density values, thus diffusion overvoltage may be not considered. For this reason, as in [16], in the present model the cell polarization characteristic has been assumed to be linear, thus considering only the ohmic losses described by the area specific resistance:

$$V_{cell} = OCV \mp ASR \cdot i \qquad [V]$$

The precise polarization curve of the r-SOC unit depends on several factors: the electrochemical reactions occurring in the unit – due to the anode and cathode gases composition – and the temperature at which they occur are considered inside the model, while others, such as degradation in time of the cell properties, have not been evaluated.

From the concerned plant design papers, two assumed values for the ASR of the entire unit are given. More precisely, atmospheric pressure and two values of temperature inside the operation range have been considered:

$$ASR_{SOC}(730\ °C, 1\ bar) = 0.6\ [\Omega \cdot cm^2]$$

$$ASR_{SOC}(800\ °C, 1\ bar) = 0.4\ [\Omega \cdot cm^2]$$

In order to evaluate the relation between ASR and the temperature of the unit, the expression given in [40] has been assumed, which was obtained as an experimental data fit from cell level studies:

$$ASR_{cell}(T,p) = 5.06 \cdot 10^{-5} \cdot \exp\left(\frac{9200}{T}\right) \cdot p^{-0.1} \qquad [\Omega \cdot cm^2]$$

It captures both temperature (expressed in Kelvin) and pressure (in bar) sensitivity; in the concerned case, only the temperature dependence has been evaluated, since the pressure is assumed to be constant at atmospheric level.

The previous expression has been then simply vertically shifted in such a way that the values of area specific resistance of the entire unit have been maintained:

$$ASR_{SOC}(T) = 5.06 \cdot 10^{-5} \cdot \exp\left(\frac{9200}{T}\right) + 0.113 \qquad [\Omega \cdot cm^2]$$

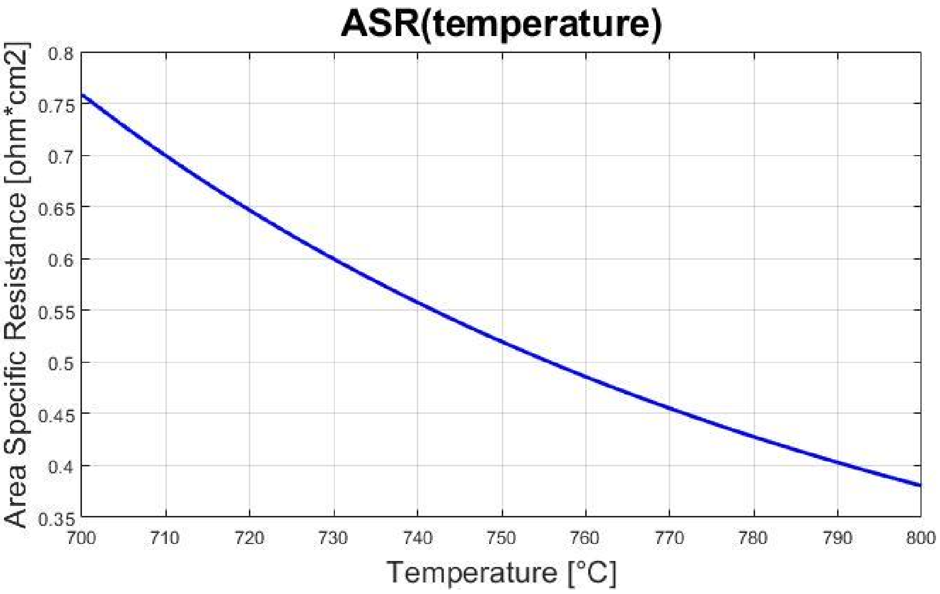

Figure 19 Modelling: Assumed ASR evolution with temperature

For the determination of the OCV the definition (2.2.1) is applied. In the case of simple hydrogen oxidation with air occurring at the nominal temperature of the cell, with assumed molar fractions of the species equal to $y_{H_2} = 0.30$, $y_{H_2O} = 0.70$ and $y_{O_2} = 0.20$, it follows:

$$OCV\left(730\ °C, H_2 + \frac{1}{2}O_2 \leftrightarrow H_2O\right) = 0.926\ [V]$$

In the dynamic model described below, both ASR and OCV have been directly evaluated inside it by knowing the stack temperature in each moment of the simulation. Also the molar fractions of the species have been directly evaluated inside the dynamic model and, as in [34], the average value between inlet and outlet section of the electrodes have been considered.

The resulting polarization curve can be drawn after evaluating the maximum current density, which is obtained from the design maximum fuel inlet flowrate. In case of H2-SOFC mode of operation, assuming a fuel utilization factor of the system equal to $FU_{system} = 0.81$, it follows:

$$\dot{V}_{MAX} = 8.7\ \left[\frac{Nm^3}{h}\right]$$

$$\dot{n}_{MAX} = \dot{V}_{MAX}\left[\frac{Nm^3}{h}\right] \cdot \frac{1}{0.0224}\ \left[\frac{mol}{Nm^3}\right] = 388.4\ \left[\frac{mol}{h}\right]$$

$$\dot{n}_{MAX}^{react} = \dot{n}_{MAX} \cdot FU_{system} = 0.087\ \left[\frac{mol}{s}\right]$$

$$I_{MAX} = \dot{n}_{MAX}^{react} \cdot z \cdot F = 16.9\ [kA]$$

The electric current density for each cell is then evaluated dividing that value by the number of cells of the unit ($n_c = 300$) and by their surface ($A = 200\ cm^2$), giving:

$$i_{MAX} = 0.281 \left[\frac{A}{cm^2}\right]$$

This cell voltage corresponding to that current density is:

$$V_{cell} = OCV - ASR \cdot i_{MAX} = 0.757 \ [V]$$

While the maximum DC power output in H2-SOFC results:

$$P_{MAX} = V \cdot I = 12.8 \ [kW]$$

Assuming an efficiency of the inverter $\eta_{inv} = 0.9$, the maximum AC power output is obtained:

$$P = 11.5 \ [kW]$$

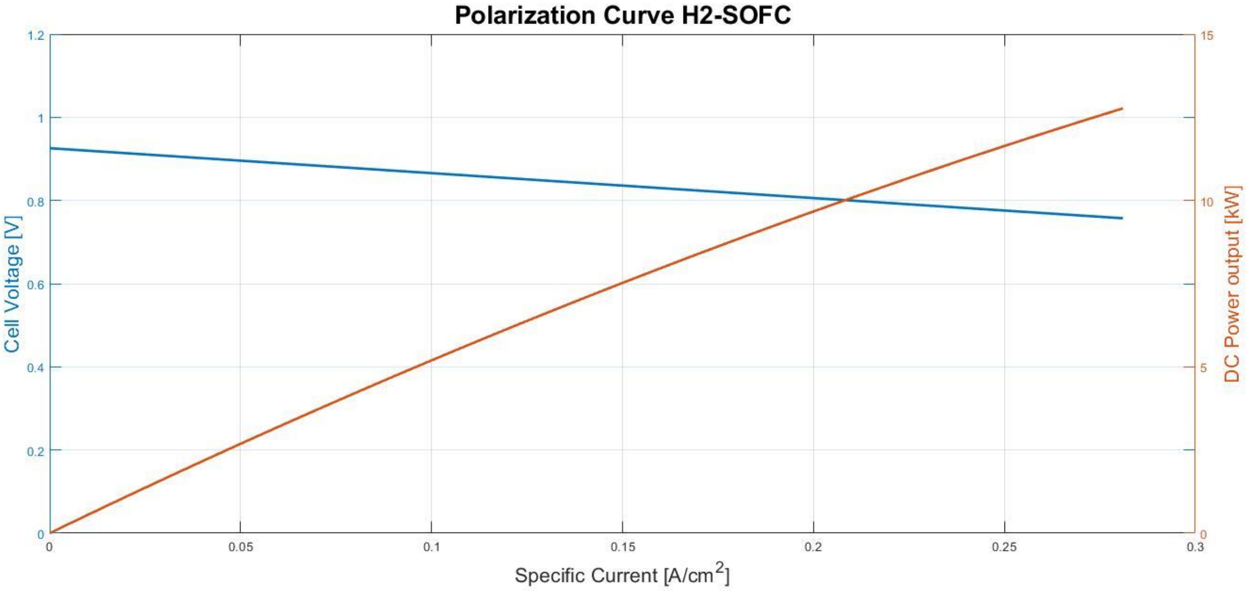

Figure 20 Modelling: Example of polarization curve for H2-SOFC

5.3 DYNAMIC MODEL

The concerned r-SOC system has been studied through a dynamic lumped parameters model in the software SIMULINK©. For each of the three modes of operation described in (3.3) a proper model has been created, with slightly differences with respect to the others that will be discussed. Moreover, at very partial load conditions the constructed models have been modified in order to simulate the system behavior at those conditions. This part will be specifically described in (5.4). After that, all the models have been united in a single comprehensive one suitable for the whole field of operation of the r-SOC system.

The mass and energy conservation equations have been always applied, while pressure drops have not been evaluated. The formulation of the first law of thermodynamics in transient conditions for open systems has been mainly used (neglecting kinetic and potential specific energy variation, as well as shear and piston work):

$$\frac{dE_{CV}}{dt} = \sum \dot{Q}_{CV} - \sum \dot{W}_{shaft} + \sum \dot{n}_i h_i - \sum \dot{n}_o h_o$$

Where:

$\frac{dE_{CV}}{dt}$ is the transient term of the equation and represents the variation in time of the energy contained in the control volume; for each component, this term has been expressed by a scalar coefficient $\tau = \rho \cdot c \cdot V$, which represents its thermal inertia, and by the temperature variation in time dT/dt.

$\sum \dot{Q}_{CV}$ represents the sum of the rate of heat transfers from and to the system, with the conventional sign choice of $\dot{Q} > 0$ if heat is provided to the control volume and $\dot{Q} < 0$ if the heat is delivered from the control volume. Heat transfers accounts also thermal losses released to the environment.

$\sum \dot{W}_{shaft}$ is the rate of work done by the system or by the environment; the applied convention is to consider $\dot{W} > 0$ for work done by the system to the environment and $\dot{W} < 0$ for work done by the environment to the system. Only electrical power in the stack module and in the electric heaters is present in the system.

$\sum \dot{n}_i h_i - \sum \dot{n}_o h_o$ represents the energy rate contribution associated to the mass flow respectively to and from the control volume.

For a better comprehension of the model, the considered system has been arbitrarily subdivided into 8 main subsystems in the SIMULINK© worksheet (*Figure21*): the electrochemical calculator, the oxidant line, the fuel line, the stack module, the afterburner line, the exhaust gas line, the mixer line and the evaporator line. The same subsystems are highlighted in the concerned plant general configuration in *Figure22*. In the following part, the construction of each subsystem is discussed, referring to the main equations and assumptions used. In general, the description refers to NG-SOFC mode of operation, which is the most complex one; where differences are present in H2-SOFC and SOEC configurations, they are described.

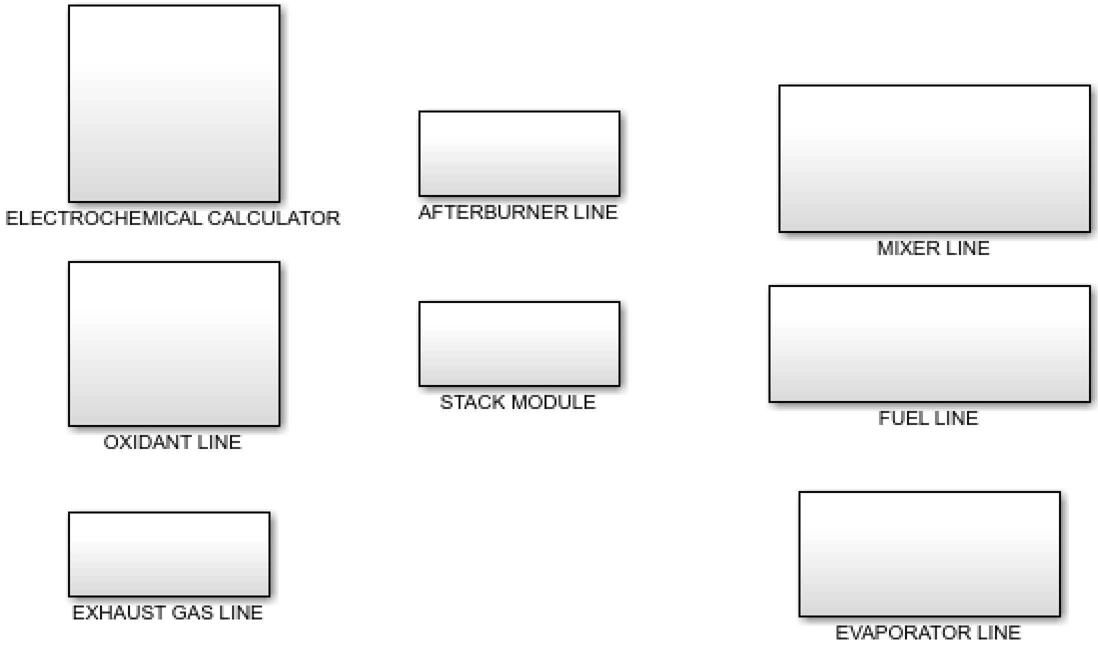

Figure 21 Modelling: SIMULINK© blocks worksheet

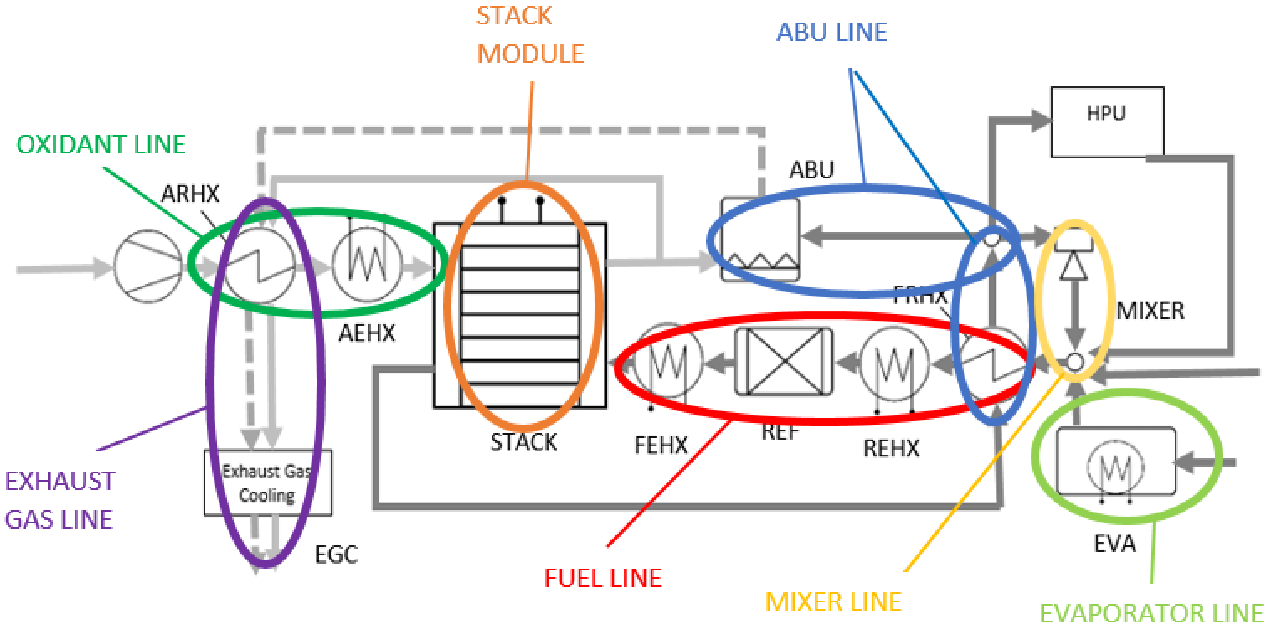

Figure 22 Modelling: Configuration of the considered blocks

Hydrogen processing unit and air blower has not been included in the dynamic model.

5.3.1 ELECTROCHEMICAL CALCULATOR

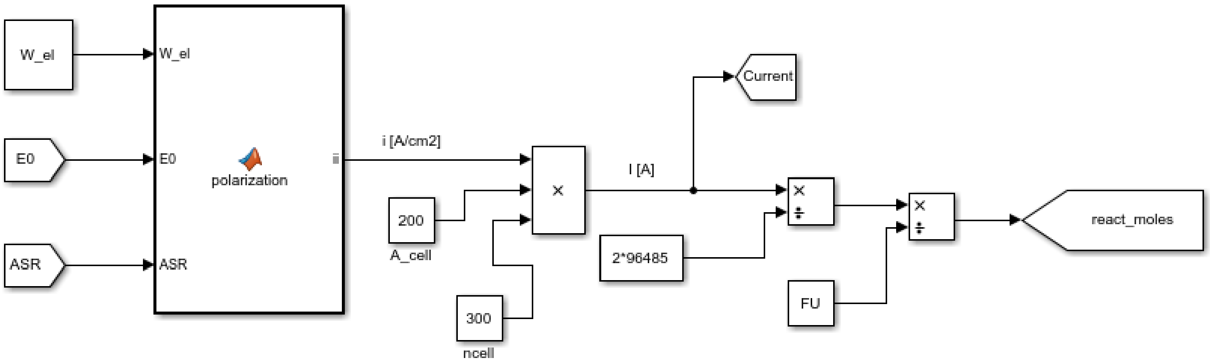

Figure 23 Modelling: Electrochemical calculator

This subsystem does not represent a physical component of the plant, but it serves as a calculator block which links the electrical part – i.e. the electrical load – to the chemical part – i.e. the required inlet fuel or steam molar flowrate. The choice of adding this subsystem inside the Simulink model has been evaluated in order to using the real values of OCV and ASR calculated in the stack module subsystem of the model.

For concerning SOFC modes of operation, by using the external input of available AC power and the internal inputs of OCV and ASR, the electric current associated to that power is obtained through the inverter efficiency and the real polarization curve of the cell. From the Faraday's law and the features of the stack (surface area of each cell and number of cells), this value corresponds to a precise hydrogen reacting flowrate value.

Since the fuel utilization is fixed constant to 0.665, the hydrogen reacting flowrate is associated to the value of moles per second of hydrogen that must exit the mixer of the fuel line to provide the required electric power in the stack module. In H2-SOFC mode it represents the real inlet hydrogen flowrate in the stack; in NG-SOFC it means the "equivalent hydrogen" flowrates, since every mole of hydrogen can be formed also by carbon monoxide and methane in the external and in the internal reformer:

$$\dot{n}_{H_2}^{eq} = \dot{n}_{H_2} + \dot{n}_{CO} + 4 \cdot \dot{n}_{CH_4}$$

This value is then used in the mixer line subsystem. In *Figure23*, the subsystem for SOFC modes of operation is represented.

For concerning SOEC mode of operation, the concept is the same. Differences are present in the polarization curve and in the fuel utilization factor that is replaced by the steam conversion factor. The calculated molar flowrate is the real steam flowrate at the outlet section of the mixer.

5.3.2 OXIDANT LINE

Oxidant line provides the air which serves both as oxidant species (containing oxygen) in the electrochemical reaction and as cooling fluid for the stack in SOFC mode of operation and both as cooling fluid and sweep gas in exothermic SOEC mode of operation. Air must enter the stack unit at a sufficiently high temperature to avoid thermal stresses in the component, thus it is heated up by a recuperator and by an electric heater. The active control of this subsystem is in the load of the electric heat exchanger, which is variated by a PID controller from 0 to 5.5 kW to reach at least 830 K in the outlet section of the subsystem. An air blower is also necessary to overcome pressure losses in the line, but it has not been considered in the dynamic model, since it has been assumed to quickly follow the load, having fast dynamic in comparison to other components [34].

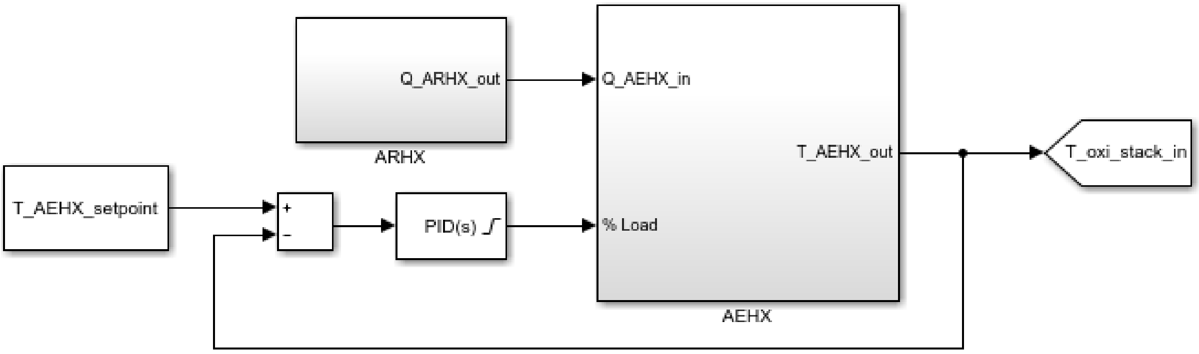

Figure 24 Modelling: Oxidant line

Nor chemical reactions nor mixing are present in this subsystem. Thus, the air composition remains constant and equal to the inlet one, i.e. oxygen 21% and nitrogen 79% molar, and the mass balance equation is trivial. For this reason, only the energy conservation equation has been presented below, as well as a brief description of the components used in the dynamic model.

- **AIR RECOVERY HEAT EXCHANGER – COLD SIDE (*ARHX*)**

The air preheater transfers the heat from the exhaust gases exiting the afterburner unit to increase the temperature of the air coming from the ambient. The thermal balance for the cold side of the component is:

$$\tau_{ARHX} \cdot \frac{dT_{ARHX}^{out}}{dt} = \sum \dot{n}_{in} \cdot \bar{h}_{in}\left(T_{AIR}^{in}\right) - \sum \dot{n}_{out} \cdot \bar{h}_{out}(T_{ARHX}^{out}) + \dot{Q}_{HT}^{ARHX}$$

Where:

$\sum \dot{n} \cdot \bar{h}(T)$ represents the contribution of the mass flow in the energy balance; the molar enthalpy of the two species have been evaluated at the air inlet temperature T_{AIR}^{in} – assumed to be constant and equal to 303 K due to the slight heating up by the air blower – and at the air outlet temperature T_{ARHX}^{out} from the component, which is computed directly with the previous equation.

$\dot{Q}_{HT}^{ARHX}$ represents the rate of heat transferred in the recuperator from the hot side to the cold side. Its evaluation has been carried out by assuming a value of effectiveness of the recuperator $\epsilon = 0.65$ after a literature review [41], by the calculation of the thermal capacity of the gases in the two sides (expressed as 1 and 2 below) of the component and by knowing their inlet temperature (T_1^{inlet} and T_2^{inlet}). Thus, the used equations are the following ones [42]:

$$\dot{Q}_{HT} = \epsilon \cdot \dot{Q}_{HT}^{MAX}$$

$$\dot{Q}_{HT}^{MAX} = \dot{C}_{min} \cdot \Delta T_{MAX}$$

$$\dot{C}_{min} = \min\left(\sum \dot{n}_i \cdot \overline{c_{p_i}}(T)\right)$$

$$\Delta T_{MAX} = |T_1^{inlet} - T_2^{inlet}|$$

- **AIR ELECTRIC HEAT EXCHANGER (*AEHX*)**

Air may be furtherly heated up in an electric heater of nominal power 5.5 kW. The thermal balance of the component is:

$$\tau_{AEHX} \cdot \frac{dT_{AEHX}^{out}}{dt} = -\dot{Q}_{losses} + W_{el} + \sum \dot{n}_{in} \cdot \bar{h}_{in}(T_{ARHX}^{AIRout}) - \sum \dot{n}_{out} \cdot \bar{h}_{out}(T_{AEHX}^{out})$$

Where:

$\dot{Q}_{losses}$ accounts for the thermal losses to ambient;

$W_{el} = W_{el}^{NOM} \cdot f \cdot \epsilon_{HT}$ represents the electrical work entering the system and it has been evaluated as the product of the rated power of the heater, the partial load of the component and the heat transfer effectiveness, assumed to be equal to 0.95;

$\sum \dot{n} \cdot \bar{h}(T)$ is the contribution of the mass flow in the energy balance, evaluated at inlet and outlet temperature for oxygen and nitrogen species, as for the recovery heat exchanger.

5.3.3 FUEL LINE

Fuel line provides the fuel mixture in SOFC mode of operation and the steam in SOEC mode of operation; the precise composition of the stream is obtained by the output of the mixer subsystem. Four are the main components which constitute the fuel line subsystem: a recovery heat exchanger which preheats the stream, an electric pre-heater, a reformer section in which the composition of the fuel entering the stack is modified and an electric heater, which modulates the power to reach at least 890 K and serves as the active control component of the subsystem.

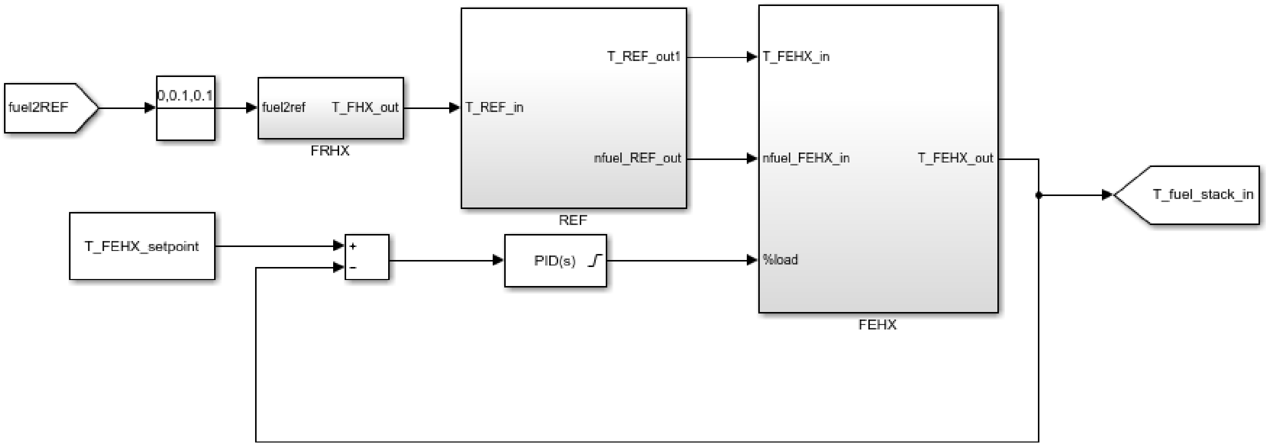

Figure 25 Modelling: Fuel line

➢ FUEL RECOVERY HEAT EXCHANGER – COLD SIDE (*FRHX*)

The fuel preheater heats up the stream by exploiting the high temperature of the gas exiting the fuel electrode of the stack module. The energy balance of the cold side of the component is very similar to the one considered in the air recovery heat exchanger:

$$\tau_{FRHX} = \sum \dot{n}_{in} \cdot \bar{h}_{in}\left(T_{FUEL}^{in}\right) - \sum \dot{n}_{out} \cdot \bar{h}_{out}(T_{FRHX}^{out}) + \dot{Q}_{HT}^{FRHX}$$

Where:

$\sum \dot{n} \cdot \bar{h}(T)$ represents the contribution of the mass flow in the energy balance; the sum is extended to 5 species: methane, carbon monoxide, carbon dioxide, hydrogen and water; in NG-SOFC mode all are present, while in H2-SOFC mode and SOEC mode only water and hydrogen are considered;

$\dot{Q}_{HT}^{FRHX}$ is the heat transferred by the hot side of the recuperator to the cold stream and it has been evaluated in the same way as for the air preheater by assuming a heat exchanger effectiveness $\epsilon = 0.8$ and knowing the two inlet temperatures of the streams in the component.

➢ REFORMER ELECTRIC HEAT EXCHANGER (*REHX*)

Reactions occurring in the reformer unit are typically highly endothermic, giving a relevant temperature decrease. An excessive decline would mean both a reduced methane conversion in the component and the risk of carbon deposition degrading the catalyst. The reformer electric heater heats up the fuel stream exiting the recuperator in order to maintain a reformer outlet temperature of at least 530 °C (803 K). The control logic is performed by a PID controller, which variates the electric power output between 0 and 3 kW. The component thermal balance is similar to AEHX:

$$\tau_{REHX} \cdot \frac{dT_{REHX}^{out}}{dt} = -\dot{Q}_{losses} + W_{el} + \sum \dot{n}_{in} \cdot \bar{h}_{in}(T_{FRHX}^{out}) - \sum \dot{n}_{out} \cdot \bar{h}_{out}(T_{REHX}^{out})$$

- **REFORMER (*REF*)**

The external pre-reformer unit serves as fuel processing component to change the fuel composition in NG-SOFC mode of operation, while in case of H2-SOFC and SOEC modes of operation the stream crosses the component without undergoing any chemical reactions. Thus, in these configurations the composition of the stream and the temperature remain constant.

In NG-SOFC mode of operation, instead, SMR and WGS reactions occur, shifting the fuel composition to reduce methane and to increase hydrogen content. For concerning the mass balance, the same relations expressed for the stack module are present, with the difference that no electrochemical reactions are present, and the non-linear system is reduced to two equations. Also in this case, the Newton-Raphson method is employed for solving.

The considered thermal balance of the component in the present model is the following:

$$\tau_{REF} \cdot \frac{dT_{REF}^{out}}{dt} = \sum \dot{n}_{in} \cdot \bar{h}_{in}(T_{REHX}^{out}) - \sum \dot{n}_{out} \cdot \bar{h}_{out}(T_{REF}^{out}) - \dot{H}_{SMR} - \dot{H}_{WGS}$$

Where:

$$\dot{H}_{SMR} = \dot{n}_{CH_4}^{react} \cdot \left[\bar{h}_{CO}(T_{REF}^{out}) + 3 \cdot \bar{h}_{H_2}(T_{REF}^{out}) - \bar{h}_{CH_4}(T_{REF}^{out}) - \bar{h}_{H_2O}(T_{REF}^{out})\right];$$

$$\dot{H}_{WGS} = \dot{n}_{CO}^{react} \cdot \left[\bar{h}_{CO_2}(T_{REF}^{out}) + \bar{h}_{H_2}(T_{REF}^{out}) - \bar{h}_{CO}(T_{REF}^{out}) - \bar{h}_{H_2O}(T_{REF}^{out})\right].$$

Both steam methane reforming and water gas shift are evaluated at reformer outlet temperature, since the main part of the reactions occur at this stage.

- **FUEL ELECTRIC HEAT EXCHANGER (*FEHX*)**

The electric heater component in the fuel line shows the same features as the one located in the oxidant line. It differs from it only for the smaller nominal power, which is equal to 1.5 kW. The minimum temperature required at the inlet section of the fuel electrode in the cells of the stack module has been assumed equal to 890 K.

Thus, the thermal balance of the component is:

$$\tau_{FEHX} \cdot \frac{dT_{FEHX}^{out}}{dt} = -\dot{Q}_{losses} + W_{el} + \sum \dot{n}_{in} \cdot \bar{h}_{in}(T_{REF}^{out}) - \sum \dot{n}_{out} \cdot \bar{h}_{out}(T_{FEHX}^{out})$$

Where all the contributions have the same meaning as in the air electric heater balance.

5.3.4 STACK MODULE

The stack module represents the stack of electrochemical cells, in which the reactions occur and electric power is delivered or absorbed. From the modelling point of view, the active control in the subsystem is performed by a PID controller which modulates the air flowrate in order to maintain an adequate level of temperature, close to the nominal value of 1003 K (730 °C).

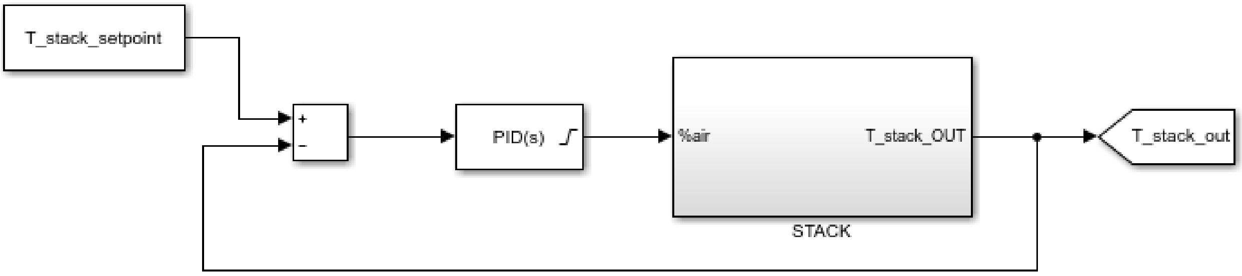

Figure 26 Modelling: Stack module

The main features of the considered polarization model have already been discussed in (5.2) in their general terms. Thus, only the main aspects related to the thermal balance are reported here. From stack temperature and species molar fractions, ASR and OCV are evaluated, while the electric current is calculated from the molar flowrate of reacting hydrogen in the stack. Thus, power and irreversible heat due to overvoltage are evaluated through:

$$\dot{W}_{el} = (OCV \mp ASR \cdot i) \cdot I \qquad [kW]$$

$$\dot{Q}_{irr} = (ASR \cdot i) \cdot I \qquad [kW]$$

The reacting moles per second in the internal reforming and in the cells are evaluated by the Newton-Raphson method as expressed in (5.2.1), as well as the outlet flowrate exiting the fuel electrode of the stack by a simple mass balance. Calling a and b the molar flowrate of reacted methane and carbon monoxide in the internal reforming, the contributions to the thermal balance of the subsystem due to those chemical reactions are:

$$\dot{H}_{SMR} = a \cdot \left[\bar{h}_{CO}(T_{stack}^{out}) + 3 \cdot \bar{h}_{H_2}(T_{stack}^{out}) - \bar{h}_{CH_4}(T_{stack}^{out}) - \bar{h}_{H_2O}(T_{stack}^{out})\right];$$

$$\dot{H}_{WGS} = b \cdot \left[\bar{h}_{CO_2}(T_{stack}^{out}) + \bar{h}_{H_2}(T_{stack}^{out}) - \bar{h}_{CO}(T_{stack}^{out}) - \bar{h}_{H_2O}(T_{stack}^{out})\right];$$

For concerning the electrochemical reaction, the same approach cannot be used. In fact, the enthalpy difference term can be expressed by:

$$\Delta\bar{h} = \Delta\bar{g} + T \cdot \Delta\bar{s} \qquad \left[\frac{kJ}{mol}\right]$$

Where the Gibbs free energy term is associated to the produced power by the stack $\dot{W}_{el}$ by the Nernst equation and it has already been included in the thermal balance: for this reason, only the entropy variation contribution is added for the electrochemical reaction. If c represents the molar flowrate of reacting hydrogen in fuel cell mode, the entropic term is obtained by:

$$\Delta\dot{S}_{HOX} = c \cdot [\bar{s}_{H_2O}(T_{stack}^{out}) - \bar{s}_{H_2}(T_{stack}^{out}) - \frac{1}{2} \cdot \bar{s}_{O_2}(T_{stack}^{out}) - \frac{\bar{R}}{2} \cdot \ln\left(\frac{y_{H_2O}^2}{y_{H_2}^2 \cdot y_{O_2}}\right)].$$

In SOEC mode of operation, the sign of the value can be simply inverted.

Besides the reaction contributions, in the thermal balance also the term due to mass flow is present. For concerning the fuel electrode side, the inlet and outlet molar flowrates of the five considered species have already been expressed. For concerning the oxidant electrode, oxygen is partly consumed in fuel cell modes and formed in electrolyser mode, while nitrogen passes unreacted through the stack. Considering $c\ [mol/s]$ the moles per second of hydrogen reacting (or formed) in the stack, the outlet composition of the oxidant electrode side is:

$$\dot{n}_{O_2}^{out} = \dot{n}_{O_2}^{in} \mp \frac{1}{2} \cdot c \qquad \left[\frac{mol}{s}\right]$$

$$\dot{n}_{N_2}^{out} = \dot{n}_{N_2}^{in} \qquad \left[\frac{mol}{s}\right]$$

The thermal balance is then completed by the term comprising thermal losses to the ambient, for which a value of $\dot{Q}_{losses} = 600\ W$ has been assumed.

Thus, considered thermal balance for the most general case, i.e. NG_SOFC mode of operation, is:

$$\tau_{stack} \cdot \frac{dT_{stack}^{out}}{dt} = -\dot{Q}_{losses} + \dot{Q}_{irr} - W_{el} + \sum_{fe} \dot{n}_{in} \cdot \bar{h}_{in}(T_{FEHX}^{out}) - \sum_{fe} \dot{n}_{out} \cdot \bar{h}_{out}(T_{stack}^{out}) + \sum_{oe} \dot{n}_{in} \cdot \bar{h}_{in}(T_{AEHX}^{out}) - \sum_{oe} \dot{n}_{out} \cdot \bar{h}_{out}(T_{stack}^{out}) - \dot{H}_{SMR} - \dot{H}_{WGS} - T_{stack}^{out} \cdot \Delta\dot{S}_{HOX}$$

In H2-SOFC and SOEC modes of operation, the contribution of SMR and WGS to the thermal balance is null, since no reactions occur.

5.3.5 AFTERBURNER LINE

In this subsystem, two components are evaluated: the hot side of the recovery heat exchanger of the fuel line (*FRHX-H*) and the afterburner (*ABU*) chamber. The stream exiting the fuel electrode part of the stack is recirculated back to preheat the fuel line and then is split into two streams by an ejector: 65% of the inlet stream is delivered back to the mixer line and then to the fuel line, while the remaining 35% is delivered to the afterburner.

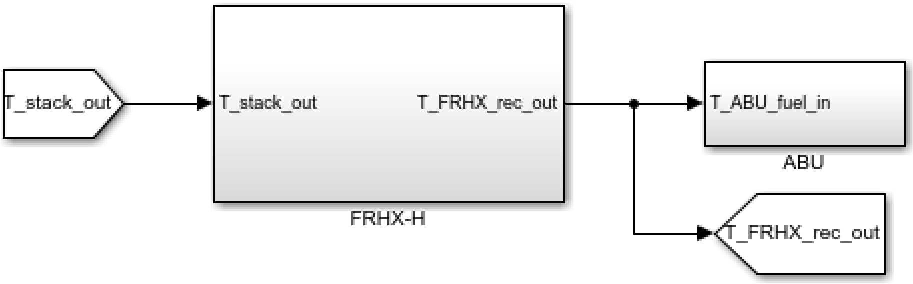

Figure 27 Modelling: Afterburner line

➢ FUEL RECOVERY HEAT EXCHANGER – HOT SIDE (*FRHX-H*)

The description of the thermal balance of the component is basically the same as FRHX, but in this case the transferred heat exits the component. Thus, it is:

$$\tau_{FRHX-H} \cdot \frac{dT_{FRHX-H}^{out}}{dt} = \sum \dot{n}_{in} \cdot \bar{h}_{in}(T_{stack}^{out}) - \sum \dot{n}_{out} \cdot \bar{h}_{out}(T_{FRHX-H}^{out}) - \dot{Q}_{HT}^{FRHX}$$

➢ AFTERBURNER UNIT (*ABU*)

The afterburner is a combustion chamber located after the electrochemical conversion unit in order to exploit the residual energy content of the exhaust gases exiting the anode and cathode ducts of the fuel cell. Usually, it works with high ratio of oxidant to fuel, thus it can be assumed that all fuel is completely utilized, leading to the hypotheses of a combustion efficiency equal to 100%. [43][12]. Therefore, the mathematical model considers that residual methane, carbon monoxide and hydrogen from the fuel electrode of the stack module are completely oxidized in the component by the oxygen coming from the oxidant electrode of the stack module. Thus, the following three reactions proceed to completion:

- $CH_4 + 2O_2 \rightarrow CO_2 + 2H_2O$
- $CO + \frac{1}{2}O_2 \rightarrow CO_2$
- $H_2 + \frac{1}{2}O_2 \rightarrow H_2O$

From the hypothesis of complete combustion, it is possible to directly evaluate the composition of the exit flow, through a simple material balance:

$$\dot{n}_{CH_4}^{out} = 0;$$

$$\dot{n}_{H_2}^{out} = 0;$$

$$\dot{n}_{CO}^{out} = 0;$$

$$\dot{n}_{H_2O}^{out} = \dot{n}_{H_2O}^{in} + 2 \cdot \dot{n}_{CH_4}^{in} + \dot{n}_{H_2}^{in};$$

$$\dot{n}_{CO_2}^{out} = \dot{n}_{CO_2}^{in} + \dot{n}_{CH_4}^{in} + \dot{n}_{CO}^{in};$$

$$\dot{n}_{O_2}^{out} = \dot{n}_{O_2}^{in} - 2 \cdot \dot{n}_{CH_4}^{in} - \frac{1}{2} \cdot \dot{n}_{CO}^{in} - \frac{1}{2} \cdot \dot{n}_{H_2}^{in};$$

$$\dot{n}_{N_2}^{out} = \dot{n}_{N_2}^{in}$$

For concerning the thermal balance, it is given by:

$$\tau_{ABU} \cdot \frac{dT_{ABU}^{out}}{dt} = -\dot{Q}_{losses} + \sum \dot{n}_{in} \cdot \bar{h}_{in}(T_{in}) - \sum \dot{n}_{out} \cdot \bar{h}_{out}(T_{ABU}^{out}) - \dot{H}_{reactions}$$

Where:

$\dot{Q}_{losses}$ is the term associated to the rate of heat dispersed to the environment;

$\sum \dot{n} \cdot \bar{h}(T)$ represents the contribution of the mass flow and are evaluated as the sum of the seven compounds considered in the mass balance (CH_4, CO, CO_2, H_2, H_2O, O_2 and N_2), while the molar enthalpy is calculated at the inlet temperature (equal to the stack exit for oxidant species and equal to the recuperator exit for the fuel ones) and at the outlet temperature, which is evaluated by the differential equation in a dynamic way;

$\dot{H}_{reactions}$ represents the rate of heat due to the three combustion reactions considered in the model, calculated as the product of the reacted moles of the species per the specific enthalpy variation of the reactions (evaluated at the outlet temperature):

$$\dot{H}_{CH_4} = \dot{n}_{CH_4}^{in} \cdot \left[\bar{h}_{CO_2}(T_{ABU}^{out}) + 2 \cdot \bar{h}_{H_2O}(T_{ABU}^{out}) - \bar{h}_{CH_4}(T_{ABU}^{out}) - 2 \cdot \bar{h}_{O_2}(T_{ABU}^{out})\right]$$

$$\dot{H}_{CO} = \dot{n}_{CO}^{in} \cdot \left[\bar{h}_{CO_2}(T_{ABU}^{out}) - \bar{h}_{CO}(T_{ABU}^{out}) - 0.5 \cdot \bar{h}_{O_2}(T_{ABU}^{out})\right]$$

$$\dot{H}_{H_2} = \dot{n}_{H_2}^{in} \cdot \left[\bar{h}_{H_2O}(T_{ABU}^{out}) - \bar{h}_{H_2}(T_{ABU}^{out}) - 0.5 \cdot \bar{h}_{O_2}(T_{ABU}^{out})\right]$$

$$\dot{H}_{reactions} = \dot{H}_{CH_4} + \dot{H}_{CO} + \dot{H}_{H_2}$$

5.3.6 MIXER LINE

The mixer line subsystem represents the physical mixing between the recirculated stream coming from the splitter and the stream of fresh fuel or steam provided from outside in order to supply the electrochemical reactions. The resulting stream exiting the mixer is delivered to the fuel line, where it passes through FRHX, REHX, REF and FEHX before entering the stack.

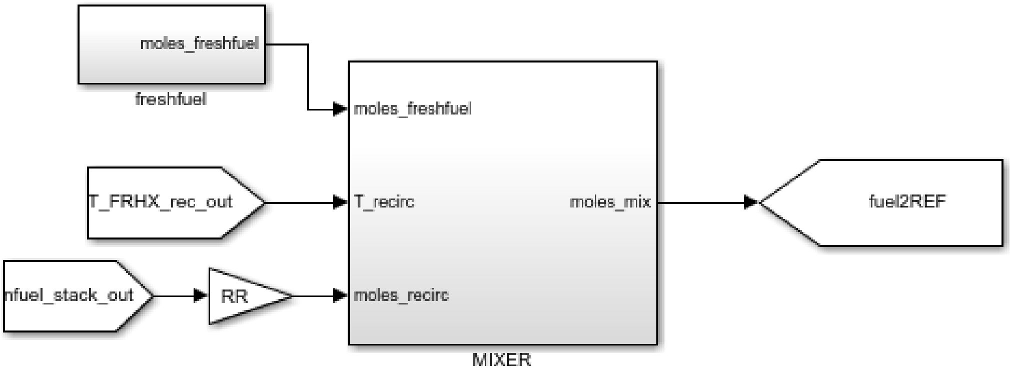

Figure 28 Modelling: Mixer line

The energy balance applied on the subsystem is simply characterized by the terms related to the mass flow, having 2 inlet streams and 1 outlet stream. Since the recirculated stream is assumed to enter the subsystem at T_{rec}, while the fresh fuel stream is assumed to be provided at T_{fresh}, the resulting thermal balance in the mixer line is:

$$\tau_{MIXER} \cdot \frac{dT_{MIXER}^{out}}{dt} = \sum_{rec} \dot{n}_{in} \cdot \bar{h}_{in}(T_{rec}) + \sum_{fresh} \dot{n}_{in} \cdot \bar{h}_{in}\left(T_{fresh}\right) - \sum_{out} \dot{n}_{out} \cdot \bar{h}_{out}(T_{MIXER}^{out})$$

Where the outlet molar flowrates $\dot{n}_{out}$ are computed for each chemical species by a simple mass balance. Since only one species for each configuration mode is considered to be present in the fresh fuel stream (methane in NG-SOFC mode, hydrogen in H2-SOFC mode and steam in SOEC mode), the resulting outlet stream composition is the same of the recirculated flow except for that species, for which the sum of the two flowrates is done.

5.3.7 EXHAUST GAS LINE

In the exhaust gas line subsystem, the outlet stream exiting the afterburner is cooled down in two stages to reach an adequate temperature condition to be released in atmosphere. In the first stage the hot stream is used to preheat inlet air in ARHX; then the residual heat value contained in the exhaust gases is exploited to heat up a pressurized water stream which is used for heat demand needs of EnviPark.

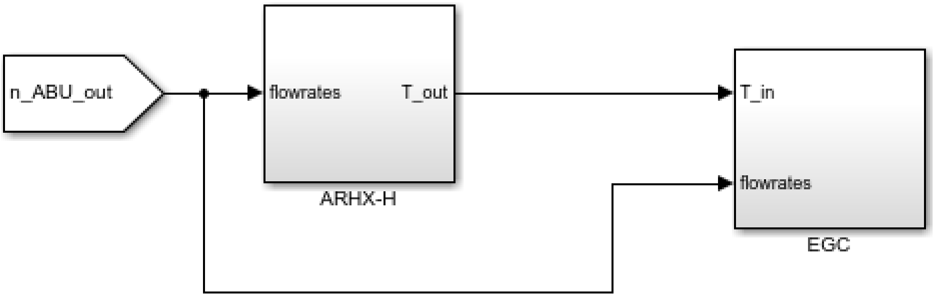

Figure 29 Modelling: Exhaust gas cooling line

- **AIR RECOVERY HEAT EXCHANGER – HOT SIDE (*ARHX-H*)**

It considers the hot side of the air recovery heat exchanger: the inlet stream is constituted by the hot exhaust gas coming from the afterburner after the combustion, while the outlet colder stream is delivered to the heat gain section.

The considered thermal balance is:

$$\tau_{ARHX-H} \cdot \frac{dT_{ARHX-H}^{out}}{dt} = \sum \dot{n}_{in} \cdot \bar{h}_{in}(T_{ABU}^{out}) - \sum \dot{n}_{out} \cdot \bar{h}_{out}(T_{ARHX-H}^{out}) - \dot{Q}_{HT}^{ARHX}$$

- **EXHAUST GAS CONVERSION (*EGC*)**

Hot gases exiting the previous component are cooled down until $T_{exhaust}^{out} = 473\ K$ (200 °C) and then released into atmosphere. A PID controller is used to modulate heat valorization water flowrate for having the desired exhaust gas temperature in the outlet section. The efficiency of the component has been considered $\epsilon = 0.7$.

$$\tau_{EGC} \cdot \frac{dT_{exhaust}^{out}}{dt} = \sum \dot{n}_{in} \cdot \bar{h}_{in}(T_{ARHX-H}^{out}) - \sum \dot{n}_{out} \cdot \bar{h}_{out}(T_{exhaust}^{out}) - \dot{Q}_{HT}^{EGC}$$

5.3.8 EVAPORATOR LINE

This subsystem is used only in SOEC mode of operation to allow the phase change of liquid water at ambient temperature into steam, which enters the fuel line subsystems and then the stack module. Outlet temperature must be enough to have steam conditions and a value of 400 K has been assumed. Heat is provided by an electric heater with rated power of 3 kW.

The considered thermal balance in the subsystem is similar to other electric heaters:

$$\tau_{EVA} \cdot \frac{dT_{EVA}^{out}}{dt} = -\dot{Q}_{losses} + \dot{W}_{el} + \sum \dot{n}_{in} \cdot \bar{h}_{in}(T_{water}) - \sum \dot{n}_{out} \cdot \bar{h}_{out}(T_{EVA}^{out})$$

5.4 MODIFICATIONS FOR LOW LOAD

The above dynamic model was created for normal load conditions, i.e. when the power output in SOFC and power input in SOEC mode of operation is high, but some relevant modifications are needed for describing peculiar lower load operating conditions. For electrolyser mode, additional constraints related to endothermic conditions are present too.

5.4.1 SOFC MODES OF OPERATION

While in normal conditions the inlet fuel stream basically follows the load in a linear way, at low power values this is not typically done, for safety reasons. In fact, too low hydrogen flowrate would mean higher possibility of fuel starvation, giving dramatically degradation of the stack. For avoiding it, typically fuel flowrate has maintained at a fixed constant level. In this work the threshold has been set to 30% of the maximum power output for SOFC modes of operation: while for higher power values the control logic on the inlet fresh fuel flowrate was the one expressed in (5.3.1), for lower values a fixed constant value of “equivalent hydrogen” is set equal to the one corresponding to the 30% conditions. Therefore, fuel utilization factor is not a input in this configuration, but it is computed inside the model.

In *Figure30* the fuel flowrate profile at various power output conditions is given as resulted from the dynamic model simulations.

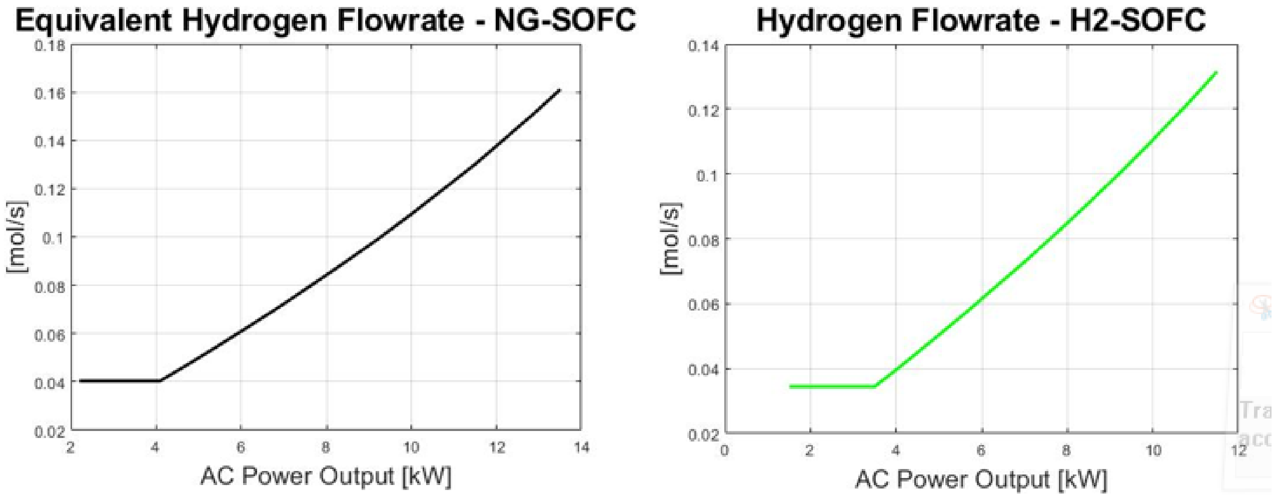

Figure 30 Modelling: Fresh fuel flowrate depending on SOFC power

For similar reasons, also the minimum air flowrate has been set constant to the 30% power conditions. Consequently, stack temperature cannot be managed in the same way as in normal conditions and a different choice must be made. To this end, AEHX and FEHX control logic is modified. While at high power levels two PID controllers modulate power delivered by the electric heaters in order to guarantee a minimum value in the oxidant line (830 K) and in fuel line (890 K) stream before entering the stack, for low-load configuration they variate the output to maintain nominal temperature in the stack. Since at partial load the exothermicity of the electrochemical reaction reduces, basically stack inlet temperature of the streams, given by the PID controllers, must increase.

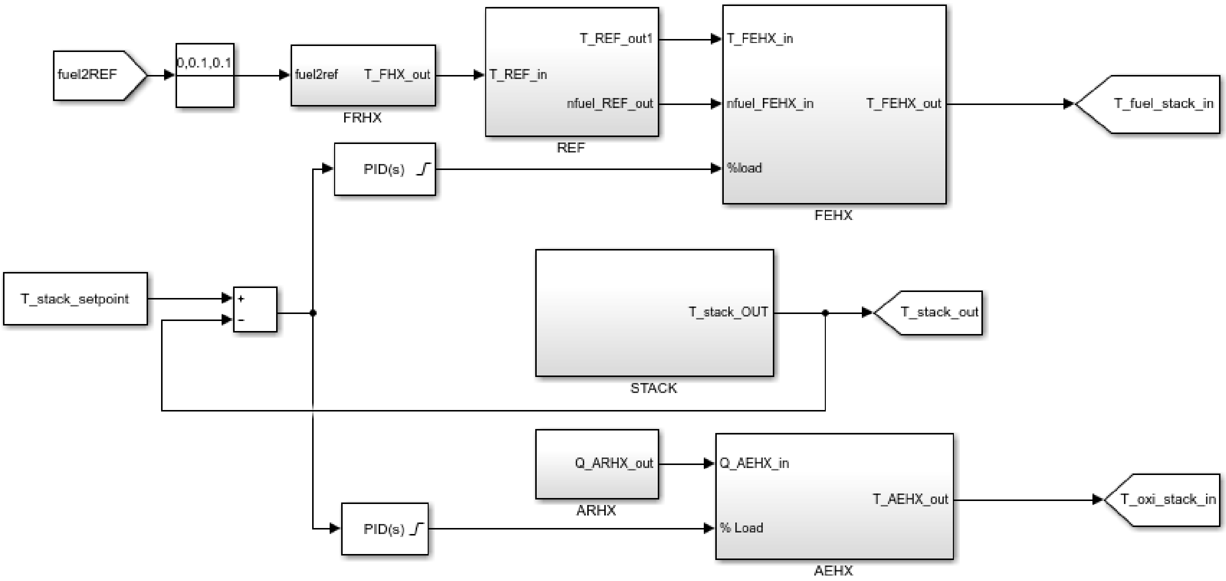

Figure 31 Modelling: SIMULINK© worksheet for low load in SOFCs

For NG-SOFC mode of operation, two additional variations are performed:

- **AFTERBURNER UNIT (*ABU*)**

Since a higher quantity of fuel species passes the stack module unreacted, the combustion reactions occurring in the afterburner unit can release a large amount of heat, with the possibility of excessively increasing the temperature. Thus, an additional fresh air stream taken from the ambient has been assumed to be injected to the combustor for avoiding thermal stresses on materials. The air flowrate is modulated by another PID controller, whose input is the afterburner temperature, for which a maximum value of 1323 K has been chosen. The inlet air has been assumed to be compressed by the blower and then delivered to the combustor.

The same modification has been done on H2-SOFC mode of operation, but additional air was not used due to lower afterburner temperature.

- **EVAPORATOR LINE**

At extremely low load condition, hydrogen conversion into steam is reduced. Consequently, gas exiting the fuel electrode would be constituted by high shares of methane, carbon monoxide and hydrogen and limited amount of steam. This can be a problem since the two reactions occurring inside the reformer needs steam. In the absence of it, they would not occur or would be reversed. For avoiding this situation, below 2.1 kW power output an increasing amount of steam is externally added together with fresh natural gas. The steam is obtained in the evaporator subsystem, taking into account power consumption of the electric heater.

5.4.2 SOEC MODE OF OPERATION

As said, electrolyser operating points show different thermal conditions: at high power the stack module is exothermic, at low power it is endothermic and between them a thermoneutral point exists. In this work, three models have been created in order to simulate the system behavior in different conditions. The one described in part (5.3) refers to exothermic conditions; the changes operated in the other two models are here described.

Below 50 kW net power input, stack inlet temperature equal to 830 K for air and 890 K for the steam-hydrogen mixture cannot be sustained, as occurs in SOFCs. However, differently from the other modes, also the air flowrate stack thermal control can be employed. In fact, inlet air does not provide reactants but is used both for thermal control and as a sweep gas. For modelling simplicity reason, in this case the air inlet temperature has been assumed and the stack temperature is managed by the PID controllers for air flowrate and fuel electrode inlet temperature. The assumption on the air temperature set point at stack inlet section has been done after some attempts, also considering not to have excessively high value.

The third model refers to very low power input conditions. The only change with respect to the previous configuration is in fresh steam flowrate, which, as in SOFC modes, it has been maintained fixed constant. The threshold value has been set to 12 kW net input power, which corresponds to around 25% of the maximum power condition referring to the AC gross power, which considers also ancillary system power consumption.

6. MODELLING RESULTS – steady-state simulations

6.1 WORKSHEET

The dynamic model previously explained has been tested in steady-state conditions in the three modes of operation. The power output (in SOFC) or input (in SOEC) in the electrochemical calculator block has been maintained fixed constant and each simulation has been carried on for a time large enough to reach steady-state conditions from the arbitrarily taken initial values at time zero of the simulation. Fifteen simulations for each mode have been performed at different power level. The resulting values of the main quantities are resumed in *Table8-9-10*. From them, interesting considerations can be made and are discussed below.

Some of the quantities included in the tables needs a definition.

The power required by auxiliaries is expressed as $\dot{W}_{el}^{AUX}$ and includes the contribution of the four electric heaters (present in the evaporator unit, upward and downward the reformer and in the oxidant line), the air blower and the hydrogen compressor in SOEC mode. Power input required by the compressors have been evaluated as:

$$\dot{W}_{compr} = \dot{m} \cdot c_p \cdot \frac{T_i}{\eta_c} \cdot \left[\left(\frac{p_o}{p_i} \right)^{\frac{\gamma-1}{\gamma}} - 1 \right] \qquad [kW]$$

The net power output in SOFCs and gross power input in SOEC have been defined as the difference and the sum respectively of the AC electric power interacting with the stack in the electrochemical calculator block and the power required by the auxiliaries:

$$\dot{W}_{el}^{net} = \dot{W}_{el}^{AC} - \dot{W}_{el}^{AUX} \qquad [kW]$$

$$\dot{W}_{el}^{gross} = \dot{W}_{el}^{AC} + \dot{W}_{el}^{AUX} \qquad [kW]$$

For SOFCs, two efficiency values are expressed. The first is the electrical efficiency of the device, defined on LHV basis as (for H2-SOFC):

$$\eta_{el} = \frac{\dot{W}_{el}^{AC} - \dot{W}_{el}^{aux}}{\dot{V}_{H_2} \cdot LHV_{H2}} = \frac{\dot{W}_{el}^{net}}{\dot{V}_{H_2} \cdot LHV_{H2}}$$

Where $\dot{V}_{H_2}$ is the volumetric inlet hydrogen flowrate of fresh fuel in the system and $LHV_{H_2} = 10.8\ [MJ/Nm^3]$ has been taken from [44] (for NG-SOFC, $LHV_{CH_4} = 35.9\ [MJ/Nm^3]$).

The second one is the global efficiency and includes the contribution of the recovered heat from the exhaust gas, too.

$$\eta_g = \frac{\dot{W}_{el}^{net} + \dot{Q}_{HR}}{\dot{V}_{H_2} \cdot LHV_{H2}}$$

For SOEC mode of operation, three efficiencies have been defined.

The first two are the conversion efficiencies, defined as the ratio between the energy content of the produced hydrogen (expressed in HHV terms, with $HHV_{H_2} = 12.8\ [MJ/Nm^3]$, taken from [44]) and the employed power in the electrolyser to produce it. Recognizing that the hydrogen compressor constitutes a large share of the inlet power and since it is not directly part of the device (in principle hydrogen could be used as exits the electrolyser and without needing compression), the second conversion efficiency, η_{conv}^*, has been calculated truncating the contribution of the hydrogen compressor. Then, a global efficiency including also the recovered heat is expressed.

$\dot{W}_{el}^{AC}$	FU	AU	V_{cell}	I	$\dot{W}_{el}^{aux}$	$\dot{W}_{el}^{net}$	$\dot{Q}_{HR}$	$\dot{V}_{H_2}$	η_{el}	η_g
$[kW]$	$[-]$	$[\%]$	$[V]$	$[kA]$	$[kW]$	$[kW]$	$[kW]$	$[l/s]$	$[\%]$	$[\%]$
2.2	0.327	11.0	0.96	2.5	2.0	0.2	3.3	0.13	4.5	75.2
2.5	0.378	12.8	0.94	2.9	1.7	0.8	3.0	0.13	15.3	76.0
3	0.465	15.7	0.92	3.6	1.5	1.5	2.7	0.15	27.1	76.0
3.5	0.555	18.7	0.90	4.3	1.2	2.3	2.3	0.16	38.0	76.6
4.1	0.665	22.5	0.88	5.2	0.9	3.2	1.9	0.18	48.3	77.1
4.8	0.665	20.4	0.87	6.1	1.1	3.7	2.4	0.21	47.6	78.0
5.5	0.665	18.9	0.86	7.1	1.3	4.2	2.9	0.24	46.9	79.6
6.2	0.665	17.7	0.85	8.1	1.5	4.7	3.4	0.28	46.1	79.1
7	0.665	16.6	0.84	9.3	1.7	5.3	4.0	0.32	45.2	79.4
8.5	0.665	15.0	0.82	11.6	2.1	6.4	5.3	0.40	43.5	79.8
9.2	0.665	14.4	0.81	12.7	2.3	6.9	6.0	0.43	42.7	79.9
10	0.665	13.7	0.79	14.0	2.6	7.4	6.8	0.48	41.7	79.9
11.5	0.665	12.6	0.77	16.7	3.1	8.4	8.5	0.57	39.7	79.8
12.8	0.665	11.7	0.74	19.2	3.6	9.2	10.1	0.66	37.8	79.6
13.5	0.665	11.1	0.73	20.7	4.1	9.4	11.2	0.71	36.1	78.9

Table 8 NG-SOFC steady-state worksheet

$\dot{W}_{el}^{AC}$	FU	AU	V_{cell}	I	$\dot{W}_{el}^{aux}$	$\dot{W}_{el}^{net}$	$\dot{Q}_{HR}$	$\dot{V}_{H_2}$	η_{el}	η_g
$[kW]$	$[-]$	$[\%]$	$[V]$	$[kA]$	$[kW]$	$[kW]$	$[kW]$	$[l/s]$	$[\%]$	$[\%]$
1.5	0.262	4.4	0.96	1.7	1.4	0.1	3.2	0.40	2.3	76.2
2	0.357	6.0	0.94	2.4	1.3	0.7	3.0	0.45	15.4	77.2
2.5	0.456	7.7	0.92	3.0	1.1	1,4	2.8	0.50	27.0	78.6
3	0.559	9.4	0.90	3.7	0.8	2.2	2.6	0.55	37.2	80.2
3.5	0.665	11.3	0.88	4.4	0.5	3.0	2.3	0.60	46.5	82.0
4	0.665	10.7	0.87	5.1	0.6	3.4	2.8	0.69	45.6	82.6
4.8	0.665	10.1	0.86	6.2	0.8	4.0	3.5	0.84	44.2	83.1
5.5	0.665	9.6	0.85	7.2	1.0	4.5	4.3	0.98	42.9	83.2
7	0.665	8.8	0.83	9.3	1.5	5.5	5.9	1.28	40.1	83.0
7.8	0.665	8.5	0.82	10.6	1.8	6.0	6.9	1.44	38.6	82.7
8.5	0.665	8.2	0.81	11.7	2.1	6.4	7.8	1.59	37.2	82.4
9.2	0.665	8.0	0.80	12.8	2.4	6.8	8.8	1.75	35.7	82.0
10	0.665	7.7	0.78	14.2	2.9	7.1	9.9	1.94	34.0	81.5
10.8	0.665	7.4	0.77	15.6	3.4	7.4	11.2	2.13	32.2	80.9
11.5	0.665	7.2	0.76	16.9	3.9	7.6	12.4	2.31	30.6	80.3

Table 9 H2-SOFC steady-state worksheet

$\dot{W}_{el}^{AC}$	SC	V_{cell}	I	$\dot{W}_{el}^{aux}$	$\dot{W}_{el}^{gross}$	$\dot{Q}_{HR}$	$\dot{V}_{H_2}$	η_{conv}	η_{conv}^{*}	η_g
$[kW]$	$[-]$	$[V]$	$[kA]$	$[kW]$	$[kW]$	$[kW]$	$[l/s]$	$[\%]$	$[\%]$	$[\%]$
0.1	0.004	0.76	0.11	5.7	5.8	1.3	0.014	2.5	2.6	24.3
1	0.04	0.87	1.0	6.9	7.9	1.3	0.12	16.4	17.4	32.8
4	0.15	1.00	3.6	8.9	12.9	1.1	0.42	35.0	39.5	43.7
6	0.24	1.06	5.1	9.6	15.6	1.1	0.59	40.8	47.1	47.8
8	0.36	1.11	6.5	10.2	18.2	1.1	0.75	44.8	52.4	51.0
10	0.50	1.14	7.9	10.7	20.7	1.2	0.91	47.6	56.3	53.4
12	0.70	1.17	9.2	11.2	23.2	1.3	1.07	49.7	59.3	55.4
15	0.70	1.20	11.3	12.1	27.2	1.4	1.31	52.0	62.6	57.2
20	0.70	1.23	14.6	13.7	33.7	1.6	1.70	54.5	66.3	59.3
30	0.70	1.27	21.3	16.6	46.6	2.1	2.48	57.3	70.8	61.7
40	0.70	1.29	27.9	19.6	59,6	2.5	3.25	58.8	73.4	63.1
45	0.70	1.32	30.8	19.1	64.1	2.7	3.57	60.1	75.4	64.2
50	0.70	1.35	33.4	16.6	66.6	2.2	3.88	62.9	79.9	66.3
60	0.70	1.40	38.7	21.0	81.0	4.6	4.50	59.9	75.1	65.6
70	0.70	1.44	43.7	25.8	95.8	7.5	5.07	57.1	70.8	64.9

Table 10 SOEC steady-state worksheet

In order to create a continuous definition of the operating range of the device from the discrete operating points collected in the previous tables, the obtained values have been used to create trendlines as a function of output (or input) AC power by best fitting curves. In the following figures, the graphical representation of the discrete values as well as the considered trendline that will be used in (6.2) are provided.

First consideration is on the SOFCs electrical efficiencies, represented in *Figure32*. As it was expected, in general terms electrical efficiency is higher in NG-SOFC than in H2-SOFC mode. However, this behavior can be seen especially at high loads, where the difference between the two values increases, while it has an opposite trend at low loads, where H2-SOFC would be preferable. This result is certainly also a consequence of the assumptions made in the model, i.e. same fuel utilization factor for both modes and fuel inlet flowrate fixed constant to a minimum value for low loads. In particular, the shift in the electrical efficiencies occurs at AC power output of around 4 kW, where H2-SOFC works in normal operation while NG-SOFC already in low-load operation. However, the resulting trend can provide some relevant indications.

Electrical efficiency depends on the energy content inside the feeding fuel and on the ancillary power required by auxiliaries. For concerning the first term, it results always higher for hydrogen than for natural gas. For concerning the auxiliary power, instead, at higher power it is lower for NG-SOFC but at around 8.5 kW the situation is the opposite. In Figures the representation of the overall ancillary power and the contributions of the three electric heaters is given for the two SOFC modes of operation. The complementary term is constituted by the required power for driving the air blower, which depends on the air flowrate.

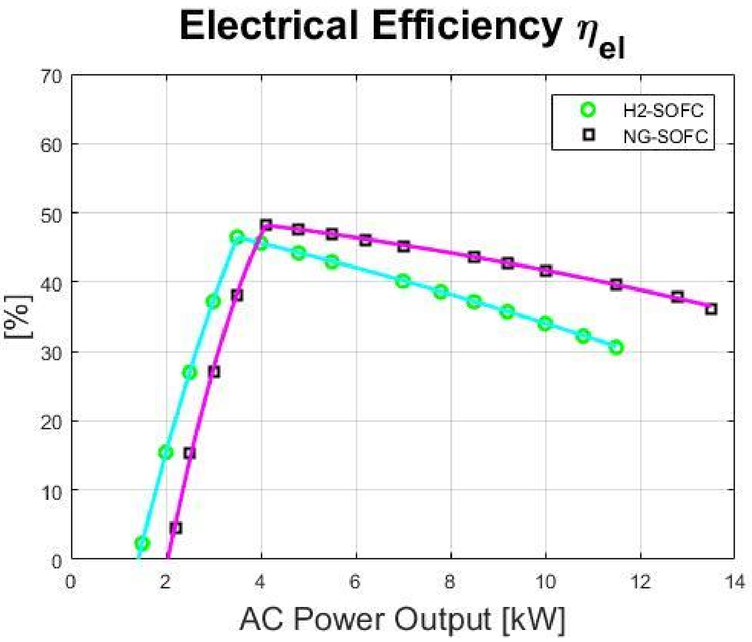

Figure 32 Results: SOFC electrical efficiency

In NG-SOFC mode of operation the endothermic steam methane reforming reaction occurring inside the stack in the internal reformer section counterbalances the exothermic electrochemical reaction of hydrogen and facilitates thermal management. For this reason, a smaller quantity of cooling air is required, giving to high air utilization factors as well as a smaller power consumption for air blower. Moreover, this results also in the absence of need to use air electric heater for a wide range of operating points, since the air recuperator provides heat enough to increase the temperature of the oxidant stream entering the stack above the minimum value of 830 K. Thus, the most relevant term in this configuration is constituted by the reformer electric preheater.

However, at low loads the trend is inverted. Since the exothermic electrochemical reaction provides a small amount of heat, the endothermic steam methane reforming can make endothermic the stack unit even in SOFC mode of operation. Thus, in these conditions the air electric heater is needed to increase the temperature even higher than the stack value, causing a rise in electric consumption. At the same time, the reformer electric heater is no more used, probably due to changes in the composition of the fuel mixture due to the low-load mode of operation, which are responsible for a reduction of the reforming conversion. The fuel electric heat exchanger, instead, shows a quite constant behavior in all the operating range.

A contrary behavior can be seen in H2-SOFC mode of operation. In this case, almost the entire ancillary power is employed in the oxidant line, both for compressing the stream in the air blower and to heat it up before entering the stack. Since the air electric heater is characterized by the highest rated power, at high load the H2-SOFC auxiliary power is higher than for NG-SOFC at the same output power. In the fuel line no power consumption is present, because the heat transfer occurring in the fuel recuperator is in general enough to have a minimum temperature of 890 K at the stack inlet.

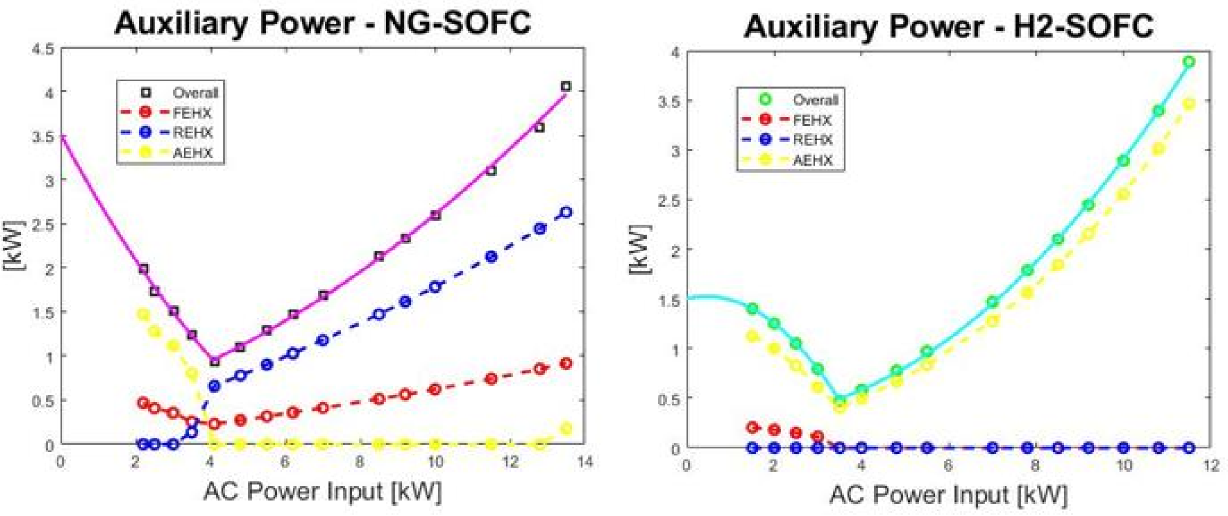

Figure 33 Results: SOFC ancillary power consumption

In SOEC mode of operation, power consumption due to hydrogen compressor is definitely the most relevant, especially at high loads and shows a quite linear trend depending on AC input power to the stack (*Figure34*). The overall auxiliary power term has instead a not uniform profile. The minimum value is reached at around 50 kW, where the transition between the model occurs. At higher input power, heat released by transport effects are much higher than heat required by the endothermic reaction of steam conversion and the stack is in exothermic conditions, needing a large amount of cooling air. This causes higher power consumption in the oxidant line, as occurs for H2-

SOFC. At 50 kW, maintaining the inlet streams in the stack at 830 and 890 K respectively, the amount of cooling air is very low, thus reducing the power consumption.

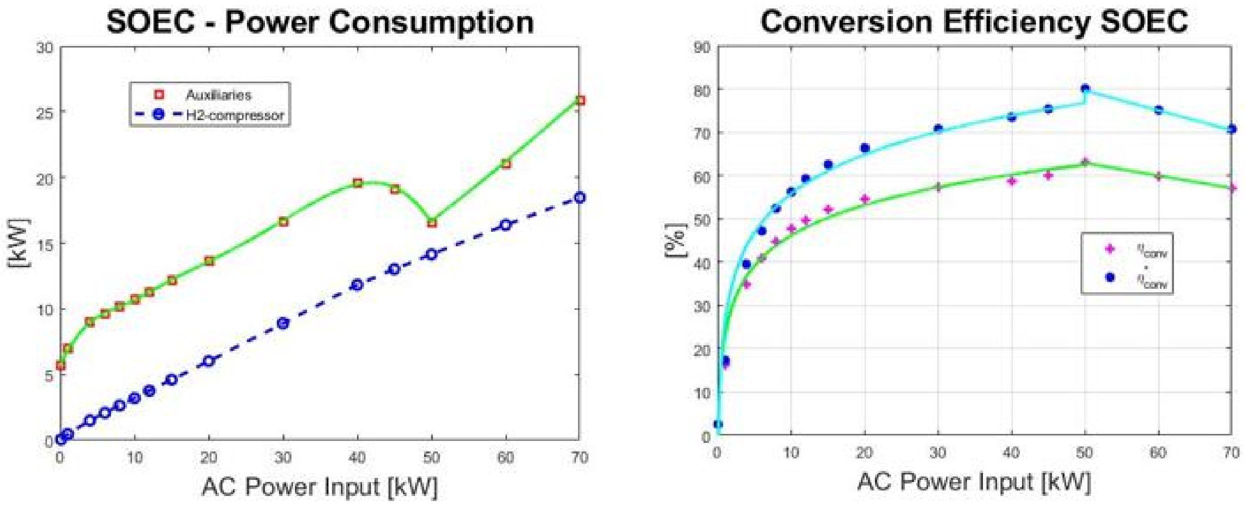

Figure 34 Results: SOEC ancillary power consumption

At low load the thermal condition of the stack is endothermic and inlet flows of steam and air must be provided at higher temperature with respect to the stack. For this reason, the electric heaters contribution results higher than the hydrogen compression term. Since in extremely low power input conditions the electrochemical reaction too needs low heat, in these points the temperature of the stack in steady-state conditions remains constant to desired 1003 K. At power levels between 5 and 30 kW, however, the endothermic term is too large to be satisfied by the auxiliaries and the steady-state temperature of the stack decreases to reach a minimum of around 930 K at 8 kW (*Figure35*). Thus, these operating points are expected to occur only for short time in transient conditions.

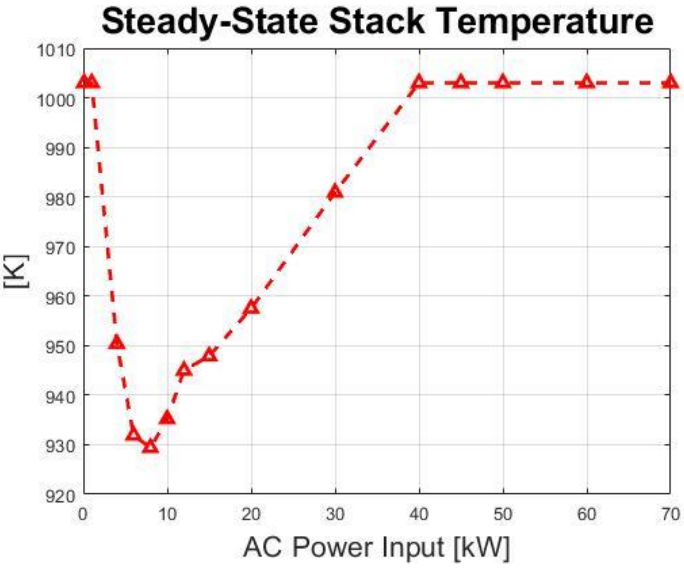

Figure 35 Results: SOEC stack temperature

The thermoneutral point is located at around 45 kW. The electrical consumption is slightly higher with respect to 50 kW-case, due to the higher inlet temperature of the streams in the stack. Probably, the transition between the simulation models used in this work for SOEC has been excessively sharp and a more uniform behavior would be obtained.

For concerning the conversion efficiency, the resulting distribution may be approximated as a logarithmic term in endothermic conditions of the stack, while it decreases with hydrogen production in exothermic conditions.

Heat constitutes a r-SOC by-product in all three modes of operation. In SOFC modes of operation the main trend is higher the power output higher the heat gain. Heat is recovered in a heat exchanger from the exhaust gases at high temperature exiting the afterburner unit after passing the air recuperator, where temperature decreases to between 630 and 700 K depending on the used fuel and operating point. Although at medium power output exhaust gases temperature is in general higher, the stream flowrate is significantly lower, because less fuel is needed and moreover less cooling air is requred. Therefore, since in hydrogen operation more air is used, heat recovery in H2-SOFC is higher.

In low-loads conditions, instead, an opposite behavior can be seen, because approximatively the same flowrate is used, but a higher amount of fuel species is present in the combustor, causing an increase in the exhaust gas temperature, whose effect prevails.

The situation is just the reverse with respect to power generation and electrical efficiency of the device. Indeed, considering the global efficiency, which accounts for the contribution of both power and heat, H2-SOFC shows a slightly superior values with respect to NG-SOFC.

In SOEC mode heat is recovered from the gas exiting the oxidant electrode of the stack. For this reason, even when the stack operates in endothermic conditions, an amount of heat can be exploited. This quantity shows a quite constant behavior at very low power input, and it is slightly increasing towards thermoneutral point. In exothermic conditions, the available heat significantly increases.

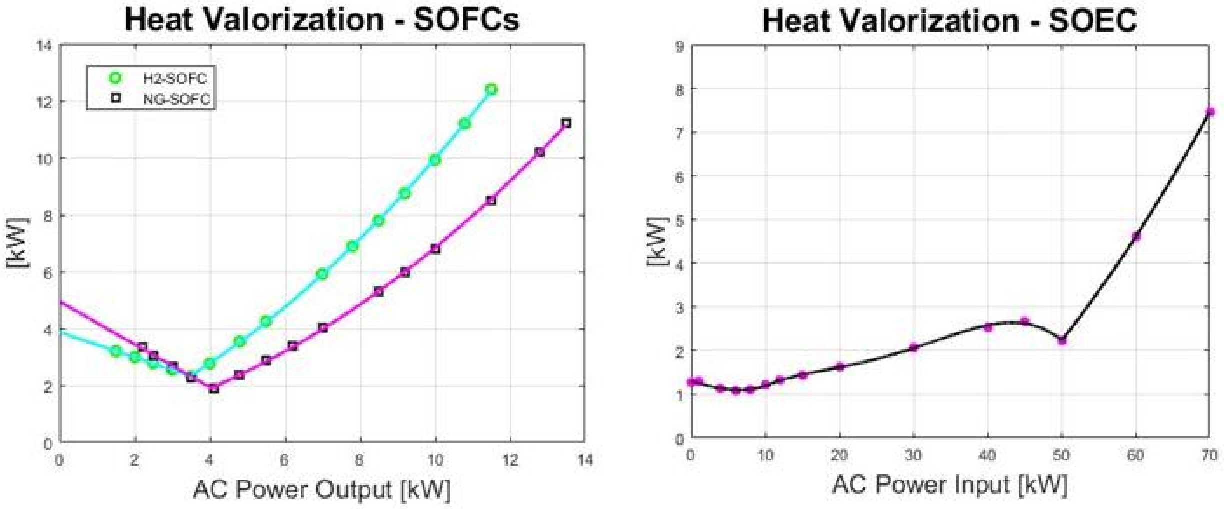

Figure 36 Results: Heat valorisation

6.2 ANNUAL SIMULATION

In part (4) hour-resolution annual energy profile of PV and hydro power plant located in EnviPark have been obtained, as well as the considered power and heat demand of building C, where the r-SOC system will be installed. In part (5) the dynamic model of the stack and BOP r-SOC system has been constructed and in part (6.1) that model has been validated through a discrete set of steady-state simulations for the three configurations at various load. In this section of the work the two parts are combined in order to perform an annual simulation of the entire system, constituted by the integration of the r-SOC plant in the EnviPark scenario. The simulation is set as a succession of steady-state r-SOC operating points during the year, with a time step of one second.

6.2.1 DESCRIPTION OF THE MODEL

The concerned microgrid can be schematized as in *Figure37*.

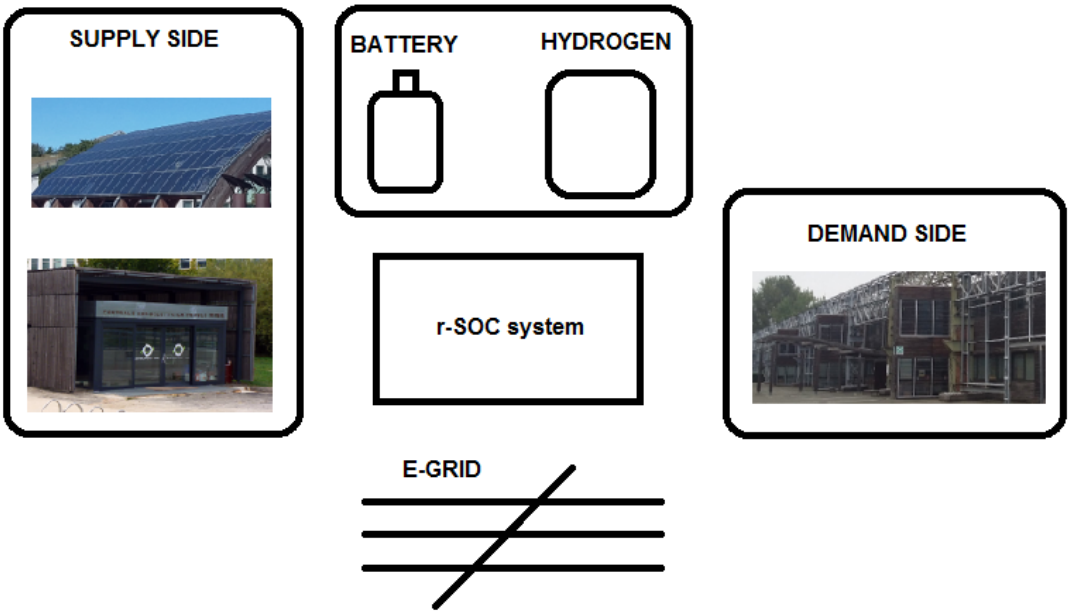

Figure 37 Annual simulation: rSOC microgrid

For each hour of the year, the difference between the power provided by the supply side and the power required by the offices in the demand side has been calculated, in order to evaluate the net power available (surplus) or necessary (deficit) by the system. Since the time of simulation of the dynamic model in Simulink is the second, the resulting hourly load has been linearly expanded to that time step. In this way, a schedule of 31 536 000 (8760 hours per year multiplied by 3600 seconds per hour) instantaneous net power values have been obtained.

Today, typically electricity grid is used to manage surplus and deficit: when power generated by renewables exceeds the power consumption of the users, it is delivered to the grid, while when the opposite situation occurs power is required from the grid. The integration of the r-SOC system and electricity storage means as battery and hydrogen vessel opens up various possibilities and the necessity to determine the operating conditions of the system.

More precisely, in this study the main priority is given to the battery unit. Thus, if in a certain moment a surplus of power is present and the battery is not fully charged, the power is delivered to the battery and not used to feed the electrolyser. On the other hand, if in a certain moment a deficit of power is present and the state of charge is not null, the required power is provided by the battery until it is not completely discharged.

The presence of the battery unit makes it necessary to choose the r-SOC mode of operation in periods when a flow to or from battery is present. Two options may be selected in the concerned system. The first one is the "hot stand-by" mode, which means to switch off the stack when battery is on and exploiting the thermal inertia of the stack not to excessively decrease its temperature. The second one, which is possible in the concerned plant, where natural gas is taken from the gas grid, is to work in NG-SOFC mode of operation and the generated power is delivered to electricity grid. Since high-temperature electrochemical devices are characterized by slower dynamicity with respect to low-temperature ones, in this work only the second option has been considered.

The hydrogen vessel, which constitutes the other energy storage technology, has the second priority. It means that in case of energy surplus and state of charge of the battery equal to 100%, the r-SOC system works in SOEC mode if the storage tank is not already full of 12 kg of compressed hydrogen. On the other hand, until a quantity of hydrogen is present in the vessel and power demand to the users is present, the r-SOC system works in H2-SOFC mode. As before, in all the other conditions the system is in NG-SOFC mode of operation in order not to switch off the device.

Another peculiar case occurs when the power surplus from the renewables is lower than 5.8 kW. As it has been seen in the steady-state worksheet for SOEC, it is the minimum power required by the electrolyser for start working, due to the presence of the auxiliary devices. Therefore, also when this condition is present, the system works in NG-SOFC mode.

The electricity grid connection of the system guarantees the possibility of exchange power with it in case of need. More precisely, power is delivered to the grid in the following two cases:

1. SOEC mode of operation: if power surplus is higher than maximum power of the electrolyser, the device works at highest power and the difference is sold to the grid;
2. NG-SOFC mode of operation: in all the cases in which this configuration is in operation in alternative to the hot stand-by, i.e. when battery is working, when surplus power is present but the hydrogen tank is full and if the power surplus is less than 5.8 kW.

Instead, power is required from the grid in the case the power demand exceeds the output power from the r-SOC operating in NG-SOFC or H2-SOFC.

Because of the way of construction of the load profile as a second-resolution linear trend among hourly values, no excessively fast variations are present in the simulation for the load following. For concerning the shifts between two modes of operation, a 5-minutes time has been assumed for changing the gases feeding the system. In this period, the power input and output of the stack have been considered zero. After the shift, the r-SOC load ramps up to reach the instantaneous load and, as in [16], the ramp slope has been assumed to be equal to 5% of the maximum load per minute in all the three modes of operation. Thus, time required to switch mode of operation and to arrive to maximum point of operation is 25 (5+20) minutes. In that time, in case of power surplus the difference between the available electricity and the required one by the electrolyser in its ramp up is delivered to the grid; in the same way, in case of power deficit the difference between the required electricity to the users and the provided one by the fuel cell is taken from the grid.

Performance of the r-SOC system clearly depends on the characteristics of supply and demand side to which it interacts. The electrochemical device uses the surplus power provided by local renewables and partly serves heat and power demands of a specific building of the Park. Four cases of interactions have been studied by the annual simulation model previously explained. They basically represent a different combination of shares of renewable supply and power demand, as expressed in *Figure38*. The most relevant results are discussed for the four cases in order to qualitatively and quantitatively evaluate the different approaches they would have on the r-SOC system performance.

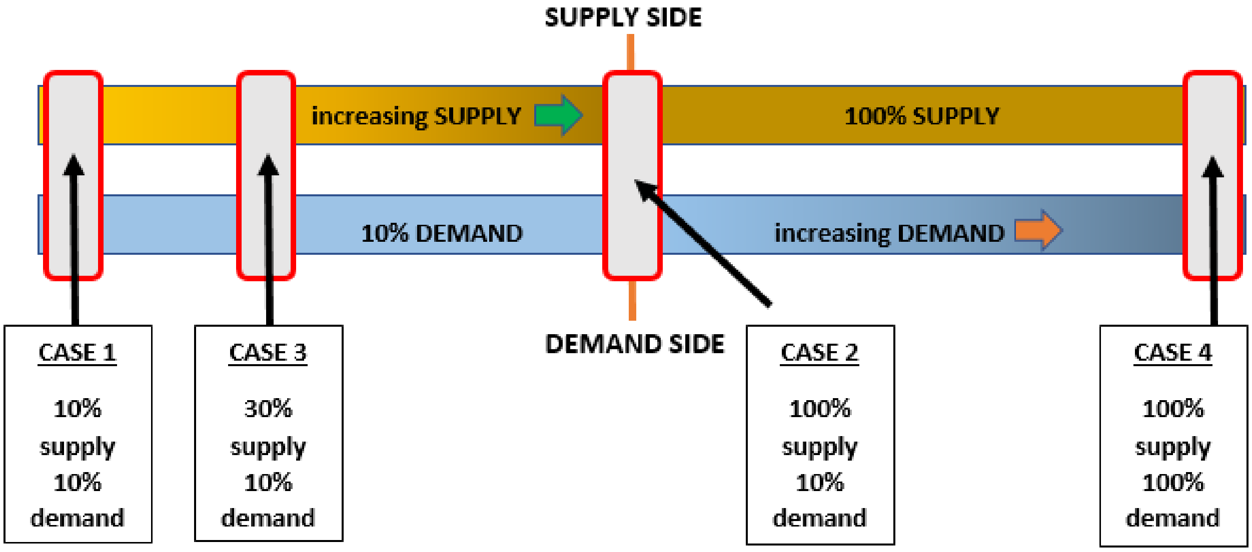

Figure 38 Annual simulation: four cases

In *Figure39* the hourly power net difference between supply and demand is provided for the four studied cases, while in *Table11* some of the main results are resumed. Those values do not represent by themselves a parameter of merit of the system but are useful in order to compare the different cases in terms of use of the r-SOC system in the EnviPark context. In fact, the ideally best system would be characterized by the instantaneous and continuous match between energy supply and demand; in that ideal system no need of r-SOC would be present and it could be unemployed. However, the renewable power generation and the energy demand of the users are in general not in balance and an energy storage technology can make the entire system greener and more affordable.

In this framework, the four cases have been discussed below not with the purpose of finding the best system integration, but to draw indications from the results obtained though the concerned annual simulation and to study how the external energy profiles by which the r-SOC system interacts can affect its performance.

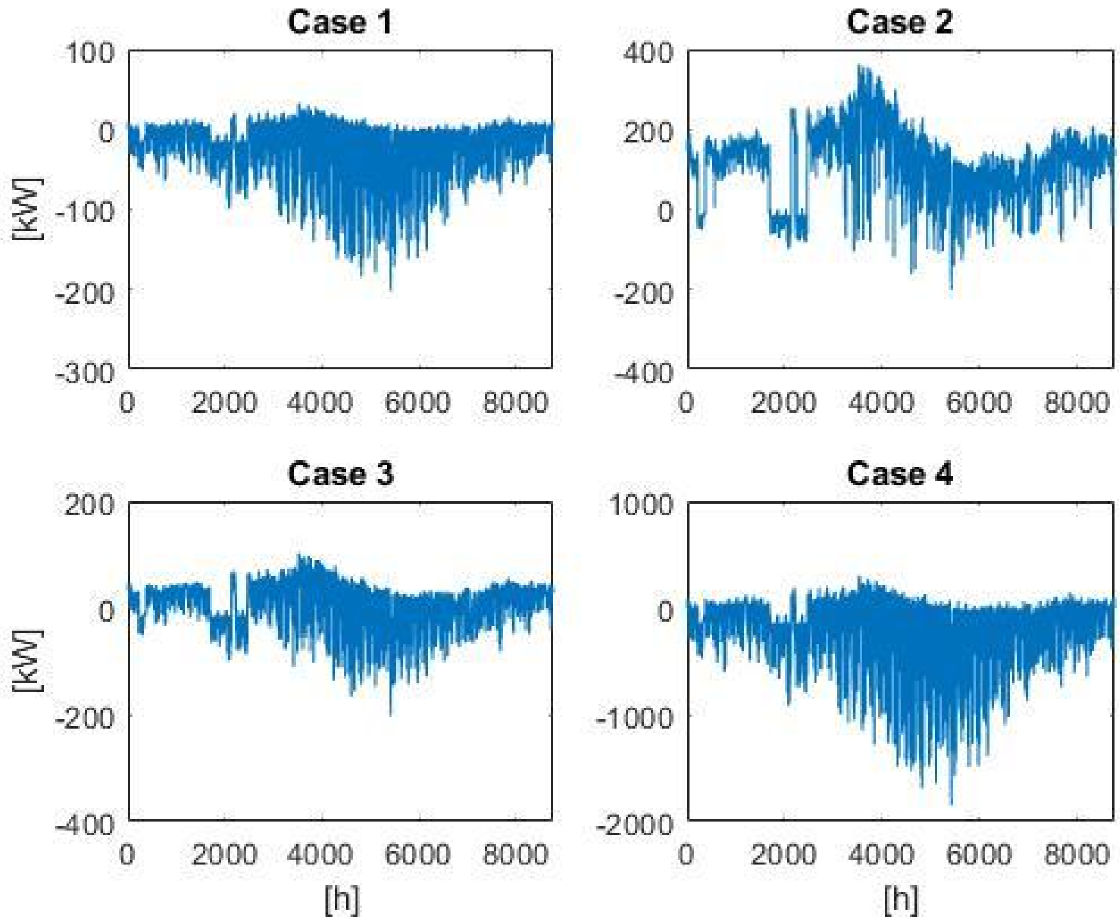

Figure 39 Annual simulation: net power for the four cases

	CASE 1	CASE 2	CASE 3	CASE 4
NG-SOFC hours of operation [h]	7942	8211	6421	5483
H2-SOFC hours of operation [h]	148	354	1044	1916
SOEC hours of operation [h]	670	196	1294	1361
Net SOFC Power Output [MWh]	70.6	79.6	66.5	64.0
Gross SOEC Power Output [MWh]	8.6	14.7	42.6	78.5
Annual Power to Grid [MWh]	24.0	1059	145.8	92.7
Annual Power from Grid [MWh]	206.8	33.1	108.8	2 343
Natural Gas consumption [Nm^3]	19 500	21 600	16 600	14 000
Number of 0-100% battery cycles	98	50	187	222
Number of 0-100% hydrogen cycles	0	9	9	25
Hours of empty hydrogen tank [h]	7321	885	2109	4552
Hours of full hydrogen tank [h]	0	7233	3561	667
Surplus Heat [MWh]	46.8	56.5	45.6	27.8
Deficit Heat [MWh]	282.0	279.8	281.7	2 857
% Heat Provided [%]	11.4	12.1	11.5	2.0
% Useful Heat [%]	43.5	40.4	44.4	67.1

Table 11 Annual simulation: results for the four cases

In counting battery and hydrogen tank cycling, only the complete cycles have been considered, i.e. the number of times the state of charge of battery (or the filling of the vessel) passes from completely empty to completely full, regardless of the time needed for the operation and of eventual partial recharge.

For the hydrogen tank, the overall hours of empty and full conditions have been calculated, by summing up all the seconds of the year in which it happens.

For concerning the heat recovery of the thermal energy by-product released by the r-SOC operation, some parameters have been inserted in the table. In general, the instantaneous produced heat can be higher or lower to the heat demand value, generating surplus and deficit heat respectively:

$$Surplus\ Heat\ (> 0) = Heat\ Produced - Heat\ Demand \qquad [MWh]$$

$$Deficit\ Heat\ (> 0) = Heat\ Demand - Heat\ Produced \qquad [MWh]$$

For $\%\ Heat\ Provided$ it has been considered the share of the annual heat demand that would be covered thanks to the electrochemical device, defined as:

$$\%\ Heat\ Provided = \frac{(Heat\ Produced - Surplus\ Heat)}{Heat\ Demand} \qquad [\%]$$

For $\%\ Useful\ Heat$ it has been accounted the share of the produced heat by the r-SOC system effectively used by the users:

$$\%\ Useful\ Heat = \frac{Heat\ Produced - Surplus\ Heat}{Heat\ Produced} \qquad [\%]$$

6.2.1 CASE 1 (10.9% supply – 10.9% demand)

The r-SOC system works for covering power demands of the building C; since its needs constitute around 10.9% of the total demands of EnviPark, the same percentage has been considered for the exploitation of the local renewables. The remaining part of green power is assumed to be used by the other buildings of the Park.

As it can be seen in *Figure39*, the load profile is considerably shifted towards demand. The maximum hourly power request is around 202 kW, while the maximum hourly power supply is 32 kW. Certainly, this configuration does not suit the r-SOC capacity, also considering that in this case SOEC mode will be always in endothermic conditions.

Moreover, as it can be seen from the results, the r-SOC system would be in NG-SOFC operation for more than 90% of time. Basically, the electrochemical device would merely substitute internal combustion engines for providing power and heat to users, but considerably underusing the hydrogen carrier.

In *Figure40* the annual profile of battery and hydrogen tank utilization are represented. The hydrogen vessel would never reach the full filling and for whole months it would be completely unused, especially between summer and autumn periods, when hydro power output is low. For more than 7300 hours, i.e. 83.5% of time, the hydrogen tank would be completely empty. Moreover, it would be employed in a very low number of times at extremely partial load. As a result, the storage would be significantly disproportionate. This is also due to the presence of the battery, which exploits power availability especially during nights to perform faster dynamic operations. However, also the battery unit would be substantially unused between August and October.

The r-SOC system would provide around 11% of the heat demand and less than half of the produced heat would be useful for the users. In fact, in winter days heat valorized from the stack operation is usually a minimum part, since hourly heat demand are also higher than 500 kWh, while in winter nights and especially in summer season it largely exceeds the needs and a relevant part must be wasted, decreasing the overall efficiency of the device.

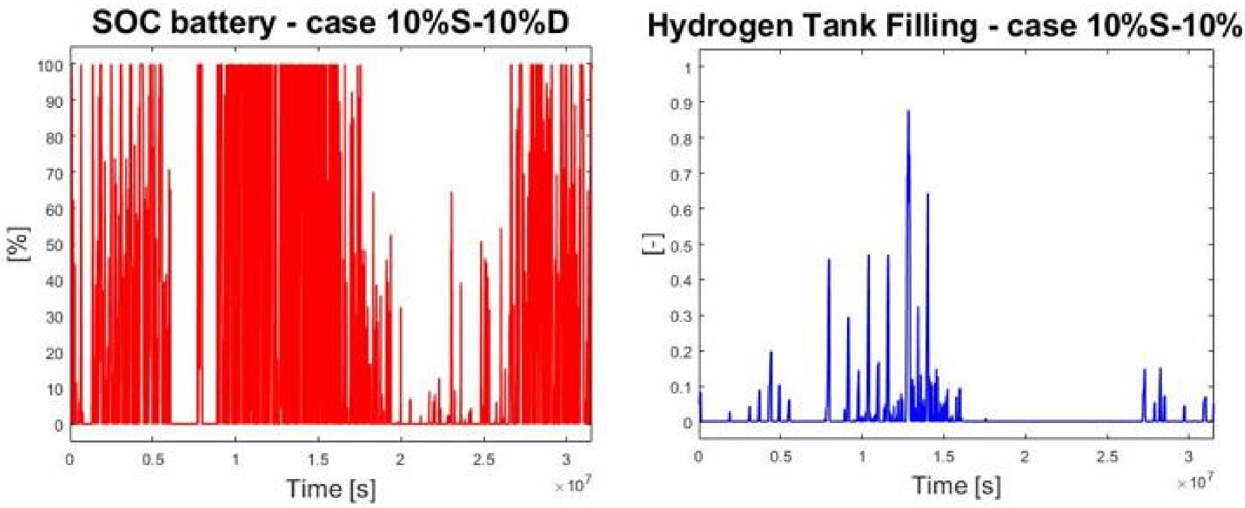

Figure 40 Annual simulation: case 1

6.2.2 CASE 2 (100% supply – 10.9% demand)

Given the results obtained for the first case, it has been chosen to consider the scenario in which the entire renewable power supply has assumed to feed the r-SOC system, whose operation refers to building C as above.

In a net power viewpoint, the situation is globally more shifted towards supply, but without excessively different peak values, giving a distribution between around 350 kW of maximum surplus and around 200 kW of maximum deficit. However, the results are even worst and represent the opposite situation with respect to the previous case.

The r-SOC system would operate for almost 94% of the year in NG-SOFC and less than 200 hours in electrolyser mode, around 3.5 times less than in case 1. However, the gross power input to electrolyser almost doubled. The fact is that a too high share of power would be supplied to the r-SOC system and the bottleneck would be constituted by the hydrogen storage capacity, which would be dramatically undersized. Electrolyser would work at very high power but for very few hours and the hydrogen tank would be entirely full for more than 7200 hours, thus limiting the possibility of employing the electrolyser mode. The battery too would be underused, with around half the cycles of the first case. Storage means are employed especially in summer, when the building C energy demand and overall renewable energy production show a balanced situation.

Provided heat would be slightly more, but a higher share of it would be not used. However, due to the high use of natural gas for both the cases, the annual results for concerning heat are similar.

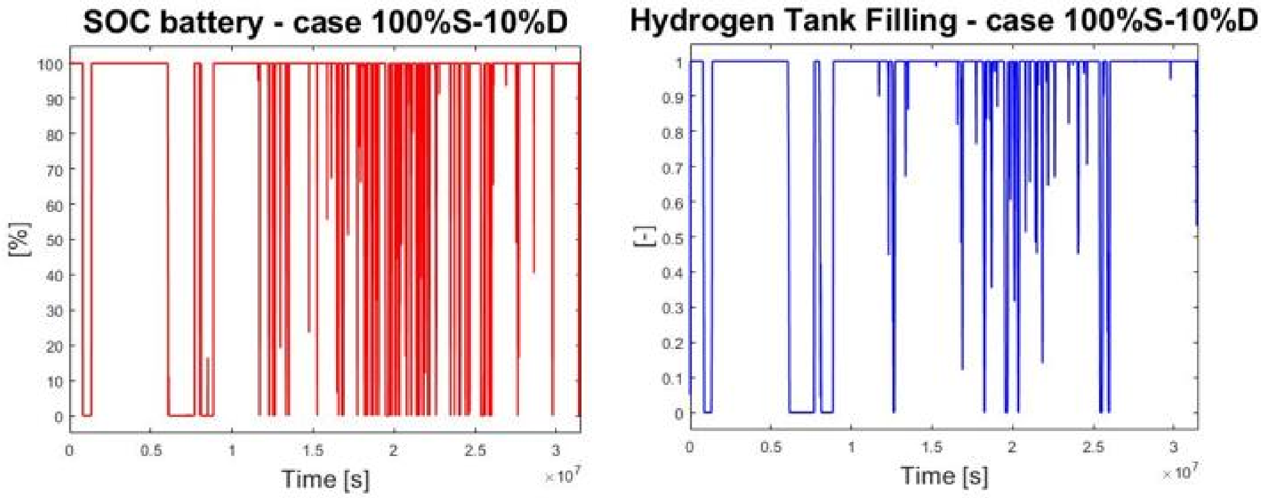

Figure 41 Annual simulation: case 2

6.2.3 CASE 3 (30% supply – 10.9% demand)

The third case represents an intermediate scenario between the previous two, in order to achieve a better integration between the r-SOC system and the EnviPark context. The demand side is maintained as building C in EnviPark, but an arbitrary share of 30% of the renewables is assumed to be exploited by the electrochemical device.

The maximum required net power is slightly more than 200 kW, around twice the maximum available. However, SOEC mode would be in operation for more than 1200 hours, around 15% of the year. Therefore, hydrogen tank would be more employed and at the same time also the H2-SOFC mode would have high share of use, seven and three times more than in first and second case respectively.

Annual battery cycles are 187, i.e. one every two days in average. It basically behaves as a daily energy storage mean, which typically is charged during nights and is discharged in working days. The hydrogen tank too, benefits from this integration: even if the total number of complete cycles is 9 as in the previous case, it is actively employed for more than 35% of the year, when a partial filling is present. In late spring and early summer, the tank is shifted towards full load and hydrogen is typically employed in weekdays during afternoon, when the battery has been discharged, while during nights the electrolyser is able to completely fill the vessel. Conversely, between summer and autumn, when higher power demand is present, the hydrogen storage is shifted towards empty conditions. Typically, the battery is discharged in a few hours and hydrogen is employed during mornings, while in nights the electrolyser is not able to fully recharge the tank.

In winter months the lower energy demand has the consequence to significantly reduce the use of hydrogen and the tank remains full for several continuously hours, with the exception of the stop periods of the hydro power plant, when stored hydrogen is fully used but remains for quite long time in empty conditions. As a general statement, more daily power variation more the rSOC system will be exploited to perform energy storage for the users; a prevalent schedule with SOFC mode during days and SOEC mode during nights seems to be the best system integration.

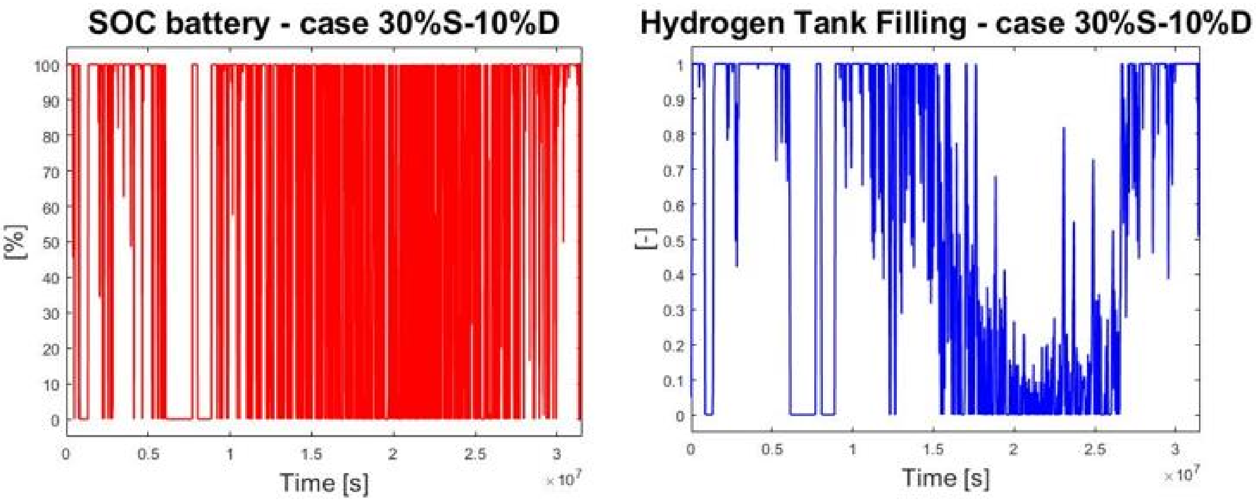

Figure 42 Annual simulation: case 3

6.2.4 CASE 4 (100% supply – 100% demand)

In the last case, the entire supply and demand side of EnviPark interacts with the r-SOC system. Power demand has been evaluated by the annual overall energy consumption value and the hourly distribution has been assumed to be the same as the calculated one for building C in part (4.2). Since the other buildings located in EnviPark are not exclusively used as offices but also laboratories are present, the concerned energy profile may not be precise, but in lack of further information it has been considered as an acceptable first approximation.

For the method by which it has been constructed, the normalized net power profile results the same as case 1, but the absolute values are around ten times larger. In this way, the results can provide more precise information on the foreseen r-SOC performance at the same normalized profile depending on the magnitude of power to which it interfaces.

The r-SOC system operates for the highest share of hydrogen configurations with respect to the previous cases: around 15% of the year in SOEC mode and even for 22% in H2-SOFC, i.e. thirteen times more than in case 1. On the other hand, also in this case more than 60% of time natural gas would be used to operate fuel cell mode.

The storage means are much more employed than in the other cases: complete battery cycles are 222 and complete hydrogen cycles 25. However, periods of continuous underuse are evident in March, during hydro power stop, and in autumn, when energy demand substantially exceeds energy supply. Moreover, more than half of the time hydrogen tank is completely empty.

The extremely high power values make very fast the charging and discharging time of the battery and typically within ten hours during nights and first hours of the day its state of charge shows a 0-100-0 load condition, while the hydrogen tank filling has a slower dynamic because it interfaces with the lower r-SOC power values.

Another consequence of the considered integration is a significant rise of the useful heat recovered from the stack operation, which is equal to 67%. This is due mainly due to the match between electrolyser operation – i.e. the mode characterized by the usually lowest heat generation – and low heat demand during night and summer.

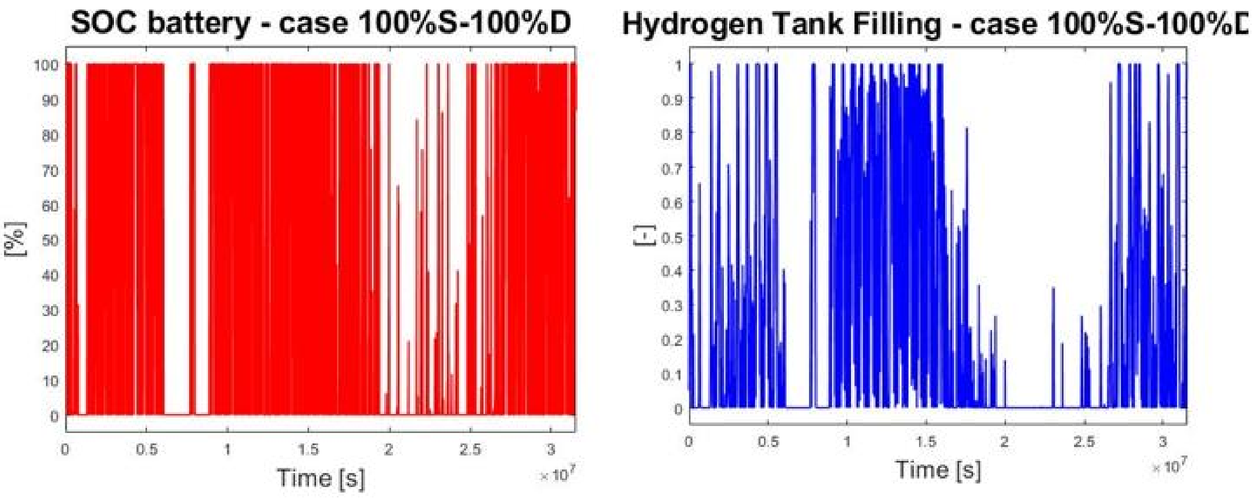

Figure 43 Annual simulation: case 4

7. MODELLING RESULTS – dynamic simulations

The dynamic model constructed on Simulink has been used so far for obtaining results in steady-state conditions and for assessing in that way the annual energy integration of the r-SOC system in a real environment as a succession of steady-state operating points. In the following part, the same model has been exploited to evaluate the concerned fuel cells system behavior submitted to some purely transient conditions and to highlight how the annual simulation results discussed above could be accurate.

7.1 RAMP UP SIMULATION

For the way in which the annual simulation model has been constructed, sharp transient conditions occur during switches in modes of operation of the r-SOC. In fact, they have been assumed to be constituted by a 5-minutes stop for inlet gas changing, over which no power input or output are involved to the stack, followed by a constant ramp up with a maximum slope of 5% per minute with respect to the maximum power. The same relative value has been considered for all the three modes of operation, even if the in absolute terms it means different ramp conditions, especially between SOFCs and SOEC.

For the three r-SOC modes of operation a dynamic simulation of the ramp up condition has been performed. Starting from nominal temperature values, the system has been subjected to the 5-minutes stop (first vertical red line in *Figures44-45-46*, after 300 seconds) and then to the prescribed power increase to reach after 25 minutes of simulation the maximum power condition (second vertical line in *Figures44-45-46*, after 1500 seconds). The maximum power value has been maintained for other 10 minutes. The stack temperature evolution has been studied for highlighting eventual excessive decrease due to zero- or low-load conditions.

In the first phase of NG-SOFC simulation the stack temperature drops down to around 992 K due both to thermal dispersion to ambient of the component and initial endothermic steam reforming reaction. It reaches a minimum after around 500 s, when the stack power output is approximately 2.2 kW, i.e. around 0.1 kW net power (considering the ancillary power consumption).

Increasing the power output stack temperature rises, because of the exothermic reaction increasingly pressing and to the temperature control of the model, which uses electrical power to rise fuel and oxidant line streams entering the stack. After around 1000 s (power output equal to 7.9 kW) a peak is present, located at 1006 K. Then temperature slowly decreases in the last part of the ramp up and in the subsequent fixed constant maximum power. At the end of the simulation, stack temperature is around 1004 K, i.e. around 1 degree higher than the nominal value.

At around 420 s a slightly variation in the curve is present. That occurs at power level where the added steam, which is required at very low loads for enabling steam reforming reactions, comes to zero. However, the temperature variation in that point is minimal.

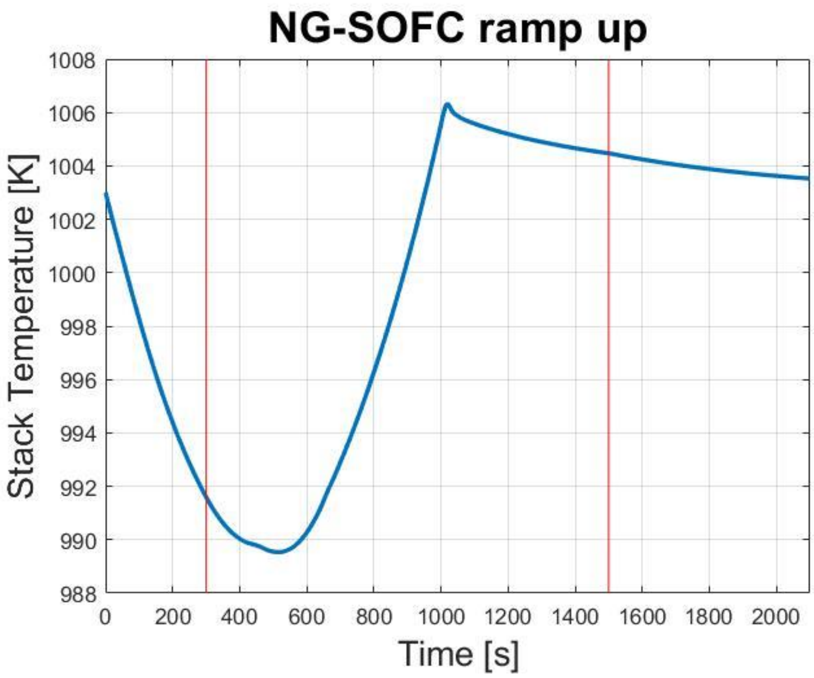

Figure 44 Ramp up: NG-SOFC

In H2-SOFC the ramp up simulation gives similar and even better results. Initial stack temperature decrease is lower, due to the absence of any endothermic reaction occurring, and its variation is around 5 degrees. Within few seconds in which the power output ramp up, stack temperature starts to rise and at 700 s (3.8 kW) it reaches the nominal value. In this case, the overtemperature is negligible and the value remains fixed constant to the nominal stack temperature for the whole time of simulation.

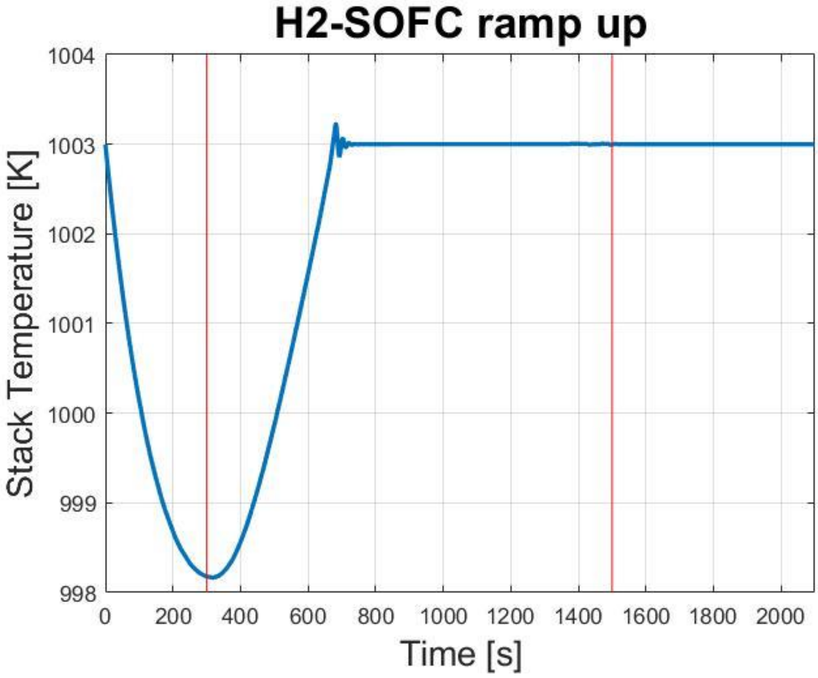

Figure 45 Ramp up: H2-SOFC

As expected, in SOEC mode of operation the most critical situation occurs. After the first 5-minutes stop, in which the transient evolution is the same of the H2-SOFC configuration, at low loads the stack is in endothermic conditions and it keeps on cooling down until around 800 s. In that time, which correspond to approximatively 30 kW input power, temperature reaches 988 K.

Approaching to thermoneutral and exothermic conditions, the stack temperature increase; the maximum is reached after around 1400 s (64 kW) and it equals to 1010 K. After a quite intense temperature oscillation, characterized by a maximum amplitude of 10 degrees, stack temperature reaches the nominal value in steady-state conditions at maximum power.

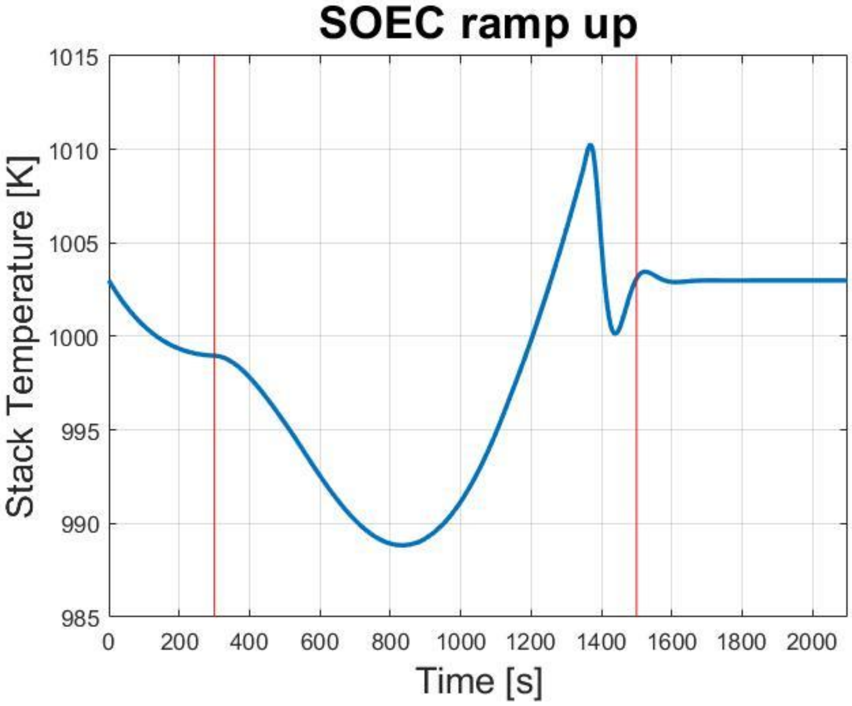

Figure 46 Ramp up: SOEC

The previous brief analysis has highlighted that the constructed dynamic model suits for all three-configurations ramp up conditions, which constitute one of the most severe transient situations occurring to the stack. Therefore, a more complete analysis has been conducted through the dynamic model, covering an entire day. 31 May has been chosen in the "30% supply – 10% demand" (case 3) scenario, because it is characterized by the sequence of the three modes of operation in various load conditions. The different dynamic models constructed for the different configuration have been united in a single model and applied in series depending on external and internal inputs, such as surplus and deficit power, battery SOC, filling of the hydrogen tank. The results are then compared to them of the annual simulation and the accuracy of the steady-state points succession model is evaluated.

7.2 DAILY SIMULATION

The r-SOC daily power profile as calculated by the annual simulation model for 31 May is represented in *Figure47*. It is a weekday, in which the net power evolution is shifted towards supply side during night and towards demand during day, when the needs of the users in the offices of the building exceeds the generated power from the local renewables.

Until around 2:15 AM the r-SOC system works in SOEC mode following the supply power profile. The curves of gross power delivered to the system (dashed red line) and the curve of the net power entering the stack unit (blue line) are roughly parallel and the difference is constituted by the ancillary power for the auxiliary system, which is quite constant due to low variation in SOEC power input.

Electrolyser mode stops when the hydrogen storage tank is completely full and the switch to NG-SOFC occurs. After the ramp-up, fuel cell mode is maintained at the highest load and the surplus power, constituted by the sum of net supply and r-SOC generation is delivered to the grid. From around 5 AM a net power demand is required, and it is provided by discharging the battery unit, which works following the load, while the r-SOC system continues its operation. After around 1 hour the battery is completely discharged and hydrogen is used.

The electrochemical device switches to H2-SOFC mode of operation, and after the ramping up it works at the highest load. The users net power demand varies along the day and the amount not covered by the r-SOC system is provided from the grid. At around 5:30 PM the energy demand is lower than the net SOFC power output and the r-SOC unit starts working at partial load following the decreasing demand. At approximately 6:20 PM the supply side exceeds the demand side and the surplus power is used to recharge the battery unit, while the r-SOC system switches to NG-SOFC as prescribed. After almost 12 hours of continuous operation, the hydrogen storage still contains more than 3 kg of chemicals.

Battery recharge lasts for around two and a half hours and is completed at 8:30 PM. As in the early morning, during the battery operation the r-SOC system works in NG-SOFC mode. Then, it switches again to electrolyser exploiting the renewable power surplus to recharge the hydrogen storage during night. Electrolyser works at high load following the input power and then at 11:56 PM reaches the highest power point.

In *Figure49* some profiles obtained from the dynamic simulation are provided.

Stack temperature does not show critical variation. The minimum value is slightly more than 988 K, i.e. 15 degrees below the nominal temperature, and the concerned dynamic is quite fast, with immediate increase to return to the desired conditions. This point occurs in NG-SOFC – to -SOEC switch and it is substantially represented by the electrolyser ramp up analysis done in the previous chapter. Other smaller oscillations are present in the other switches: at around 2 AM from SOEC to NG-SOFC, at around 6 AM between NG-SOFC and H2-SOFC, at around 6 PM from H2-SOFC to NG-SOFC, as it has been seen. The maximum value also occurs in the last switch, but the variation is less than 3 degrees.

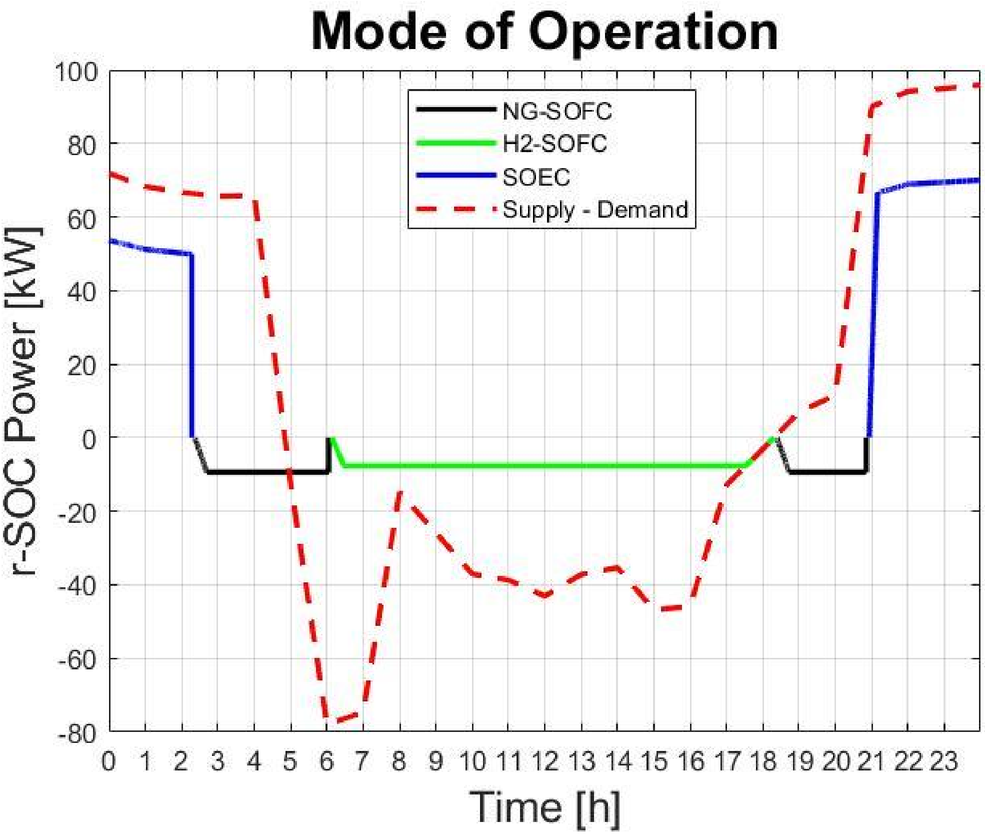

Figure 47 Daily Simulation: Modes of operation and Power values

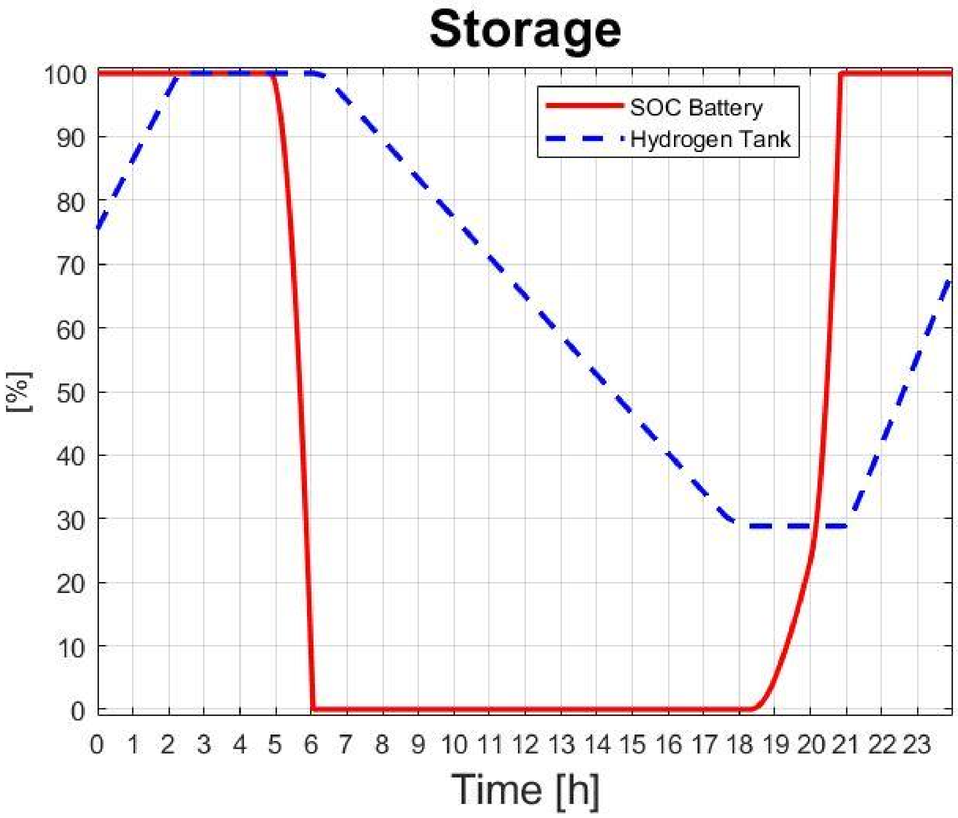

Figure 48 Daily Simulation: Energy Storage Means Profile

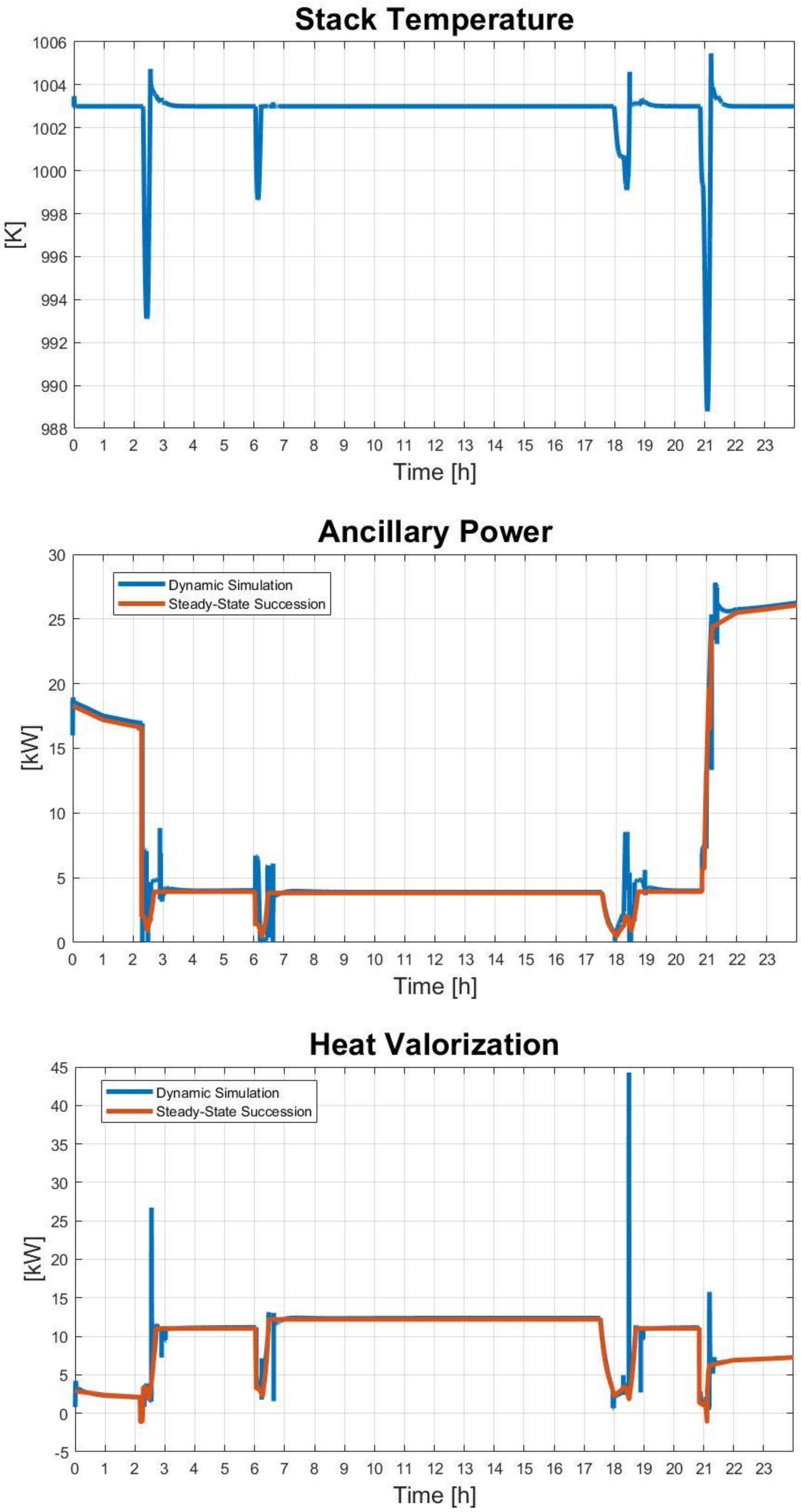

Figure 49 Daily Simulation: Stack temperature, Ancillary power and Heat Valorisation

The second figure shows the ancillary power consumption, which evaluates the contribution of air blower, electric heat exchangers and hydrogen compression. A substantial agreement between the steady-state points succession model and the dynamic model can be seen. The two curves basically show a constant overlap in steady-state conditions, occurring when fuel cells work at maximum power point. This is not surprising since this was one of the considered points for the construction of the steady-state succession model. However, also for load following conditions the two curves are very close and a good approximation is performed. During the switches the major differences are present; in the dynamic model power consumption has visible oscillations caused to rapid variations in the electric heater load to follow rapidly changing conditions. Consequently, while in the steady-state model the power consumption is low in these conditions, from the dynamic simulation it is highlighted that some peaks are present. However, also in this case a quite good approximation has been obtained through the steady-state model.

The third figure represents the heat recovered from the r-SOC operation in the exhaust gas cooling unit. Also in this case a good agreement between the two models has been obtained. In some switching points the steady-state model too comprises some quick oscillations which are obtained also in the dynamic model (for example in SOEC – to – NG-SOFC switch during night). Some relevant and discontinuities have been obtained in the dynamic simulation, that are probably due to rapid variations in the heat valorisation water flowrate, for which a maximum value has not been set in the model. However, also in this case the profiles are strongly similar.

Another interesting aspect is to evaluate the difference in the hydrogen tank filling, which is not part of the simulated model but to which the concerned system interacts by delivering and requiring hydrogen stream. The first switch occurs because of the complete filling of the storage; in *Figure50* the hydrogen tank filling evolution in these conditions is represented. The difference between the two models is only slightly more than 100 seconds.

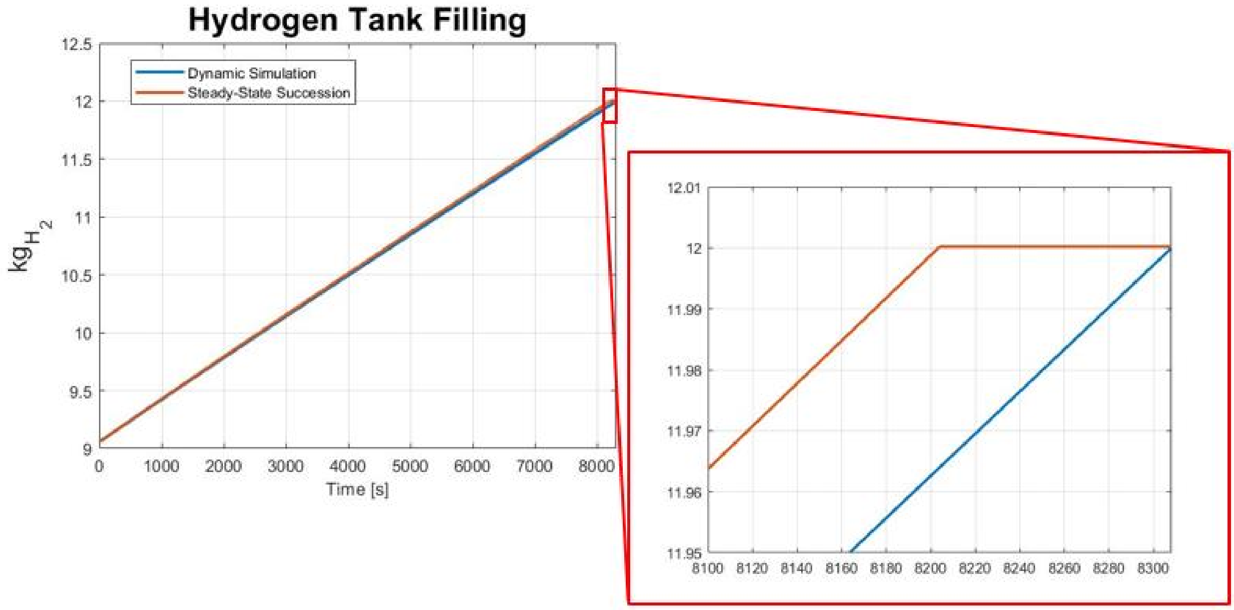

Figure 50 Daily Simulation: Time of hydrogen tank filling

In *Figure51* the representation of the hydrogen mass contained in the tank at the end of the day is given. In the dynamic simulation the result is 8.092 kg, while the predicted value from the steady-state model was 8.286 kg, i.e. a relative error of 2.3%. Taking into consideration that the hydrogen mass value depends not only on the last three hours of SOEC operation, but also on the discharge mode in H2-SOFC operation for around 10 hours, a pleasing agreement has been obtained.

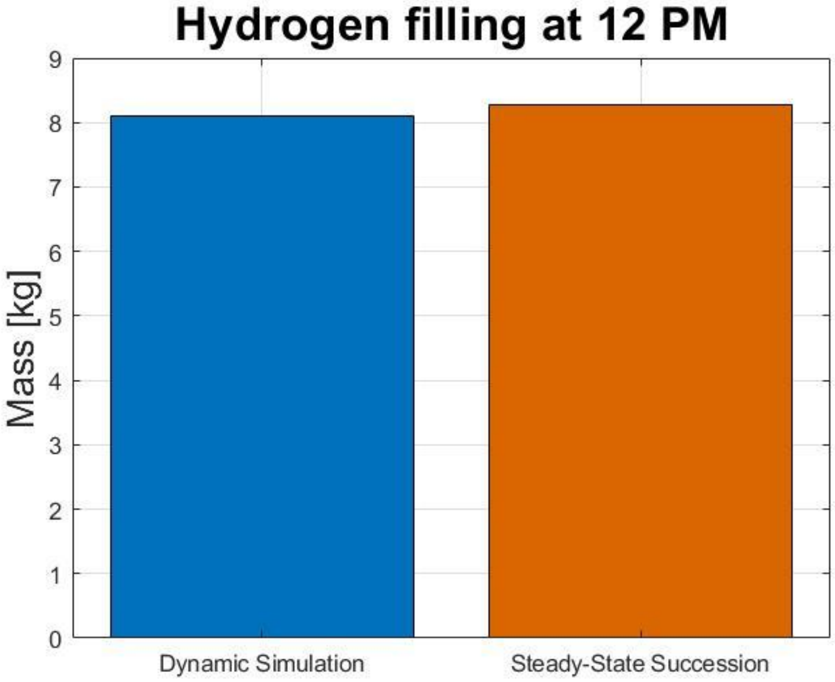

Figure 51 Daily Simulation: Hydrogen tank filling at the end of the day

In *Figures52-53* the overall ancillary power consumption and heat recovery in the entire day are compared between the two models. In both the cases the results of the dynamic simulation are slightly higher than them of the steady-state model. This is mainly due to higher oscillations during switching periods occurring in the dynamic model. The relative difference between the two results is around 3% for concerning the daily ancillary energy consumption (183.0 kWh vs 188.6 kWh) and less than 1.5% for the heat valorisation (230.1 kWh vs 233.6 kWh).

The results of the dynamic simulation for an entire day have shown an impressive agreement to the predicted values by the steady-state points succession model. Relative difference between some significant quantities have not been higher than 3%. For concerning ancillary power consumption and heat recovery, the dynamic results have been slightly higher, due to oscillations occurring in switching conditions.

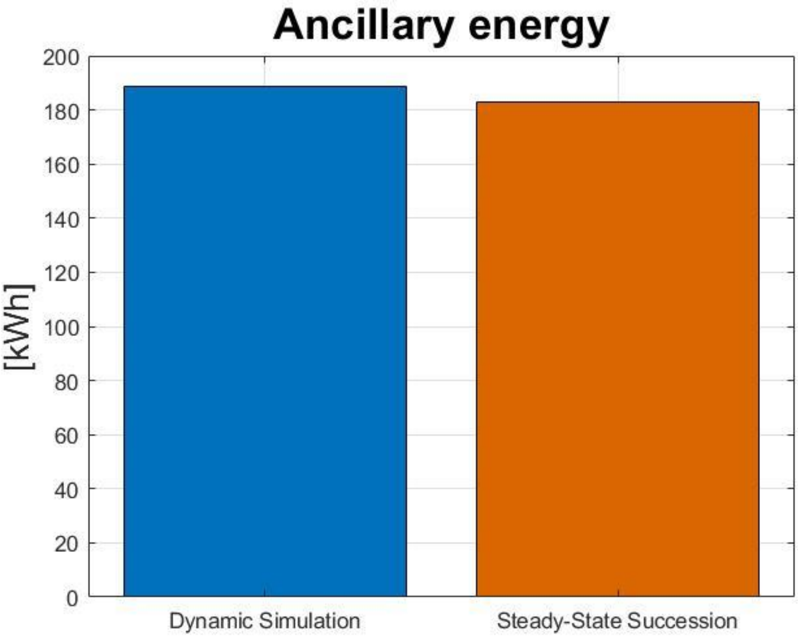

Figure 52 Daily Simulation: Daily Ancillary Energy Consumption

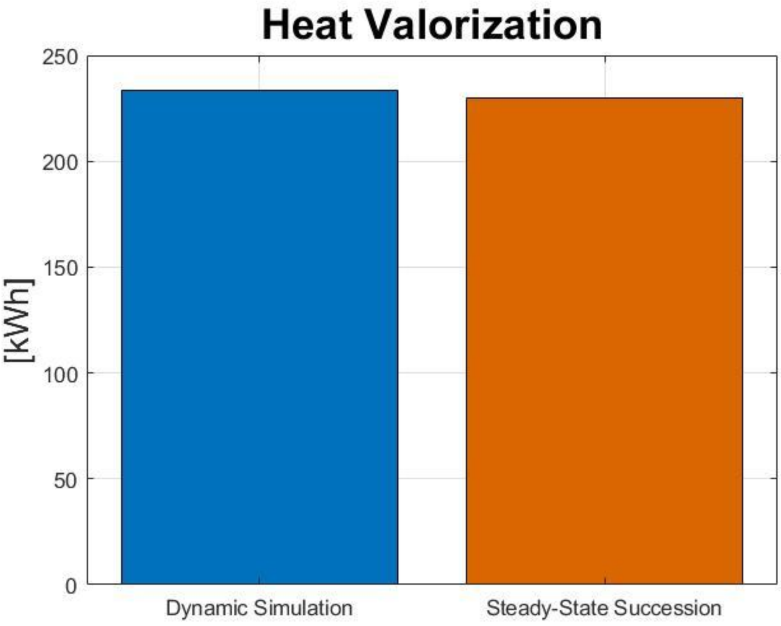

Figure 53 Daily Simulation: Daily Heat Recovery

8. REGULATIONS OVERVIEW

In this chapter a regulations overview for concerning hydrogen and fuel cells is presented.

In the first part, the main three Italian regulations that have been considered for design and construction of the concerned plant are briefly discussed. Their focus is on the fire prevention for plants and components. DPR n. 151 deals with fire prevention measures in terms of checking procedure for several components, including storage vessels. DM 3/2/2016 is related to the safety distances to be maintained for fire prevention in a natural gas storage. DM 13/7/2011 refers to fire prevention in the installation of CHP units, especially referring to internal combustion engines. The main consideration after this overview is the lack of specific regulations for concerning hydrogen and fuel cells, which obliges operators to refers to standards originally thought for other fuels and technologies.

In the second part of the chapter, following some documentations provided by *HyLaw*, the legislative situation in a European viewpoint has been considered. The main resulting aspects connected with this overview is the presence of relevant differences among the European countries for concerning requirements, procedures and incentives for installation and operation of hydrogen and fuel cells. Moreover, lack of distinction among the methods for producing hydrogen and on the plant-size has been highlighted, as well as an absence of clear thresholds for the application of some regulations and procedures.

8.2 ITALIAN LEGISLATION

8.1.1 DECREE OF THE PRESIDENT OF THE REPUBLIC n. 151 - 1 August 2011

(*DECRETO DEL PRESIDENTE DELLA REPUBBLICA, 1° agosto 2011, n. 151*). *Regolamento recante semplificazione della disciplina dei procedimenti relativi alla prevenzione degli incendi*

As expressed in Article 2, the Regulation identifies the activities subjected to checks of fire prevention and it disciplines the verification of fire safety conditions, which under the Italian existing regulation are given to National Fire Brigades officers.

The activities subjected to above checks of fire prevention are reported in tabular form in Annex 1 of the regulation. For the concerned project, it refers to compressed flammable gases repositories in movable vessels (activity n. 3a): vessels with overall geometric capacity higher or equal than 0.75 m^3 are categorised and they fall into Category B if their volume is within 10 m^3 and into Category C if it is higher.

N.	ACTIVITY	CAT. A	CAT. B	CAT. C
3	Tanks filling, repositories, resales of flammable gases in mobile vessels:			
	a) compressed, with total geometric capacity higher than or equal to 0.75 m^3		Resales, repositories up to 10 m^3	Tanks filling, repositories over 10 m^3

Table 12 Categorization of storage vessels for fire prevention procedures

Thus, the volume of the tank, that is connected to the design pressure of the storage, strongly determines the bureaucratic procedures to be carried out: if the vessel is characterized by a geometric capacity smaller than 0.75 m^3 no additional activity for fire prevention is necessary, while if it is larger than 0.75 m^3 checks by Fire Brigades are requested. In this case, it must be submitted a draft, requested an authorization and waited for the successful outcome of the checking procedure performed by Fire Brigades, so leading to a significant increase in time. As expressed in the Regulation, the drafts are considered by the Fire Service *Comando Provinciale* and within 30 days additional documentation may be requested; from the date of submission of the entire documentation, the Fire Service Command has 60 days for giving a response in terms of compliance with the regulation and with technical criteria for fire prevention. Typically, time for the entire procedure is even larger.

The application for authorization must be submitted before the facility comes into operation, through a certified notice of commencement of work. The Fire Service Command verifies the formal compliance of the request, of the documentation and of the annexes and releases a receipt in case of successful outcome of the checks.

For the activities included in Category B, the checks performed by Fire Brigades are constituted by technical inspections that are intended to verify the compliance with the regulations and with the fire safety requirements. The checks are arranged according to sampling methodology or sectorial programs, for categories and in any case in hazardous situations that are reported and detected. In case of negative result, the Command takes substantiated measures to forbid the continuation of the activity and to remove the possible harmful effects that are product by the same, with the exception, wherever possible, that the interested party shall ensure the conformity of the activity to the fire safety regulation within a period of 45 days. In case of successful outcome, the Command releases a copy of the minutes of the technical inspection if requested by the owner of the activity.

For the activities included in Category C, the main features for procedures and checks are the same as for the ones present in the previous category. Checks are constituted by technical inspections, but not using the sampling methodology. Moreover, in case of successful outcome, the Command releases the fire prevention certificate within 15 days from the date in which the technical inspections were performed.

In the subsequent articles of the Decree the following aspects are then listed:

- the requirements connected to the periodic renewal (it must be done each 5 years) of the certificate for fire safety, via a statement that no variations have been done to the fire safety conditions, accompanied by the required documentation;
- the obligations related to the operation of the facility, and in particular maintaining a good performance level in the systems, in the devices and in the equipment, guaranteeing the efficiency state of fire safety measures, performing control checks and maintenance operations in accordance with the deadlines specified by the Command in the fire prevention certificate, ensuring that there is information about fire risks connected to the specific activity;
- the indications for possible derogations;
- the information required for the possible verification during operation;

- the correlations of the Decree with previous procedures and rules in the Italian legislation or concerning similar topic.

Those aspects are not very relevant for the concerned project, since the facility related to rSOC will be tested in a real scale for about 8000 hours.

For the concerned plant, the main aspect related to this Decree is that the choice of the storage pressure of the hydrogen tank plays an important role not only from the operative point of view, but also from the authorization one; the limit value for the geometric capacity of the tank is of 0.75 m^3, which corresponds for the concerned storage to a pressure in the vessel of almost 200 bar, which is exactly the considered design pressure. If a lower pressure were chosen, e.g. for decrease CAPEX in hydrogen compressors and tank, time required for bureaucracy for the installation significantly increases.

8.1.2 DECREE OF THE MINISTRY OF THE INTERIOR - 3 February 2016

(*DECRETO DEL MINISTERO DELL'INTERNO, 3 febbraio 2016*). *Approvazione della regola tecnica di prevenzione incendi per la progettazione, la costruzione e l'esercizio dei depositi di gas naturale con densità non superiore a 0.8 e dei depositi di biogas, anche se di densità superiore a 0.8.*

The decree defines the specifications concerning fencing, safety distance and components in natural gas storage facilities, depending on its type and size. In the absence of dedicated regulation about hydrogen storage in the existing Italian legislation, the standard operating procedure is to assimilate hydrogen to natural gas and to consider the limits imposed by the present decree.

In Articles 2 and 3 the main views of the Decree are listed. The objectives are: minimizing the possible causes and initial events for which a fire may be produced, ensuring the stability of the load-bearing structures in order to guarantee a rescue to occupants, limiting the production and the propagation of a fire within the premises and among adjacent spaces, ensuring that occupants could have the possibility to get out unscathed from the premises and guaranteeing that the rescue team could operate safely.

The most important item of the decree is constituted by the technical rule concerning the fire prevention, that is presented in the Annex of the document. In Section I and Section II respectively, general rules and dispositions regarding fixed vessels are presented, while Section III refers to the storage in mobile vessels, which is the part related to the concerned project. The main guidelines expressed in this part of the decree are reported in a bulleted list, as well as some considerations about the concerned project:

- **Permitted operating pressure.** The maximum permitted operating pressure are the design pressure of the pressure tanks, that are governed by the existing regulation.

- **Storage Capacity.** It is evaluated in [m^3] using the following formula:

  $$C = V \cdot \frac{P}{P_0}$$

  Where V is the geometric volume of the tanks, expressed in [m^3]; P is the maximum permitted operating absolute pressure expressed in [bar], as reported by the operator; P_0 is the barometric absolute pressure, expressed in [bar] and conventionally assumed to be equal to 1 bar.

Depending on the storage capacity, the vessels are classified into 4 categories:

- Category 1: over 10 000 m^3
- Category 2: over 5 000 m^3 and up to 10 000 m^3
- Category 3: over 850 m^3 and up to 5 000 m^3
- Category 4: over 75 m^3 and up to 850 m^3.

Considering the design values of pressure and geometric volume, the storage capacity is:

$$C = 0.75 \cdot \frac{200}{1} = 150\, m^3$$

Thus, the concerned vessel belongs to category 4. It is the lowest category and the one with the least restrictive dispositions.

- **Degree of Safety.** On the basis of the construction characteristics of the storage buildings, the storage vessels and the parking spaces for vehicles for gas transport, the mobile vessels are categorized with two degrees of safety:
  - Safety of 1st degree: if the containment of splinters or other bits of material projected in case of explosion is provided both sideways and upward;
  - Safety of 2nd degree: in the case the said containment is provided only laterally.

- **Location.** Vessels shall be installed in areas compatible with the urban planning tool.

- **Fencing.** The area of relevance of the vessel shall be bordered by a dedicated fencing that shall be continuous, robust, made of non-combustible materials and suitable for preventing the access and the approach to the hazardous elements of the vessel. By the term hazardous elements are considered the following elements, as expressed by the decree:
  - The buildings, the items and the areas intended for the storage tanks;
  - The parking spaces for the vehicles used for natural gas transport, if present;
  - The compressor plants and the decompression cabins;
  - Every other element that may constitute a danger of explosion or fire in usual operating conditions.

  The fence shall have a height of at least 1.80 m and shall be placed no less than the protection distance from the said hazardous elements, which is equal to 5 m for vessels in category 4 (table following). Moreover, at least two gateways shall be present in the fencing, one of which with a minimum width of 2.50 m. They must be reasonably spaced from each other and suitable to ensure both the access to emergency vehicles and the way out of people, in case of necessity. For concerning underground vessels included in category 4, the fencing may present a single gateway even for only pedestrian access, with a minimum width of 0.80 m, provided that it is sufficient for maintenance and control activities.

- **Safety Distance.** Three different safety distances are expressed by the decree, with different values depending on the degree of safety and on the category of the vessel. The limits are shown in tabular form, following the decree.

a) 1st degree of safety vessels			
Storage Capacity	**Protection [m]**	**Internal Safety [m]**	**External Safety [m]**
Category 4	5	-	10
Category 3	5	-	20
Category 2	5	-	25
Category 1	5	-	30

b) 2nd degree of safety vessels			
Storage Capacity	**Protection [m]**	**Internal Safety [m]**	**External Safety [m]**
Category 4	5	7.5	15
Category 3	10	10	20
Category 2	10	15	25
Category 1	10	15	30

c) Category 4 vessels without degree of safety			
Storage Capacity	**Protection [m]**	**Internal Safety [m]**	**External Safety [m]**
Category 4	20	20	30

Table 13 Safety distances depending on storage vessel category

The above values represent the minimum distance that shall be maintained among the previously said hazardous elements and some specific elements, that are listed in the definition of the three distances. In particular:

- **Protection distance (*Distanza di protezione*).** In addition to the distance related to the fencing, the value represents the minimum width of the strip of land, cleared and devoid of vegetation that could constitute fire danger, that shall be kept among the hazardous elements.
- **Internal Safety distance (Distanza di sicurezza interna).** To maintain among the hazardous elements; it shall increase by 50% and, in any case, it shall be not less than 7 m, with respect to buildings intended for offices and services connected to the activities of the facility.
- **External Safety distance (Distanza di sicurezza esterna).** To maintain with respect to the perimeter of the nearest external building or to the borders of the building areas.

Moreover, the safety distances shall increase by 50% in the case that the buildings to protect, both internal and external, are intended for activities:

- With presence of the public with a crowd higher than 100 units;
- Intended for the community, included in Annex I, DPR n. 151, 1st august 2011;
- Characterized by disposal and use of flammable, combustible or exploding products.

In the concerned project, the above increase is not required.

Finally, some dispositions about the distance to power lines are present in the technical rule of the decree; however, they are not impactful for the concerned project.

- **Construction characteristics.** In this section some requirements with respect to the construction characteristics of the items are defined. Specifically, vertical elements shall be realized in reinforced concrete or in prefabricated elements, and in the latter case some additional dispositions are required. For concerning premises that are located above ground and used as storage of vessels, minimum values for the thickness of the perimeter and interior walls, for the width of the ventilation and entrance openings, for the covering characteristics related to systems characterized by 1st and 2nd degree of safety are indicated.

8.1.3 MINISTERIAL DECREE - 13 July 2011

(*D.M. 13 luglio 2011*). *Approvazione della regola tecnica di prevenzione incendi per l'installazione di motori a combustione interna accoppiati a macchina generatrice elettrica o ad altra macchina operatrice e di unità di cogenerazione a servizio di attività civili, industriali, agricole, commerciali e di servizi.*

The Decree identifies the safety standards against the risks of fire and explosion concerning the fixed and mobile terrestrial installations of internal combustion engines (ICE) coupled with power generators or other operating machines and cogeneration units. It applies to new installations with total rated power not higher than 10 000 kW and with different dispositions depending on the total rated power between 50 kW and 10 000 kW, between 25 kW and 50 kW and below 25 kW.

In the Decree, the term total rated power refers to the mechanical power made available to the shaft by the set of the first motors that constitute the installation of combine heat and power (CHP) units. It is stated by the manufacturer and must be reported in the identification plate of the CHP unit. The present decree repeals all the previous regulations concerning the same field and specifically the Ministerial Decree 22 October 2007. One of the major differences between the two regulations is in the categorization of the installations, that in the previous decree was performed in terms of total electrical power, with the same minimum value of 25 kW. Taking into account an average mechanical-to-electrical efficiency, it is possible to consider that the range of applicability of the present decree is translated to total electrical power between 28 and 12000 kVA [45].

For the installations with total rated power lower than 25 kW (*TITOLO IV*), the dispositions contained in the regulation are quite few. The installer carries out the assembly phase of the plant according to the prescriptions provided by the manufacturer of the CHP unit. The prescriptions are reported in the instruction manual; moreover, the rules of good practice should be considered. After the placement, the installer on its own responsibility attests that the CHP unit is installed in a workmanlike manner.

The dispositions for the installations with higher total rated power are instead much larger and stricter. First, the installation is allowed out of the ground, or in spaces located on the first underground floor where the walking surface is not placed less than 5 meters below the reference floor. For the last location, plants must be fed by liquid fuels characterized by a flash point equal or higher than 55 °C or by gaseous fuels with ratio between density of the gas and density of the air not above 0.8. For different values of the total rated power of the plants, different dispositions concerning attestation, structures, size, access and communications, gates, ventilation are requested by the regulation.

For instance, for facilities with total rated power higher than 25 kW, the space in which the installation is placed shall not have openings for which is possible a direct communication to spaces intended for other uses. Moreover, the access to the room can be constituted by a direct entry from the outside with uncovered spaces, or by a ventilated hallway from the outside with precise features, or by fireproof gaps in which no devices are placed that can make difficult the access.

For the concerned r-SOC system, the total rated power in fuel cell modes of operation is smaller than the 25 kW-threshold. Thus, any particular bureaucratic limitation is created by this Decree.

8.2 HYDROGEN REGULATION AND PROCEDURES IN AN EUROPEAN OVERVIEW

The novelty of the concerned plant with respect to the traditional facilities, both from the point of view of technology and regulations, stands in the employment of fuel cells and in the use of hydrogen. Apart for the DPR 151 1/8/2011, which is a regulation containing the procedures for fire prevention, in the other two decrees previously expressed the difference in the field of application is evident: DMI 3/2/2016 refers to natural gas vessels and not to hydrogen, while DM 13/7/2011 refers to internal combustion engines and not to fuel cells. This is due to the lack in the Italian legislation of regulations up to date with the latest technology improvements and at the same time to the limited penetrations of fuel cells and hydrogen in the market yet. However, this situation creates a sort of vicious circle, because at the same time the new technologies installation is hindered by the absence of a clear and specific legislation able to discriminate and simplify the procedures for these technologies.

This situation is quite similar all over the Europe and the world, as the reports provided by the HyLAW project put in evidence. HyLAW stands for Hydrogen Law and removal of legal barriers to the deployment of fuel cells and hydrogen applications. The project started in January 2017 bringing together 23 nations: Austria, Belgium, Bulgaria, Denmark, Finland, France, Germany, Hungary, Italy, Latvia, Netherlands, Norway, Poland, Portugal, Romania, Spain, Sweden and United Kingdom. The aim of the project was to boost the market uptake of hydrogen and fuel cell technologies providing market developers with a clear view of the applicable regulations and calling the attention of policy makers on legal barriers to be removed. The duration of the project was of 2 years, with the end scheduled in December 2018, but the created database is claimed to be maintained by Hydrogen Europe for at least three years after the conclusion of the project [46].

The main information related to the situation in Europe about hydrogen from the viewpoint of procedures and requirements presented in the next part of the work come from the *D4.1 Cross-country comparison* report [47] and the *National Policy Paper – Italy* report [48] by HyLAW. The reports deal with various processes related to hydrogen and fuel cells; however, in this text only the aspects connected to the concerned project are exposed, i.e. hydrogen production and storage, electricity grid connection for electrolysers and stationary fuel cells.

8.2.1 PRODUCTION OF HYDROGEN

There are 3 main legal and administrative processes (LAPs) related to the production of hydrogen:

1. Land Use Plan, including zone prohibition. It refers to the tool used by the governments to manage the development of land within their jurisdictions in an efficient and ethical way, by discriminating the areas of the region in different categories, allowing only specific activities inside them.
   In almost all the countries covered by the study, the production of hydrogen is considered an industrial activity, regardless of the technology and of the production method: thus, such activity would only be permitted in industrial areas or, under specific conditions, in commercial areas. If the limitation in industrial zones is understandable for steam methane reforming, which is a chemical industrial process which typically produces hydrogen in large quantities in centralized facilities, the situation would be different in the production via electrolysis, usually characterized by decentralized production of small quantities of hydrogen and near-zero GHG emissions. While it is theoretically possible to change a land use plan, the process of undertaking such a change is lengthy and costly.

2. Permitting process. It refers to the steps for which the applicant produces forms to a regulatory agency or a competent authority to ensure in advance that the proposed operation will be following the applicable standards.
   The required processes for a hydrogen production plant is subjected to significant differences throughout the nations. While in Austria and UK the process is steered by a single authority, in most other countries the various required permits (such as construction, environmental, operating) must be obtained from different local, regional, national authorities, with variations among the nations or even within countries.
   The general process consists of various steps, including the applications for building permit, for a permit to handle and store flammable gases, for an (integrated) environmental permit, for design approval and for operating permit to be lodged by the applicant and the subsequent verifications made by the competent authorities. It is in general irrespective of the production method used by the plant; on average, the entire process takes around one year to complete, but with relevant variations depending on the scope of the project and the authorities involved: as explicitly underlined by the cross-country report, "in Italy much longer periods have been reported by industry, as the controlling entities have the right to decide upon own discretion".
   From an EU wide perspective, the permitting process represents a significant barrier for the deployment of hydrogen technology; this is due to length, cost and uncertainty of the outcome associated to the process and the absence of simplified processes for small quantity production and for production methods different from the chemical production facilities typical of steam methane reforming.

3. Permitting requirements. It refers to the several legal requirements, such as regulations and standards, necessary for hydrogen production approval. The most important ones derive from EU Directives, but, while the overall requirements are similar across all the countries, significant differences in interpretation and implementation exist.
   The main EU Directives that specifically apply to production of hydrogen and generate obligations on operators and manufacturers are the following:

  - Seveso Directive (2012/18/EU). The Directive deals with the control of major-accident hazards involving dangerous substances. It contains general obligations and requirements for operators, including safety report, internal and external emergency plans, actions to be taken and other obligations to competent authorities and Member States. Hydrogen is classified in Annex 1 Part 2 as a dangerous substance and the thresholds are set to more than 5 tons as lower-tier requirements and more than 50 tons as upper-tier requirements; thus, for quantities less than 5 tons of hydrogen none of the obligations above applies.

  - ATEX Directive (2014/34/EU). The Directive defines the essential health and safety requirements and conformity assessment procedures to be applied to products intended for use in potentially explosive atmospheres and placed in the EU market. Thus, it is significant in design and construction of hydrogen production plants. Obligations to manufacturers, importers and distributors are present, as well as definition of conformity assessment procedures, EU declaration of conformity and CE marking.

  - IED Directive (2010/75/EU). The Directive deals with industrial emissions in the perspective of integrated pollution prevention and control. Definition of emission limit values and monitoring requirements are present for several typologies of plants. Production of hydrogen is included in chemical industry activities in Annex 1, but no quantitative thresholds are present.

  - SEA and EIA Directives (2001/42/EC, 2011/92/EU, 2014/52/EU). The three Directives (and their subsequent amendments) define a strategic environmental impact assessment procedure. Projects listed in Annex I shall be subjected to assessment, while for projects listed in Annex II each Member States shall determine if an assessment is necessary on a case-by-case examination or in a threshold perspective. Hydrogen production and storage may fall both in the first (Integrated chemical installations) or in the second class (production of chemicals or storage facilities for chemical product).

The scopes of the above requirements are the protection human life, property and the environment, but some inconsistencies and potentially unintended consequences are expressed by the HyLAW project, and mainly two are mentioned:

- The absence of clear thresholds in discrimination for the size of the production plants, leading often to the same complication in the requirements for small decentralized units as well as for large centralized facilities. In particular, in the application of the IED the interpretation of “industrial scale” may be misleading, while the application of the EIA and SEA Directives for the specific cases is often left to the discretion of the authorities.
- The lack of any distinction among the various methods to produce hydrogen, which is a feature common to all the above requirements.

8.2.2 STORAGE OF HYDROGEN

Two LAPs related to the storage of hydrogen as a compressed gas, cryogenic liquid and in metal hydrates are indicated:

1. Land Use Plan, including zone prohibition. The situation is similar to the hydrogen production described above. For almost all the countries, hydrogen storage units can only be installed in locations belonging to industrial areas, due to the traditional view of hydrogen as an industrial gas, or in some cases in commercial areas. The lack of distinction considering the quantities of hydrogen stored is mentioned as a barrier to the deployment of the technology. An exception is found in Sweden, where different levels of requirements for prohibition zones depending on the quantity of hydrogen stored are present.
2. Permitting requirements. The storage of hydrogen is in general subjected to permitting requirements connected to risk assessment (SEVESO Directive, if more than 5 tons of hydrogen are stored), health and safety requirements (referring mainly to the ATEX Directive) and environmental impact assessment procedures (as envisioned by the SEA and EIA Directives). While in six countries studied (Austria, France, Germany, Hungary, Spain and Sweden) various simplified processes for demonstration and small-scale projects exist, in Italy the operating permit from the municipality is based on different local regulations; the requirements typically include the authorization from the local Fire Department, from the regional environmental protection agency (ARPA) and local safety authority (ASL).
   The main criticism expressed by the HyLAW report related to the permitting requirements refers to the application of SEA and EIA Directives, leading to high costs on operators and further delays. Moreover, in some cases, very restrictive safety distances are imposed.

8.2.3 ELECTRICITY GRID ISSUES FOR ELECTROLYSERS

Hydrogen production via electrolysis needs access to electricity that can be obtained entirely through a connection to an electricity grid (e-grid) or using also local electrical renewable sources; in any case, access to e-grid is in general required.

The regulatory framework covering the electricity grid and transmission/distribution networks in Europe has shifted to a liberalized market system and opened the electricity sector to market competition over the past 20 years. The main EU legislation framework related to the regulation of the grid access has been part of three “energy packages”, which has been complemented by Commission Regulation 2016/1388 for establishing a network code on demand connection. According to the Regulation, the connection of an electrolyser to the e-grid as an energy consuming function should be performed at the local level by the low voltage Distribution Network Operator (DNO). However, different load thresholds are present in the various countries and in some cases both DNO and TSO (Transmission System Operator) access and connection approvals are required: in Italy, the connection to the e-grid is operated by any of the commercial/public electricity companies as DNO if the power required is less than 10 MW, while for higher power the connection can be operated only by the TSO company Terna. In general, there are no significant differences between connecting an electrolyser or connecting other installations of a similar load demand, also considering the procedural steps to follow.

Electrolysers are a possible key element in the framework of Power-to-Gas (P2G). A P2G facility typically includes an electrolyser directly connected to the e-grid or directly connected to a renewable energy system to draw electricity needed for electrolyser to generate hydrogen, which can be temporarily stored and then used in fuel cells, ICE turbines or other power-electric generation system, or injected into the natural gas grid if specific requirements are ensured. In this way, P2G allows the direct connection between electricity grid and gas grid and it is recognized as having a significant role to play in decarbonizing and sustaining energy independency. However, the current legal framework has no provisions for P2G systems under either e-grid and gas grid common rules and the actual plants operate “by exception” or under a specific demonstration program. The absence of clear legal definition and coverage has the consequence of creating a substantial barrier to P2G deployment, with uncertain and difficult definition of specific burdens and supporting policies. This situation is common to Italy and to the other European countries.

P2G plants can play an important role in the electricity grid balancing, or load balancing, which is an ancillary service required by the transmission and distribution system operators to ensure the integrity and stability of the electricity grid. When the network shows more power than needed, an electrolyser can be switched on to consume the power producing hydrogen, that can feed a fuel cell to provide power when the network shows less power than required to maintain load/frequency. However, not all the countries, including Italy, have accepted yet electrolyser operations for ancillary services within their regulatory framework.

8.2.4 STATIONARY POWER FUEL CELLS

Stationary fuel cells are a distributed generation technology, which means they produce power and heat at the site of the consumers and for the purpose of their immediate supply with energy [47]. They usually fall into the Micro-CHP paradigm, i.e. cogeneration units with a maximum capacity below 50 kW, as expressed in the Energy Efficiency Directive 2012/27. Following the HyLaw approach, three LAPs have been identified, which are related to the stationary fuel cells connection to the gas grid at supply side, to the electricity grid at demand side and for concerning the existing financial support mechanisms for their market roll out.

1. Requirements for connection to the gas-grid. At present, there is not a common EU framework for the connection of residential fuel cells to the gas grid. The connection must be performed by trained and qualified installers, usually by gas network operators. The requirements for the connection highly depend on the specific country, because are typically stipulated by the distribution network company. However, it is not considered a barrier in the potential diffusion of the technology.
2. Requirements for connection to the electricity-grid. As for the previous point, there is not a common EU framework for the connection of micro-CHP fuel cell plants to the electricity grid at present. A connection agreement with the electricity network operator is in general required; the requirements are typically general and not consider the specific case of fuel cells and, moreover, vary a lot in the different nations: in some countries a quite expensive technical documentation and even the carrying out of a feasibility study is needed, thus causing higher costs and delays, while, for example in Netherlands and Sweden, a simple

registration is required for injecting the produced power by the fuel cell in the electricity grid.

In the Energy Efficiency Directive, stationary fuel cells are included in high-efficient cogenerations. Thus, priority access and dispatch in the electricity grid should have been present, as well as for renewable energy technologies. However, even if the European Directive has been transposed to all countries, almost all of them failed to adopt simplified grid connection procedures for micro high-efficiency cogenerations, such as residential fuel cells.

3. Support mechanisms. Since residential stationary fuel cells are in market entry phase yet and they must compete with up-to-now more mature technologies, support mechanisms are necessary in the legal framework at European and country level, as it happens for other technologies: fuel cells fed with natural gas may be compared to high efficiency micro CHP plants, while for fuel cells fed with green fuels, such as hydrogen, the same preferential treatment as of technologies generating electricity from renewable sources may be. At present, significant differences are present among countries for this aspect. Most of the European countries show no support for stationary fuel cells, while for the others in general fragmented and ineffective measures have been carried out. An exception is Germany, where a specific program promoting the purchase of below 5 kW stationary fuel cells is present, as well as other incentives measures. Other countries, including Italy, support them as any other cogeneration units, with feed-in tariffs and certificates. CAPEX support and incentives for self-production are present only in few countries.

   For concerning European legislation, Directive 2018/844 aims to promote the use of smart technologies in buildings; however, it depends on national implementations of the Directive if micro-CHP fuel cells plants are included in technologies for reducing CO_2 emissions.

9. RISK ANALYSIS

In this part of the work a preliminary risk analysis for the concerned plant is presented. For the purpose, the plant has been subdivided into 6 main nodes and for each of them the identification of the most relevant hazards has been carried out, following information on failure modes and deviations obtained from literature and from risk analysis studies performed on similar plants. For each deviation, the main possible causes that may originate it and the main effects that it may create are shown, as well as the detection, prevention and mitigation measures suggested for improving the safety of the plant. The worksheet available in (11) resumes all this part.

In the second part of the chapter, after a brief description of the properties of hydrogen for concerning safety, some quantitative assessments of damage to people connected to some of the deviations highlighted in the worksheet are presented, especially considering hydrogen use. The analysis has been carried out using semi-empirical models and Probit equations to assess the expected damage to people in case of fire and explosion.

9.1 RISK ANALYSIS WORKSHEET CREATION

The representation of the 6 considered nodes of the system for the risk analysis purpose is given in *Figure54*. They are the natural gas supply, the gas processing unit (also subdivided into heat exchangers, fuel line and oxidant line), the stack module, the afterburner unit, the exhaust gas cooling unit and the hydrogen processing unit.

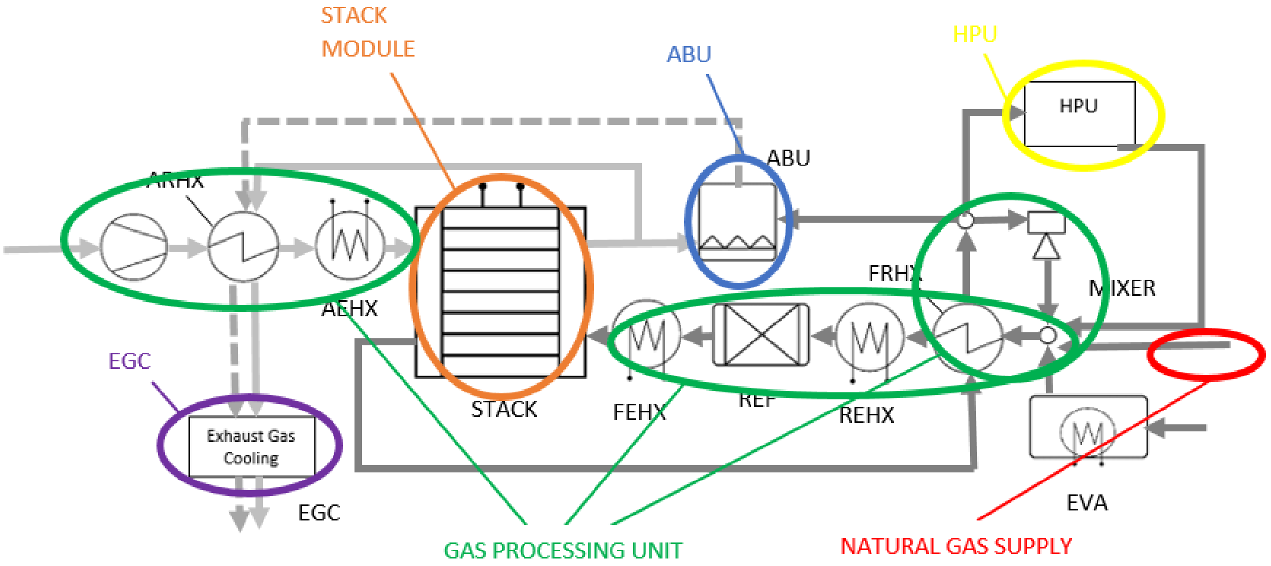

Figure 54 Risk analysis: system configuration

In the presented worksheet (11) some relevant deviations from the expected function have been presented for each node, as well as the list of possible causes and effects connected to them. The identification of these aspects has been done after a literature review on typical failures in fuel cells – based systems and from risk analysis performed to similar plants. Due to the lack of information on the precise configuration of the system, as for example for the number and the position of valves and other components, this approach has been considered the best for carrying out a risk analysis.

In each row of the worksheet, the possible deviation is associated to a category and three discrete levels of frequency, damage and risk, in order to preliminarily assess which deviations could be the most critical and for which a more precise analysis would be required. The frequency level has been evaluated through information found in literature and by using OREDA tables [49], which provide a useful database on rates of failure of simple component, such as compressors, heaters and valves. The assumed levels from 1 to 5 are given in *Table14* as function of number of events per year.

Frequency		
1	Not expected	$f < 10^{-3} ev/y$
2	Less than 1 event in 100 years	$10^{-3} \leq f < 10^{-2}\ ev/y$
3	Less than 1 event in 10 years	$10^{-2} \leq f < 10^{-1}\ ev/y$
4	Less than 1 event in 3 years	$10^{-1} \leq f < 3x10^{-1}\ ev/y$
5	More than 1 event in 3 years	$f \geq 3x10^{-1} ev/y$

Table 14 Risk Analysis: Frequency levels

For concerning the effects generated by the deviations, they have been classified into three categories:

- damage to people (P): it is measured in terms of injuries and deaths and has been more precisely analyzed in the following part with semi-empirical models;
- economical damage (M): it refers to both impossibilities to exploit the potential of the system, such as covering thermal and electrical load in SOFC modes of operation or producing hydrogen in SOEC mode of operation (*TEH loss*), and ruptures of components causing a money expenditure to recover or substitute them;
- environmental damage (E): since dangerous substances for environment contamination are not used in the plant, it refers only to the pollutant levels that may be released in atmosphere in exhaust gas stream after the combustion.

Information on the considered damage levels is given in *Table15*.

Damage	People (P)	Economical (M)	Environmental (E)
1	Negligible Impacts	Negligible Impacts (Loss of TEH for no more than 1 hour and no relevant ruptures)	Emissions out of standard for less than 1 day
2	Injuries to workers for no more than 3 working days	Loss of TEH for no more than 1 day or ruptures for no more than 1000 €	Emissions out of standard for less than 1 week
3	Injuries to workers for no more than 2 weeks	Loss of TEH for no more than 1 week or ruptures for no more than 10 000 €	Emissions out of standard for less than 1 month
4	Single death or injuries for no more than 1 month	Loss of TEH for no more than 1 month or ruptures for no more than 100 000 €	Emissions out of standard for more than 1 month
5	Multiple deaths and injuries	Loss of TEH for more than 1 month and ruptures for more than 100 000 €	-

Table 15 Risk Analysis: Damage levels

Three risk matrices have been constructed (*Figure55*) in order to evaluate if the couple frequency-damage for an accident must be considered:

- Acceptable (green cells): the calculated risk is low and no additional safety measures may be considered unless the correct development of prescribed safety procedures;
- ALARP – As Low As Reasonably Practicable (yellow cells): at this stage of the analysis, it means that the risk could be unacceptable and a more precise calculation on the precise final configuration of the plant or with more precise damage evaluation models should be carried out;
- Unacceptable (red cells): the calculated risk is high, so that the considered configuration is a priori unacceptable and relevant corrective measures shall be implemented.

f P	1	2	3	4	5
1	🟩	🟩	🟩	🟨	🟨
2	🟩	🟩	🟨	🟨	🟥
3	🟩	🟨	🟨	🟥	🟥
4	🟨	🟨	🟥	🟥	🟥
5	🟨	🟥	🟥	🟥	🟥

f M	1	2	3	4	5
1	🟩	🟩	🟩	🟩	🟨
2	🟩	🟩	🟨	🟨	🟨
3	🟩	🟨	🟨	🟨	🟥
4	🟩	🟨	🟨	🟥	🟥
5	🟨	🟨	🟥	🟥	🟥

f E	1	2	3	4
1	🟩	🟩	🟩	🟨
2	🟩	🟩	🟨	🟨
3	🟩	🟩	🟨	🟨
4	🟩	🟨	🟨	🟥
5	🟨	🟨	🟥	🟥

Figure 55 Risk analysis: Risk matrices

The last three columns of the worksheet refer to the safety measures considered and suggested in the plant. Detection purpose is to detect the occurrence of undesired or unexpected conditions in physical parameters of the system – such as temperature, pressure or release sensing – in order to promptly intervene to stop the possible evolution of the accident. Prevention measures are connected to limiting the occurrence of the causes responsible for the accident and at this stage of the analysis are mainly related to performing an adequate and periodical maintenance on the different parts of the system. Mitigation measures acts on the effects of the accident to reduce the connected damage; they are for example safety procedures for shut-down of the system, operational changing or fire-fighting appliances.

Four main operational configurations have been considered in the analysis. They are NG-SOFC mode, H2-SOFC mode, SOEC mode and the configurations related to start-up and shut-down of the system as well as the switching conditions between two of the first three configurations. For each row of the worksheet, the identification of the operational condition in which it may occur is provided.

As the result of the risk analysis, 16 main possible deviations have been identified. After the following quantitative analysis about damages mainly related to the use of hydrogen in the plant, the main results of the analysis are provided.

9.2 SEMI-EMPIRICAL MODELS FOR EVALUATION OF DAMAGE

9.1.1 HYDROGEN

Hydrogen is a gas at room temperature, characterized by a critical temperature of 33.18 K and by a triple point temperature of 13.95 K [50]. It is a colorless and odorless gas, with the lowest molecular weight (2.106 g/mol), the lowest density (0.0899 kg/m^3 at standard condition) and the lowest viscosity among the gases. Moreover, it shows the highest diffusion coefficient in air (0.61 cm^2/s, i.e. almost four times the value of methane) [51]. For these reasons, it has a high propensity to leak, it rapidly mixes with the ambient air upon release going upwards, due to high buoyancy [52]. This fact is positive for safety viewpoint in unconfined areas, but is negative in closed rooms, where hydrogen can rapidly accumulate underneath the roof.

The most relevant chemical property of hydrogen is its flammability [53]. Indeed, it is an extremely flammable gas, characterized by a very wide flammability range and classified in category 1a in CLP regulation: LEL in air is 4.0% (while it is 5.0% for methane) and UFL is 75.0% (15.0% for methane). It reacts with all oxidant species, such as oxygen, chlorine and nitrous protoxide, with extremely exothermic reactions. The minimum ignition energy is very low, around ten times less than the one required by LPG and hydrogen flames are very hot and not visible in daylight. Auto-ignition temperature is 585 °C.

Even if in general hydrogen is not corrosive, some metals show the embrittlement phenomenon if are in contact with hydrogen. It means that individual hydrogen atoms can diffuse through the metal structure and then recombining to form hydrogen molecules, having the effect of reducing the ductility and tensile strength of the material and generating cracking inside it. Therefore, steel tanks for pressurized hydrogen are constructed with a special alloy [53].

For concerning environmental and health hazards, hydrogen shows less problems. If it is released in atmosphere, hydrogen is not dangerous nor for the ozone layer nor for the greenhouse effect; if it is used as a fuel in a combustion process, hydrogen produces only water molecules and no carbon species or dangerous products are created. Hydrogen is not toxic for people but may cause asphyxiation if inhaled in very high concentration, because of its substitution to the oxygen of air. However, since the hydrogen concentration lower limit for asphyxiation risk is 17%, which is much higher than the 4%-limit for fire and explosion risk, in general it is much more probable to produce an explosion before having health hazards [53]. Thus, only dangers related to its flammability are typically considered.

As expressed in the Joint Research Center reference report on hydrogen safety [54], a hydrogen accident usually follows a typical sequence of events, which is characterized by an unintended release of the gas, the mixing of hydrogen with air creating a flammable mixture and the ignition of the flammable cloud which can cause, depending on the specific conditions, flames or explosions.

In the concerned plant, hydrogen is produced in SOEC mode of operation at low pressure in the stack module located in a closed and ventilated room. Then, it passes to the HPU, located outside, and is compressed and stored in a vessel at high pressure (200 bar) as a compressed gas. In H2-SOFC mode of operation it is expanded to relieve its pressure inside the HPU, and it is delivered to the stack module, where it is converted into steam generating power and heat.

A schematic representation of the concerned system for hydrogen risk analysis is provided in *Figure56*. The inner zone is constituted by the closed and ventilated room where the stack module is located; low pressure levels in ducts are present. The hydrogen processing unit is situated in the outer zone and high-pressure conditions can take place between the compressor unit and the storage tank. Between the two zones hydrogen is exchanged at low-pressure condition.

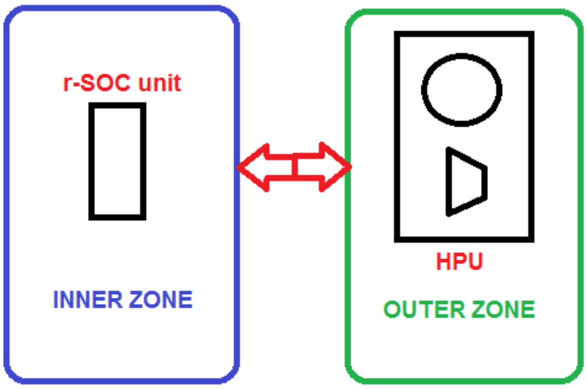

Figure 56 Risk Analysis: Schematic representation of outer and inner zone

The main quantities for describing the two zones are here provided. They have been used in the following part for a quantitative evaluation of the damage to people. Simple semi-empirical methods have been used in free field conditions. Safety distances have been obtained for the various scenario, that have been compared with the legislative prescribed distances in case of no physical barrier is present. This is not the case of the concerned plant, but this has been considered the way to have a fair comparison between the calculated free-field effects and the real damage.

For concerning the inner zone, the dimensions of the room where the r-SOC stack will be located are collected in *Table17*, as well as the approximated net volume calculated taking off the volume occupied by a big pipe. Moreover, the enclosure has a fixed vent opening towards outside in the upper part of one wall.

Room Dimensions [m]	6.7 x 4.6 x 3.3
Net Volume [m^3]	92.6
Opening Dimensions [m]	4.5 x 0.5

Table 16 Risk Analysis: Enclosure characteristics

For concerning the outer zone, the assumed storage vessel conditions are resumed in *Table18*. They have been obtained by considering the maximum hydrogen pressure and contained mass data and assuming a reference temperature condition. Density and volume have been obtained from the hypothesis of ideal gas.

Pressure [bar]	200
Temperature [K]	298
Density [kg/m^3]	16.3
Mass of hydrogen [kg]	12
Volume [m^3]	0.737

Table 17 Risk Analysis: Storage vessel characteristics

9.1.2 JET FIRE SCENARIO

A jet fire is a turbulent diffusion flame resulting from the immediate ignition of a turbulent jet, that typically occurs when a compressed flammable gas is accidentally released. The present scenario considers the case of a leakage from the high-pressure circuit in the hydrogen processing unit, between the compressor unit and the hydrogen storage. For assessing the consequences the following approach has been used: two models have been employed one after the other to obtain the released hydrogen flowrate and the dimensions of the jet flame, which are used to evaluate the surface emissive power of the flame and the radiative heat flux, which can be directly associated to the effects to people through Probit equations. Depending on the size of the leakage, different results are obtained. For this reason, three hole-sizes have been considered: small size (1 mm), medium size (4 mm) and big size (10 mm).

The first part of the procedure deals with the evaluation of the gas conditions in case of accidentally release through a hole from a vessel. The main assumptions of the considered model are mono-dimensional outflow, lumped parameters, velocity vector orthogonal to the surface of the hole and mean velocity as the modulus.

Since the critical ratio for hydrogen ($\gamma = 1.406$ is the ratio between specific heat capacity at constant pressure and specific heat capacity at constant volume) is:

$$r_{cr} = \left(\frac{2}{\gamma + 1}\right)^{\frac{\gamma}{\gamma - 1}} = 0.527$$

the gas release from vessel pressure to ambient pressure is in sonic conditions. Moreover, an adiabatic outflow has been considered and to be conservative the maximum value at the initial time has been assumed to be constant for the released flowrate. For the small size hole, the main calculated values at the outlet section at initial time are given in *Table19*.

Pressure $[bar]$	Density $[kg/m^3]$	Temperature $[K]$	Velocity $[m/s]$	Flowrate $[kg/s]$
105.4	10.3	247.7	1199	0.0097

Table 18 Jet Fire Scenario: Released hydrogen quantities

The second part of the procedure considers the immediate ignition of the released gas flow to create a jet fire. The main values of the fire have been calculated below.

For the flame length evaluation, the following relation has been assumed [55]:

$$L_{flame} = 0.00327 \cdot (\dot{m} \cdot \Delta\mathrm{H_{comb}})^{0.478} \qquad [m]$$

The maximum radius of the flame is given by the following relation [55]; to be conservative it has been considered constant for all the length of the flame:

$$R_{flame} = \frac{0.1244 \cdot L_{flame}}{2} \qquad [m]$$

The most important parameter for defining a fire in a solid flame model is the surface emissive power (SEP), which represents the heat flux due to heat radiation. It is defined as:

$$SEP = \frac{F_{rad} \cdot \dot{m} \cdot \Delta H_{comb,gas}}{A} \qquad \left[\frac{W}{m^2}\right]$$

Where:

- $F_{rad} = 0.15$ for hydrogen [56] representing the fraction of heat radiated from the flame.
- $\Delta H_{comb,gas}$ $[J/kg]$ is the heat of combustion of hydrogen (120 000 kJ/kg [57]).
- A $[m^2]$ is the surface emitting area of the solid flame.

The radiative heat flux received by a target is a fraction of the surface emissive power and it is given by the following formula:

$$q = SEP \cdot F_{view} \cdot \tau \qquad \left[\frac{W}{m^2}\right]$$

Where F_{view} is the view factor, which depends on the relative direction between the flame surface and the target surface, while τ represents the air transmissivity, which accounts for the absorption and scattering phenomena which reduce the heat flux to the target and for which especially water vapour and carbon dioxide contained in the air are responsible.

The view factor has been evaluated using the following formula [58], which is valid for cylindrical flame surface and target at ground level and in vertical position.

$$F_{view} = \frac{1}{\pi \cdot H} \cdot \arctan\left[\left(\frac{L^2}{H^2 - 1}\right)^{\frac{1}{2}}\right] + \frac{L \cdot (X - 2 \cdot H)}{\pi \cdot H \cdot \sqrt{X \cdot Y}} \cdot \arctan\left[\left(\frac{(H-1) \cdot X}{(H+1) \cdot Y}\right)^{\frac{1}{2}}\right] - \frac{L}{\pi \cdot H} \cdot \arctan\left[\left(\frac{H-1}{H+1}\right)^{\frac{1}{2}}\right]$$

Where $H = d/R$, $L = L_{flame}/R$, $X = (1 + H)^2 + L^2$ and $Y = (1 - H)^2 + L^2$.

The air transmissivity has been evaluated through the Wayne equation [59]:

$$\tau = 1.006 - 0.0117 \cdot \log A - 0.02368 \cdot (\log A)^2 - 0.03188 \cdot \log B + 0.001164 \cdot (\log B)^2$$

Where:

$A = 288.65 \cdot R_H \cdot d \cdot p_{sat}/T_{air}$ is the term due to water vapour: R_H is the relative humidity of the air, which is between 0 and 1 and a value of 0.6 [59] has been used; p_{sat} represents the saturated water vapour pressure expressed in mmHg; T_{air} is the ambient air temperature and it is assumed to be 293 K.

$B = 273 \cdot d/T_{air}$ is the term due to carbon dioxide.

The consequences to people of jet fire have been evaluated by using three Probit equations provided by TNO [54], valid for first degree burn, second degree burn and fatality respectively:

$$\Pr(first\ degree\ burn) = -39.83 + 3.0186 \cdot \ln V$$

$$\Pr(second\ degree\ burn) = -43.14 + 3.0186 \cdot \ln V$$

$$\Pr(fatality) = -37.23 + 2.56 \cdot \ln V$$

Where V is a parameter accounting both for thermal radiation and time of exposure of the target:

$$V = q^{\frac{4}{3}} \cdot t \qquad [\left(\frac{W}{m^2}\right)^{\frac{4}{3}} \cdot s]$$

Moreover, three levels of damage have been considered, depending on the heat flux received by the target [54]:

	Consequences	Thermal Radiation $[kW/m^2]$
No harm level	No harm for long exposure	1.6
Severe injuries	Second degree burns after 20 seconds	9.5
High lethality	100% lethality in 1 minute	25

Table 19 Jet Fire Scenario: Consequence levels

The previous procedure has been carried out for 3 different sizes of the hole: a small size (1 mm), a medium size (4 mm) and a big size (1 cm). In *Table21* the resulting distances to which the three consequence levels are reached in the three cases are resumed, while in *Table22* the results are expressed in terms of time of exposure of a constant heat flux to have a half probability ($Pr = 5.0$) to receive a first degree, a second degree burn and to die at a distance of 10 and 30 meters from the flame.

DISTANCES [m]	$\boldsymbol{d = 1\ [mm]}$	$\boldsymbol{d = 4\ [mm]}$	$\boldsymbol{d = 10\ [mm]}$
No harm level	3.8 m	13.7 m	34.9 m
Severe injuries	0.7 m	2.4 m	6.2 m
High lethality	0.3 m	1.2 m	2.3 m

Table 20 Jet Fire Scenario: Results 1

TIMES [s] – distance 2 m	$\boldsymbol{d = 1\ [mm]}$	$\boldsymbol{d = 4\ [mm]}$	$\boldsymbol{d = 1\ [cm]}$
First Degree Burn	60.9 s	11.6 s	3.4 s
Second Degree Burn	182.3 s	34.6 s	10.0 s
Fatality	315.4 s	59.8 s	17.2 s
TIMES [s] – distance 10 m	$\boldsymbol{d = 1\ [mm]}$	$\boldsymbol{d = 4\ [mm]}$	$\boldsymbol{d = 1\ [cm]}$
First Degree Burn	819.5 s	91.4 s	25.9 s
Second Degree Burn	2453 s	273.4 s	77.5 s
Fatality	4245 s	473.1 s	134.0 s

Table 21 Jet Fire Scenario: Results 2

9.1.3 EXPLOSION SCENARIO

An explosion is a release of energy occurring in a sufficiently short time to generate a pressure wave going away from the source and can be heard [60]. Explosions can be classified into two categories: chemical explosions – where chemical reactions are present in the energy release phenomenon – and physical explosions – where not.

In the concerned plant, hydrogen is present at high pressure in the storage vessel. Two main cases have been considered to possibly occur that can create the explosion scenario:

1) Quick expansion of the compressed hydrogen due to a collapse of the vessel. This scenario, even if very rare, may be due to a fire in the proximity of the vessel, which heats up the compressed gas, causing mechanical stress on the component (physical explosion).

2) Release into atmosphere of a large quantity of hydrogen, forming a vapour cloud, and delayed ignition of the cloud, causing a vapour cloud explosion (chemical explosion).

A detailed evaluation of the effects of an explosion is possible only by using CFD models created ad hoc with very precise knowledge of the concerned physical system and characteristics of the area. However, for approximated assessment of the overpressure generated by an explosion, quick methods based on empirical correlations have been developed in the past. One of most used method is the equivalent TNT mass method. It equals the damages generated by the concerned explosion and the consequences of the detonation of a certain quantity of TNT (Trinitrotoluene).

For a chemical explosion, the TNT mass is calculated through the following expression:

$$M_{TNT} = \epsilon \cdot M_{gas} \cdot \frac{\Delta H_{comb,gas}}{\Delta H_{comb,TNT}} \qquad [kg]$$

Where:

- ϵ represents the efficiency or "yield" of the explosion. Its determination is quite complex since it comprises all the effective differences between the TNT detonation and the vapour cloud explosion; however, it is typically assumed to be between 0.01 and 0.1 [61].
- M_{gas} $[kg]$ represents the mass of hydrogen in the cloud; to be conservative, the maximum total mass of hydrogen contained in the pressure vessel has been assumed.
- $\Delta H_{comb,gas}$ $[kJ/kg]$ is the heat of combustion of hydrogen (120 000 kJ/kg [57]).
- $\Delta H_{comb,TNT}$ $[kJ/kg]$ is the released heat from a TNT explosion (4 686 kJ/kg [62]).

For concerned the physical explosion scenario, the equivalent TNT mass have been calculated with the following relation [60]:

$$M_{TNT} = 0.024 \cdot \frac{p_{storage}[bar] \cdot V_{storage}[m^3]}{\gamma - 1} \cdot \left[1 - \left(\frac{1}{p_{storage}[bar]}\right)^{\frac{\gamma-1}{\gamma}}\right] \qquad [kg]$$

From the equivalent TNT mass previously calculated, the scaled distance parameter has been evaluated at different distances d from the source of the explosion, by:

$$Z = \frac{d}{M_{TNT}^{\frac{1}{3}}} \qquad [m \cdot kg^3]$$

The peak overpressure of the shock wave may be directly found from the value of the scaled distance, through the following empirical relation [63]:

$$P_s = 80800 \cdot \frac{\left[1 + \left(\frac{Z}{4.5}\right)^2\right]}{\sqrt{1 + \left(\frac{Z}{0.048}\right)^2} \cdot \sqrt{1 + \left(\frac{Z}{0.32}\right)^2} \cdot \sqrt{1 + \left(\frac{Z}{1.35}\right)^2}} \qquad [kPa]$$

The consequences to people generated by the blast wave have been evaluated through the following Probit equation [54], provided by AICHE, which considers the case of death due to lung hemorrhage.

$$Pr = -77.1 + 6.91 \cdot \ln(P_s[Pa])$$

Moreover, as for the jet fire scenario, the following three levels of damage have been considered:

	Consequences	Overpressure $[kPa]$
Negligible harm	People knocked down by the pressure wave	10.3
Severe injuries	50% probability of eardrum rupture	34.5
High lethality	100% probability of fatality from missile wounds	48.3

Table 22 Explosion Scenario: Consequence levels

The previous procedure has been carried out for chemical explosion for three different values of yield: 0.01, 0.03 and 0.1. They correspond to an equivalent TNT mass method of 3.1, 9.2 and 30.7 kg respectively. Since in the physical explosion equation, the equivalent TNT mass results 6.9 kg, the effects for this scenario would be between the first two cases and in the following part have not been developed.

The peak overpressure of the blast wave at different distances has been calculated for the three cases; in *Table24* the results of the model are resumed: the distances at which the three damage levels are reached are expressed, as well as the distance for which a 50% probability of death due to lung hemorrhage occurs according to the Probit equation ($Pr = 5.0$):

DISTANCES [m]	$\boldsymbol{\epsilon = 0.01}$	$\boldsymbol{\epsilon = 0.03}$	$\boldsymbol{\epsilon = 0.1}$
Negligible harm	14.1 m	20.3 m	30.3 m
Severe injuries	6.7 m	9.6 m	14.3 m
High lethality	5.6 m	8.1 m	12.0 m
50% Probit	3.4 m	4.9 m	7.3 m

Table 23 Explosion Scenario: Results

9.1.4 INTERNAL RELEASE SCENARIO

The last scenario considers a release of hydrogen in a low-pressure pipe occurring in the enclosure where the r-SOC stack module is located.

For evaluating the hydrogen released flowrate, the same formulas as in the jet fire scenario for compressed gas release have been used. In this case, the thermodynamic conditions of gas are different: the pressure has been assumed to be equal to 0.05 barg and the nominal temperature of the stack (1003 K) has been considered for the leakage stream. The outflow is in subsonic conditions and the results of the outstream quantities for a hole diameter equal to 1 mm are collected in *Table25*. The ideal gas hypothesis and adiabatic expansion have been assumed.

Pressure $[bar]$	Density $[kg/m^3]$	Temperature $[K]$	Velocity $[m/s]$	Flowrate $[m^3/s]$
1	0.026	923	1514	0.00119

Table 24 Internal Release Scenario: Released hydrogen quantities

The calculated volumetric hydrogen flowrate $\dot{V}_{leak}$ has been considered constant during time, since it has been assumed that the leakage occurs in a fuel line pipe, where the stream is driven at a fixed pressure.

The Lower Explosive Level (LEL) for concerning hydrogen is 4.0% in volumetric term. For safety reason, the concentration limit for preventing fires and explosion in enclosures is lower. In this work, a value equal to half of LEL has been used. Given the room dimensions (*Table17*), the assumed critical value ($CV = 1\%$) and the calculated release flowrate, time to reach critical value in the enclosure has been computed as:

$$t = \frac{V_{room} \cdot CV}{\dot{V}_{leak}} = 1557\ [s]$$

In case of release, the hydrogen sensing system must intervene within that time in order to stop the fuel flow and to avoid reaching the critical concentration inside the enclosure. Moreover, the presence of the high vent opening guarantees air natural recirculation which can disperse hydrogen increasing safety. The effect is also enhanced due to high buoyancy of hydrogen.

As a reference value, the required ventilation rate in terms of air change per hour (ACH) not to accumulate hydrogen in the room results [64]:

$$ACH = \frac{\dot{V}_{leak}\left[\frac{m^3}{s}\right] \cdot 3600\ \left[\frac{s}{h}\right]}{V_{room} \cdot CV} = 2.31$$

9.3 RESULTS

The evaluation of the damage to people caused by a release of hydrogen in different parts of the r-SOC system has been carried out mainly through semi-empirical models. Due to lack of precise knowledge of the system characteristics and to some significant assumptions that have been made, the following exposed results represent a preliminary assessment on the possible effects to people caused by some specific scenarios. In a more advanced project stage, the presented results should be compared to them obtained from more accurate methods.

The jet fire scenario has given a maximum distance for not having consequences equal to 34 m. However, the severe injuries level has been reached at no more than 7 m in the worst case. For smaller hole size, damage level is substantially reduced. By using the Probit equations, at a distance equal to 10 m from the flame source fatality has been obtained to occur after more than 2 minutes of exposure, while for the less impacting considered case, more than a minute of exposure has been calculated for having first degree burns at 2 m.

In the worst case considered for the explosion scenario, a safety distance of around 30 m has been obtained as without consequences to people. Blast overpressure high lethality levels have been reached at no more than 12 m and the Probit equation referring to death due to lung hemorrhage has given 7.3 m as the distance threshold. For concerning the other considered case in the sensitivity analysis, a safety distance of no more than 20 m has been obtained. Severe injuries can occur at less than 10 m.

Since these results have been obtained for free field conditions, a comparison to the safety distance prescribed by the Italian legislation for pressurized vessel without degree of safety has been considered fair. In this case, the fencing shall be placed at 20 m from the tank, while external buildings at 30 m. Consequently, serious consequences to people are extremely improbable.

The internal release scenario has shown has highlighted how, considering a possible hole size for hydrogen leakage in the enclosure where the stack module is located, more than 25 minutes are necessary before having risks of flammable mixtures in case of no ventilation. In this case, the large vent present in the upper part of the enclosure wall should be adequate for avoiding major risks.

The preliminary risk analysis worksheet has been created on the basis of literature review and performed risk analysis on existing plants and after the described assessment of damage to people. 16 deviation conditions have been highlighted, of which 3 have been considered acceptable and the other 13 has been marked as ALARP. None of the evaluated deviation has resulted a priori unacceptable. The most critical scenarios have been obtained for production damage due to rupture of expensive components and systems. In a more advanced stage of project, a more structured and precise risk assessment should be performed, especially considering the ALARP deviations that have been highlighted.

10. CONCLUSIONS

In this Master thesis work a stationary reversible solid oxide cells (rSOC) system has been analyzed as a renewable energy storage within the framework of a microgrid.

System concept has been based on an existing research project for which the installation is envisaged in 2020, and, in the absence of precise knowledge of the entire system characteristics, data from other similar plant have been used to integrate.

The electrochemical system is coupled with a compressed hydrogen storage vessel and can operate in three main configurations: in addition to hydrogen fuel cell and steam electrolyser, the stack can be fed with natural gas taken from the grid to generate power. The rSOC system has been analyzed as integrated in a real microgrid system constituted by Environment Park, Turin, Italy. The supply side is constituted by a hydro power plant and a small photovoltaics, while the demand side consists of an office building. For both an hourly resolution annual energy profile has been constructed, using PVGIS software for photovoltaics and typical US office profile for the demand, while for hydro plant real measured data have been used.

The rSOC stack and most of the balance of plant components have been dynamically modelled in SIMULINK©. Starting from a typical rSOC concept, the system configuration has been gradually modified for taking into consideration all operating points and the three configurations.

The created model has been tested through steady-state simulations to obtain a worksheet of 15 operating points at various power levels to cover all the operating field of the plant. Results have been consistent with them expected. In normal operation electrical efficiency in NG-SOFC mode has been slightly higher than in H2-SOFC reaching a maximum value of 48.3%. Conversely, maximum heat gain has been obtained in hydrogen mode and the highest global efficiency has been 83.2%. Ancillary power distribution has been analyzed and a relevant consumption has resulted in the hydrogen compression in electrolyser mode. From the stack temperature analysis, all considered operating points has maintained the nominal temperature in steady-state conditions, except for some points in electrolyser endothermic cases, where a maximum decrease of around 70 degrees has resulted.

The steady-state points have been interpolated to create a continuous field of operation. It has been used to perform second-resolution annual simulations in MATLAB©, jointly with the created energy profiles for supply and demand side, in order to analyze the integration of the rSOC system in the real environment. NG-SOFC has been assumed in all the moments in which the other two modes are unable, depending on the hydrogen storage filling; the microgrid is then completed by a battery unit, to which the main priority in both charge and discharge has been considered. Four cases have been studied using the steady-state points succession model, depending on the share of renewables intended for interacts with rSOC.

With high and low shares, the results have been similar and NG-SOFC have resulted definitely the most employed configuration, for more than 90% of time. In case of excessive shift towards demand side, electrolyser has resulted unable to work and the hydrogen tank has resulted empty for most of the time; conversely, in case of excessive shift towards supply side, hydrogen tank has resulted full for most of the time with the consequence of limiting also in this case the electrolyser operation.

The case with 30% share of renewables has resulted the best for energy storage framework, with high utilization of both battery and hydrogen. For 2338 hours electrolyser or hydrogen fuel cells mode were in operation and for more than 35% of time hydrogen tank has been actively used. The best integration has occurred in summer and autumn, were a general balance between energy supply and demand is present. In this case, the rSOC system has worked mainly as a daily energy storage, characterized by a hydrogen filling during nights and a hydrogen use in morning or afternoon depending on the discharging time of the battery. In periods when a general unbalance between supply and demand is present, the results have been worst, without exploiting the complete capacity of the rSOC system. The last case, in which all the supply side has been considered and the demand side has been increased for around ten times, has shown how interacting with higher power values a general increase in the hydrogen utilization is present, also due to fast charge and discharge of the battery.

Then, the dynamic model has been used to study specific transient conditions occurring in the system during switches among the three configurations, highlighting a maximum stack temperature decrease of 15 degrees. Finally, an entire day simulation has been performed totally using the dynamic model and the results have been compared to them found using the steady-state model for the same day. A remarkable agreement has been obtained. Daily profile of all the studied quantities have shown visible differences only in the switch periods, where oscillations found in the dynamic simulation has not been predicted by the steady-state model. However, considering the entire day the relative difference between the results for concerning hydrogen tank filling, ancillary energy consumption and heat recovery has been lower than 3%.

In the last two chapters, authorization and risk analysis parts have been carried out.

Three Italian regulations for concerning the rSOC installation in Environment Park has been discussed, pointing out some critical aspects impacting on the design parameters. In a European perspective, the current situation related to standard and regulation for hydrogen and fuel cells have been analyzed. A general lack in distinction of the methods by which hydrogen is produced and regarding plant sizes has resulted, as well as facilitations and incentives for decarbonizing solutions based on hydrogen, electrolysers and fuel cells. Today, regulations and standards still represent a barrier for hydrogen deployment.

A preliminary risk analysis worksheet has been finally presented. The study has been done relying on analysis performed on similar plants and on literature review. A more precise focus has been led to risks connected to hydrogen use, and a preliminary assessment of the levels of damage to people caused by some accident scenarios has been carried out. Jet fire and explosion scenario have been performed on the hydrogen storage at high pressure and a sensitivity analysis on hole size and yield of explosion respectively has been done. Simple semi-empirical methods in free field conditions have been mainly used and the effect distances have been compared to them prescribed by the Italian legislation in the absence of physical barriers. The third scenario has dealt with hydrogen release at low pressure occurring in the enclosure where the stack module is located. In all the cases, any critical scenario has been obtained.

11 APPENDIX

θ [°]	α [°]	θ [°]	α [°]	θ [°]	α [°]
180 (North)	11	300	10	60	31
185	5	305	9	65	33
190	5	310	9	70	35
195	5	315	9	75	32
200	5	320	2	80	28
205	5	325	2	85	18
210	4	330	2	90 (West)	13
215	11	335	2	95	2
220	11	340	2	100	2
225	10	345	2	105	2
230	10	350	2	110	2
235	9	355	2	115	2
240	9	0 (South)	2	120	2
245	6	5	2	125	2
250	7	10	2	130	2
255	7	15	2	135	2
260	8	20	17	140	2
265	8	25	17	145	2
270 (East)	8	30	26	150	2
275	9	35	25	155	8
280	9	40	24	160	9
285	10	45	23	165	10
290	10	50	22	170	10
295	10	55	21	175	10

Table 25 Appendix: Supply side: Considered angular views

RISK ANALYSIS WORKSHEET

NATURAL GAS FEEDING

code	FUNCTION	DEVIATION	CAUSE	EFFECTS	CAT	F	D	R	DETECTION	PREVENTION	MITIGATION	H2	NG	EL	SS
1	Supply the natural gas to the fuel line of the GPU and then to the stack for the electrochemical reactions	Presence of sulphur in the natural gas composition	Failure in the clean-up section before the GPU	If low concentration (<100 ppb) no damages; if higher, possible deactivation of catalysts in the pre-reformer and irreversible degradation of the stack	P	3	3	🟧	Monitoring of the natural gas composition before entering the GPU	Frequent maintenance of the clean-up unit	In case of signal of sulphur presence, switch the line not to deliver it to the GPU and the stack, use hydrogen for fuel if present or shut-down the system, intervention to substitute the clean-up unit		X		

GAS PROCESSING UNIT

HEAT EXCHANGERS

code	FUNCTION	DEVIATION	CAUSE	EFFECTS	CAT	F	D	R	DETECTION	PREVENTION	MITIGATION	H2	NG	EL	SS
2.1	Guarantee adequate conditions of temperature through recovery heat transfer of electric power	Not sufficient heat provided to the streams entering the stack unit	Problems in electric feeding for electric heaters; failures, obstructions or fouling in the component	Off-design temperature conditions in the stack unit; possibility of thermal stresses and damages on the stack unit; possibility of not cover the load or not exploiting the power	P	3	3	🟧	Control system of the module; temperature sensing on the streams	Maintenance and cleaning of the heat exchangers	Shut-down in case of no other safety measures can act	X	X	X	X

OXIDANT LINE

code	FUNCTION	DEVIATION	CAUSE	EFFECTS	CAT	F	D	R	DETECTION	PREVENTION	MITIGATION	H2	NG	EL	SS
2.2.1	In SOFC mode of operation: deliver the oxidant species (oxygen contained in the air) to the stack unit for the electrochemical reaction; in SOEC mode of operation provide the sweep gas necessary for correct operation	Not sufficient oxidant flow supply	Failure or malfunction in the air blower or problems in electric feeding	Off-design conditions in the stack unit due to lack of oxidant species; over-heating of the stack; impossibility to cover the load or the power; if continuous operation, possibility of damages to the stack	P	3	4	🟧	Control system of the module	Maintenance of the blower and presence of filters to avoid obstructions	If the air flowrate is lower but sufficient for cell operation, reduction of the load required by or the power delivered to the stack; if not, safety position of the system is necessary (injection of nitrogen and no power)	X	X	X	X
2.2.2			Rupture in an oxidant line due to accidentally shearing or due to fatigue; accidentally release from a valve		P	2	4	🟧	Control system of the module	Maintenance of the valves and of the lines		X	X	X	X

FUEL LINE															
code	**FUNCTION**	**DEVIATION**	**CAUSE**	**EFFECTS**	**CAT**	**F**	**D**	**R**	**DETECTION**	**PREVENTION**	**MITIGATION**	**H2**	**NG**	**EL**	**SS**
2.3.1	In SOFC mode of operation: deliver the fuel (natural gas, hydrogen, a mixture of also CO, CO2 and H2O after the recirculation loop and the reformer) to the stack unit for the electrochemical reaction; in SOEC mode of operation provide the steam (mixed with produced hydrogen) for the electrolysis reaction occurring in the stack	Not sufficient fuel flow supply or steam supply	Rupture in a fuel line due to accidentally shearing or due to fatigue; accidentally release from a valve	Off-design conditions in the stack unit due to lack of fuel species; impossibility to cover the load or the power	P	2	2	🟩	Control system of the module	Maintenance of the valves and of the lines	Depending on the position of the rupture, possibility of shutting down the system	X	X	X	X
2.3.2				Release of a gas stream rich in hydrogen (and natural gas and carbon monoxide for SOFC mode), with possibilities of fire and explosion in case of ignition	H	2	3	🟨	Control system of the module, sensing system for inflammable species in the atmosphere	Maintenance of the valves and of the lines	Shut-down system for limit if possible the released flowrate; evacuation of hydrogen (and other gases) towards vents; fire-fighting system	X	X	X	X
2.3.3		Non-desired outlet composition of the stream from the GPU to the fuel electrode of the stack	Failure or malfunction in the pre-reformer	Off-design conditions in the stack unit with possibility of damages	P	2	4	🟨	Monitoring of the fuel line gas composition exiting the GPU	Frequent maintenance of the pre-reformer chemical reactor	If possible, change parameters of the line for continuous operation; if fuel composition is dangerous for the stack, switch the lines and turn to safety position		X		

STACK MODULE															
code	**FUNCTION**	**DEVIATION**	**CAUSE**	**EFFECTS**	**CAT**	**F**	**D**	**R**	**DETECTION**	**PREVENTION**	**MITIGATION**	**H2**	**NG**	**EL**	**SS**
3.1	Performing the electrochemical reactions which convert the fuel mixture and the oxidant stream to electricity (SOFC mode) and the water steam and electricity into hydrogen and oxygen separated streams	No reaction in the unit	Degradation of the stack; absence of required thermodynamic conditions for the chemical conversion; causes due to former components (lack of fuel or steam in the fuel line or of oxidant in the oxidant line of the GPU)	SOFC mode of operation: no power production and demand not covered; SOEC mode of operation: no hydrogen production; sending to ABU a mixture rich in reacting elements (see ABU); damages to the unit	P	2	3	🟧	Control system of the module	Maintenance of the stack unit with particular attention to catalysts degradation, carbon deposition; substitution of catalyst every year and of the stack every three years	Shut-down the system	X	X	X	

AFTERBURNER UNIT

code	FUNCTION	DEVIATION	CAUSE	EFFECTS	CAT	F	D	R	DETECTION	PREVENTION	MITIGATION	H2	NG	EL	SS
4.1	Post-combustion of the gases exiting the stack unit	Problems in the combustion, with partial or total lack of the reaction in the component	Failure or malfunction in ABU; problems in former components (see stack unit)	Off-design conditions in stack unit (due to heat recovery from ABU exhaust gases), with possible lack of produced power and heat	P	2	3	🟨	Control system of the module	Frequent maintenance (check of ABU at least once a year to coincide with checks on the stack unit)	Shut-down in case of no other safety measures can act	X	X		
4.2				Release in atmosphere of an exhaust gas stream rich in hydrogen and carbon monoxide	E	2	2	🟩	Sensing system for hydrogen and carbon monoxide and periodical analysis on emissions		If detected, shut-down of the system to limit the amount of hydrogen and carbon monoxide release	X	X		

HYDROGEN PROCESSING UNIT															
code	**FUNCTION**	**DEVIATION**	**CAUSE**	**EFFECTS**	**CAT**	**F**	**D**	**R**	**DETECTION**	**PREVENTION**	**MITIGATION**	**H2**	**NG**	**EL**	**SS**
5.1	SOFC H2 mode of operation: deliver the stored hydrogen from the high pressure vessel to GPU after a pressure reduction section; SOEC mode of operation: receive the produced hydrogen from the stack unit, separation from water, increase the pressure by a compression stage and stored in high-pressure vessel; storage of hydrogen	Leakage of hydrogen in vessel, lines, compressor or turbine components of HPU	Degradation or accidentally release from valves	Release of hydrogen, with possibility to create a flammable athmosphere with risks of fire and explosion	H	2	3	🟨	Control system and H2 sensing system outside HPU and where hydrogen release may occur	Maintentance of vessel and lines of HPU; safety design for accidentally errors in valves position	Passive and active ventilation system to reduce risks of reaching LFL; containment structure of the unit	X	X	X	X
5.2.1		Overpressure in the vessel	Failure in active and passive control system of the vessel (possibly due to degradation of components)	Risk of physical explosion, rupture of the vessel and hydrogen release with possibility of jet fires, flash fires and chemical explosions; domino effect possibility	H	1	3	🟨	Pressure sensing in the vessel	Presence of a passive relief valve in order to reduce pressure if other control systems do not work properly; maintenance of the safety systems	Reducing the possibility of ignition; presence of safety distance from the vessel component			X	
5.2.2				Rupture of the vessel and possible damages to other components of the plant	P	1	5	🟨			Presence of the safety distance from the vessel component and physical barriers to other components				

5.3		No hydrogen delivered to storage in case of SOEC mode	Leakage (see 5.1); failure or malfunctioning in the hydrogen compressor stage; obstuction in the lines or valves; no reactions in the stack module	Lack of hydrogen production with no exploitation of available electricity	P	2	2	🟩	Filling sensing in the vessel and control system	Maintenance of vessel, compressors, lines and valves of HPU	Shut-down of the system			X	

EXHAUST GAS COOLING

code	FUNCTION	DEVIATION	CAUSE	EFFECTS	CAT	F	D	R	DETECTION	PREVENTION	MITIGATION	H2	NG	EL	SS
6	Cooling the exhaust gases from the ABU and exploit their heat content in a heat exchanger to provide heat to demand side	Not sufficient heat transfer in the unit	Malfunction in the heat exchanger component, due to failures, obstruction or fouling or problem due to former parts of the plant (ABU)	Not sufficient heat to cover the demand	P	3	2	🟨	Control system and temperature sensing in the streams	Maintenance of the unit	Shut-down of the system	X	X		

NITROGEN SYSTEM

code	FUNCTION	DEVIATION	CAUSE	EFFECTS	CAT	F	D	R	DETECTION	PREVENTION	MITIGATION	H2	NG	EL	SS
7	Feed the purge gas (nitrogen is used) for safety reason in start-up and shut-down operating conditions	Not sufficient purge gas supply	Rupture or accidentally release from a valve in the purge gas line, failure in control system, failure in nitrogen tank	Emergency shut-down of the system; possibility of damages to the stack; impossibility to start-up the module; possibility of safety problems	P	2	4	🟨	Control system	Maintenance of the purge gas line, valves and nitrogen tank; check of the nitrogen amount in the tank	Emergency shut-down of the system performed, detecting the lack or not sufficient supply of purge gas				X

12 REFERENCES

[1] “Paris Agreement, https://unfccc.int/process/conferences/pastconferences/paris-climate-change-conference-november-2015/paris-agreement.” .

[2] “IRENA (2019), Hydrogen: A renewable energy perspective, International Renewable Energy Agency, Abu Dhabi,” 2019.

[3] “https://www.iea.org/statistics/.” .

[4] “IEA (2019), The Future of Hydrogen, Seizing today’s opportunities, Report prepared by the IEA for the G20, Japan, All rigths reserved.”

[5] “IEA, Technology Roadmap, Hydrogen and Fuel Cells, All rights reserved,” 2011.

[6] *IEA 2018, World Energy Outlook 2018*. .

[7] “Hydrogen Council (2017), How hydrogen empowers the energy transition,” no. January, p. 28, 2017.

[8] S. Popov and O. Baldynov, “The Hydrogen Energy Infrastructure Development in Japan,” *E3S Web Conf.*, vol. 69, pp. 1–11, 2018.

[9] B. Gupta, “Fuel Cell Seminar, SlideShare,” 2015. .

[10] A. Godula-Jopek, *Hydrogen Production: By Electrolysis*. 2015.

[11] C. H. Wendel, “Design and Analysis of Reversible Solid Oxide Cell Systems for Electrical Energy Storage,” 2015.

[12] M. L. Ferrari, U. M. Damo, A. Turan, and D. Sánchez, *Hybrid Systems Based on Solid Oxide Fuel Cells*. 2017.

[13] J. Larminie and A. Dicks, *Fuel cell systems explained: Second edition*. 2013.

[14] J. Kupecki, J. Jewulski, and J. Milewski, “Multi-Level Mathematical Modeling of Solid Oxide Fuel Cells,” in *Clean Energy for Better Environment*, 2012.

[15] K. Nikiforow and P. Koski, “Report on ejector modelling , characterization and testing in FCS,” pp. 1–27, 2017.

[16] G. Buffo, “Modeling, techno-economic analysis and optimal operation of a Reversible Solid Oxide Cell (ReSOC) polygeneration system,” 2017.

[17] M. Dillig and J. Karl, “Thermal management of high temperature solid oxide electrolyser cell/fuel cell systems,” *Energy Procedia*, vol. 28, pp. 37–47, 2012.

[18] F. Petipas, A. Brisse, and C. Bouallou, “Thermal management of solid oxide electrolysis cell systems through air flow regulation,” *Chem. Eng. Trans.*, vol. 61, pp. 1069–1074, 2017.

[19] “Scheda Tecnica Impianto fotovoltaico di Environment Park.”

[20] “https://re.jrc.ec.europa.eu/pvg_tools/en/tools.html.” .

[21] “https://photovoltaic-software.com/pv-softwares-calculators/online-free-photovoltaic-

software/pvgis.” .

[22] “https://re.jrc.ec.europa.eu/pvg_static/en/manual.html.” .

[23] “https://www.infobuildenergia.it/notizie/in-italia-e-la-prima-centrale-idroelettrica-in-citta-1067.html.” .

[24] “https://www.envipark.com/impianto-idroelettrico/.” .

[25] F. Zagarella, “Estimating the buildings hourly energy demand for smart energy district planning.,” 2019.

[26] G. Giolitti, “Analysis of the hotel sector as a potential market for fuel cell-based cogeneration systems,” 2019.

[27] F. Accurso, “Techno-economic evaluation of SOFC-based cogeneration systems for the hospital sector,” 2019.

[28] “https://www.energy.gov/eere/buildings/commercial-reference-buildings.” .

[29] “https://openei.org/doe-opendata/dataset/commercial-and-residential-hourly-load-profiles-for-all-tmy3-locations-in-the-united-states.” .

[30] M. Dell’Isola and F. Fuoco, “Available Online: http://www.docente.unicas.it/useruploads/000370/files/fabbisogno_di_energia_termica_dell’edificio_per_la_climatizzazione_invernale_ed_estiva_parte_2.pdf.” .

[31] D. Maillet, D. Petit, and J. Battaglia, “Lecture 3 : Models and measurements for thermal systems , types of inverse problems,” pp. 1–34, 2011.

[32] R. Bove and S. Ubertini, “Modeling solid oxide fuel cell operation: Approaches, techniques and results,” *J. Power Sources*, vol. 159, no. 1 SPEC. ISS., pp. 543–559, 2006.

[33] “https://webbook.nist.gov/chemistry/.” .

[34] G. D’Andrea, “Dynamic modelling of an integrated biogas SOFC plant with experimental validation,” 2015.

[35] “NIST-JANAF Thermochemical Tables (1998), NIST Standard Reference Database 13, DOI: 10.18434/T42S31, https://janaf.nist.gov/.” .

[36] A. F. Massardo and F. Lubelli, “Internal reforming solid oxide fuel cell-gas turbine combined cycles (IRSOFC-GT): Part A- Cell model and cycle thermodynamic analysis,” *J. Eng. Gas Turbines Power*, vol. 122, no. 1, pp. 27–35, 2000.

[37] M. Ni, “Modeling and parametric simulations of solid oxide fuel cells with methane carbon dioxide reforming,” *Energy Convers. Manag.*, vol. 70, no. 852, pp. 116–129, 2013.

[38] A. Le Gal La Salle, F. Ricoul, O. Joubert, A. Kerihuel, and A. Subrenat, “Electrochemical Study of a SOFC with Various H2-CO-CH4-CO2-N2 Gaseous Mixtures,” *Fuel Cells*, vol. 17, no. 2, pp. 144–150, 2017.

[39] “https://it.mathworks.com/matlabcentral/fileexchange/43097-newtonraphson.” .

[40] R. J. Braun, C. Wendel, and R. Braun, “Modeling and design of a novel solid oxide flow battery system for grid-energy storage A1109 Modeling and Design of a Novel Solid Oxide Flow Battery System for Grid-Energy Storage,” no. November, 2015.

[41] P. Di Giorgio and U. Desideri, “Potential of reversible solid oxide cells as electricity storage system,” *Energies*, vol. 9, no. 8, 2016.

[42] C. Bonacina, A. Cavallini, and L. Mattarolo, *Trasmissione del Calore*. 1989.

[43] J. Milewski, K. Świrski, M. Santarelli, and P. Leone, “Advanced methods of solid oxide fuel cell modeling,” *Green Energy Technol.*, 2014.

[44] M. F. Torchio, *Tabelle di Termodinamica Applicata e Trasmissione del Calore*. 2012.

[45] “Regola Tecnica di prevenzione incendi DM 13 luglio 2011, Guida Tecnica all’Installazione, https://www.energyservice2005.it/DownloadDocument.ashx?file=1501&k=70GORA&lang=1.” .

[46] “https://www.hylaw.eu/about-hylaw.” .

[47] “HyLAW, D4.1 Cross-country Comparison,” 2018.

[48] “HyLAW National Policy Paper - Italy.”

[49] “OREDA (2009), Offshore Reliability Data, 5th Edition.” .

[50] “DIPPR Tables for hydrogen.”

[51] M. Santarelli, “Tecnologie dell’idrogeno e celle a combustibile, Proprietà dell’idrogeno,” 2000.

[52] *Hydrogen Fundamentals from HySafe, http://www.hysafe.org/download/997/BRHS_Ch1_Fundamentals-version%201_0_1.pdf*, no. 1. .

[53] “Raccomandazione di sicurezza - RS23 Proprietà e rischi dell’idrogeno, The Linde Group.”

[54] D. Baraldi *et al.*, *Prioritisation of Research and Development for modelling the safe production, storage, delivery and use of hydrogen*. 2011.

[55] O. A. Rosyid, “System-analytic Safety Evaluation of the Hydrogen Cycle for Energetic Utilization,” 2006.

[56] G. Leroy, S. Duplantier, G. Leroy, and S. Duplantier, “1D iterative model for predicting thermal radiation from jet fire,” 2014.

[57] M. Andreotti, “Modellazione di esplosioni in ambienti confinati: valutazione degli effetti su edifici residenziali e possibili strategie di mitigazione,” 2015.

[58] A. L. Anderson, “Assessment of thermal radiation arithmetic’s for jet flames,” 2018.

[59] X. Z. Wang, Y. Q. Fan, K. Bin Zhou, and Y. Yu, “Multi-Layer Cylindrical Flame Model for Predicting Radiant Heat Flux from Pool Fire,” *Procedia Eng.*, vol. 211, no. m, pp. 768–777, 2018.

[60] “Notes of the course of ‘Localizzazione e impatto ambientale’, prof.ssa Sobrero, Politecnico di Torino, a.y. 2018/19.” .

[61] F. Isorna, G. Mair, E. Lopez, and R. Rengel, “Analysis of high-pressure hydrogen and natural gas cylinders explosions through TNT equivalent method,” no. July, 2015.

[62] K. B. Lopes and P. Fernando, “Analysis of the Effects of Explosion of a Hydrogen Cylinder on the Transfer of Radioactive Liquid Wastes At Nuclear Power Stations,” 2011.

[63] A. R. Soman and G. Sundararaj, “Consequence Assessment of Vapour cloud Explosion Involving Hydrogen Release,” *Int. J. Emerg. Technol. Adv. Eng.*, vol. 2, no. 11, pp. 291–297, 2012.

[64] A. Bhatia, “Battery Room Ventilation and Safety,” no. 877, 2015.